# Transport Phenomena in Nano/Molecular Confinements

*Masoumeh Nazari[1,‡], Ali Davoodabadi[1,‡], Dezhao Huang[2], Tengfei Luo[2,3,] † and Hadi Ghasemi[1,†]*

[1]Department of Mechanical Engineering, University of Houston, 4726 Calhoun Road, Houston, Texas, 77204, United States.

[2]Department of Aerospace and Mechanical Engineering, University of Notre Dame, Notre Dame, Indiana 46556, United States.

[3]Department of Chemical and Biomolecular Engineering, University of Notre Dame, Notre Dame, Indiana 46556, United States.

‡Equal Contributor

†**E-mail:** hghasemi@uh.edu and tluo@nd.edu

## Abstract

Transport of fluid and ions in nano/molecular confinements is the governing physics of myriad embodiments in nature and technology including human physiology, plants, energy modules, water collection and treatment systems, chemical processes, materials synthesis and medicine. At nano/molecular scales, the confinement dimension approaches the molecular size and the transport characteristics deviates significantly from that at macro/micro scales. A thorough understanding of physics of transport at these scales and associated fluid properties is undoubtedly critical for future technologies. This compressive review provides an elaborate picture on the promising future applications of nano/molecular transport; highlights experimental and simulation metrologies to probe and comprehend this transport phenomenon; discusses physics of fluid transport, tunable flow by orders of magnitude and gating mechanisms at these scales; and lists the advancement in the fabrication methodologies to turn these transport concepts to reality. Properties such as chain-like liquid transport, confined gas transport, surface charge-driven ion transport, physical/chemical ion gates and ion diodes will provide avenues to devise technologies with enhanced performance inaccessible through macro/micro systems. This review aims to provide a consolidated body of knowledge to accelerate innovation and breakthrough in the above fields.

Keywords: nanochannel, liquid transport, ion transport, interface, molecular confinement, ionic diodes, energy harvesting, nanofluidics, molecular simulation, carbon nanotubes

## Introduction

The overwhelming contributions of flow of a liquid (and particularly water) through miniature confinements in nature has made this phenomenon an attractive subject for researchers. Understanding the physics of small-scale confined liquid flow not only provides a clear explanation for many natural processes, but also and most importantly, enables researchers to

exploit this concept to advance different technologies. The capillary rise of water through plant xylems driven by negative pressures resulted from evaporation of water in leaves is an important example of liquid flow in small confinements. Synthetic trees and leaves are microfluidic devices developed to mimic this natural transpiration process[1–3] and that along with other microfluidic devices can be used for passive pumping applications,[4–6] energy harvesting[7] and thermal management (evaporation-induced cooling).[8–11] Ion channels are another example of natural systems relying on transport phenomena through small conduits. They play a pivotal role in different systems in human body such as neural, retinal and muscular system by controlling the ion flux across protein membrane [12] for a wide range of functions such as signal transduction, muscle development, release of neurotransmitters, hormone secretion, fever control, and brain function.[13–20] Another example are aquaporins (the natural water channels) that are employed in kidneys for urea filtration. They separate urea waste and re-adsorb about 200 liters of water while consuming only 100 kJ of energy a day; whereas, the energy required to desalinate 200 liters of salty sea water using state-of the-art membranes is about 3 MJ, *i.e.*, 30 times larger.[21] This example highlights the economic importance of developing nanofluidic devices such as synthetic water channels.

Systems incorporating fluid transport through small-scale confinement can be broadly divided into microfluidics and nanofluidics according to the characteristic length of the confinement. Nanofluidics have been separated from larger (macro-/micro-) scale problems and have a dedicated field due to the observed characteristic difference at nano/molecular dimensions *i.e.*, the inapplicability of the continuum theories.

Microfluidics have been developed for a variety of applications including sample preparation, separation, sensing, oil recovery and detection. Microfluidics are also useful in predicting the

phase behavior in bulk systems, while obviating the need for large-scale experiments. In fact, since most of fluid properties in micro-scale remain the same as in bulk systems, microfluidic devices can be studied in lieu of original-size systems owing to advantageous features such as rapid heat and mass transfer, easy access for visualization as well as precise control of temperature and pressure and compositions. Bao *et al.*[22] discussed the extensive list of properties in oil and gas industry that can be studied using microfluidic systems.

Nanofluidics have become a major player in many industrial and scientific applications such as energy conversion, chemical sensing, separation and biotechnology.[20,23–25] These devices are of great importance in biotechnology, as the extremely small dimensions increase their sensitivity and allow for isolation and studying of individual macromolecules. Additionally, they can be employed to develop artificial materials that mimic the functionality of their biological counterparts *e.g.*, ion channels, water channels and glucose channels. Smart nanochannel membranes inspired by aquaporins (biological ion channels) are an example of nanofluidics utilization to develop such materials.[20,23] Wettability adjustment in these channels allows for controlled transport of water and ions; where a stimulus can be used to induce wetting state in the intrinsically hydrophobic channels. Transport through nanoscale confinement, also, offers additional functionalities such as nanofluidic transistors,[26] nanofluidic diodes.[27] A detailed discussion about applications of nanochannel-based devices is provided in chapter 2 of this review, where five main categories *i.e.*, energy harvesting, chemical reactions, separation, drug delivery and nanofabrication are discussed.

Unlike microfluidics, the properties of fluids in nano-scale confinements can significantly deviate from the bulk, primarily due the growing contribution from surface forces. These changes become even more pronounced when the dimensions shrink to sub-nanometer (molecular) scales.

At these scales, the physicochemical properties of the surfaces play a major role and surface properties can be tuned for optimized electric charge-induced transport phenomena. Bocquet and Charlaix[28] reviewed the properties that distinguishes nanofluidics from transport phenomena in bulk. Bocquet and Tabeling[21] pointed out the importance of nanofluidics and the challenging nature of studying nanoscale phenomena and urged additional research endeavors. Several review articles have discussed the importance of nanofluidic devices and the wide spectrum of their applications;[29–31] but a comprehensive review on applications, metrology, flow properties in nanochannels and nanochannel-based materials with especial focus on their transport phenomena is missing. The ever-growing demand for nanofluidic devices and the foreseen rise in its applications underscore the significance of understanding the physics of mass/ion transport through nano/molecular scale channels. Chapter 4 discusses the transport properties observed in nano/molecular channels.

To investigate the transport phenomena at nano/molecular scales, different methodologies can be employed. Theoretical and simulation-based investigations are very important tools for scientific endeavors, however, in most cases, they do not suffice, independently. Theoretical study of real-life phenomena often requires simplifications that can introduce potentially large errors in the analysis results; and sometimes theoretical solution may not be feasible for more complicated problems. On the other hand, simulations, despite being of extreme significance, produce results that typically cannot be verified without favorable experimental evidence. Hence, direct experimental observations are imperative to make reliable conclusions. In chapter 3, the most useful instruments and techniques for experimental investigation of transport phenomena in nano/molecular channels as well as the suitable molecular simulation methodologies are discussed. Fortunately, recent technological advances have facilitated the fabrication of nanoscale devices,

where nanochannels with dimensions down to a few angstroms and excellent precision can be developed. Chapter 5 provides a comprehensive discussion on the latest methodologies for fabrication of nanofluidic devices. Considering the recent findings about nano/molecular scale transport as well as the developments in the fabrication techniques, we realized the necessity for a comprehensive review. In chapter 6, the importance of development of nano/sub-nanofluidic devices and the main challenges in characterization of transport phenomena at nano/molecular scale are summarized. Additionally, considering state-of-the-art technology and the potential of nanofluidic devices for employment in different applications, the roadmap for future research endeavors is envisioned.

## Applications

### Energy harvesting

Nanofluidic channels have shown great promise for applications in energy harvesting facilities from electrical power generation to ion pumps. This wide variety of applications can be divided into four main categories according to their driving force for mass/ion transport: concentration-driven, pressure-driven, light-driven and temperature-driven.

The transport phenomena in nanochannels can take place due to a gradient in concentration. Often, mass/ion transport through the channels is maintained by salinity gradient between two reservoirs at the opposite ends of the channels, which can be utilized to generate electricity. In other words, the Gibbs free energy of mixing stored in the system when two fluids with different salinities are separated by an ion selective membrane ($\Delta G_{mix}$ in Eq. 1) can be harvested directly in the form of electrical power.

$$\Delta G_{mix} = -RT\left[\left[\sum x_i \ln(\gamma_i x_i)\right]_M - \phi\left[\sum x_i \ln(\gamma_i x_i)\right]_D - (1-\phi)\left[\sum x_i \ln(\gamma_i x_i)\right]_C\right] \quad (1)$$

In Eq. 1, $R$ is the universal gas constant, $T$ is the absolute temperature, $x_i$ is the mole fraction of species $i$ in the mixture ($M$), dilute solution ($D$) and concentrated solution ($C$). $\phi$ represents the ratio of the total moles in $D$ solution to the total moles in the system. Also, the activity coefficient, $\gamma$, accounts for nonideal behavior of the species and is a function of the temperature, pressure, and solution composition.[32,33] Note that the calculated $\Delta G_{mix}$ gives the theoretical upper bound for the amount of energy that can be harvested but the actual obtainable energy is always less than $\Delta G_{mix}$ due to the inevitable increase in entropy during the mixing process. Different technologies such as pressure retarded osmosis, reverse electrodialysis, and capacitive mixing can be used to extract power from salinity gradient. A variety of membranes have been employed for this purpose, as well. For example, as shown in **Fig. 1A**, very large electric currents with power densities up to 4 $kWm^{-2}$ can be achieved as the liquid moves through a single boron nitride nanotube connecting two reservoirs with different concentrations.[34] In another study, Feng *et al.*[35] utilized the concentration-driven (osmotic pressure-driven) flow to harvest energy and were able to obtain surprisingly large power densities of ca. $10^3$ $kWm^{-2}$; values that exceed their counterparts from boron nitride nanotube configuration by two to three orders of magnitude and are about a million times larger than typical power densities obtained from classical exchange membranes.[36] These large amounts of generated energy can be attributed to the application of single-layer molybdenum disulfide ($MoS_2$) nanoporous membrane with atomic-scale thickness as osmotic nanopower generators (**Fig. 1B**). Indeed, low membrane resistivity and good ion selectivity are the most

important requirements for enhanced energy harvesting. Since membrane resistivity decreases for smaller thicknesses, membrane properties pertinent to through-plane water transport *e.g.*, power density and ion mobility increase for thinner membranes. This explains the excessively high powers generated from the atomically thin layer of $MoS_2$ membrane. Aside from these extremely thin membranes, alternative and more accessible membranes can also be optimized to produce higher energies. Zhang *et al.*[37] tried to maximize energy harvesting from the blue energy (another term to describe the osmotic potential in the fluids) by optimizing the membranes with sub-micron scale thickness. To this end, they designed ultrathin and ion-selective Janus membranes, depicted in **Fig. 1C**, that were prepared through phase separation of two block copolymers. They analyzed the effect of membrane thickness and channel structure on ion transport *via* both experiments and continuum simulations and showed that power densities of ca. 2.1 $Wm^{-2}$ were achievable by using asymmetric membranes with thicknesses of approximately 500 nm.

Pressure driven transport through nanochannels can also be employed to generate electrical energy. In electro-chemo-mechanical energy conversion (ECMEC), the mechanical energy of pressure driven flow and the chemical energy of electric double layer (EDL) induced in nanochannels, is converted to electrical energy. In fact, the charge imbalance created within the EDL near the charged nanochannel walls are moved by the liquid flow, leading to a net electrostatic potential difference along the channel. This potential gradient can be harvested in form of electric current (electrical energy). Indeed, the downstream migration of the mobile ions of the EDL establishes a streaming potential ($E_s$) that along with the streaming current ($i_s$) can generate an electric power of $P = \frac{1}{4} i_s E_s$. Chen *et al.*[38] grafted end-charged polyelectrolyte brushes onto nanochannel walls, as shown schematically in **Fig. 1D**. The end-charged brushes localized the maximum EDL charge density away from the wall, thereby enabling a larger magnitude of

pressure driven transport to transfer the ions downstream. The results indicated that the application of the brushes led to generation of substantially enhanced streaming potential and improved efficiency of ECMEC compared to brush-free nanochannels. By comparing the performance of different brush structures, they also optimized the brush properties such as grafting density and number of monomers to harvest maximum energy.

It must be noted that the obtainable power efficiency through pressure driven energy conversion techniques is very limited. For example, van der Heyden *et al.*[39] could only achieve an efficiency of 3.2% for electrokinetic power generation despite using channels as small as 75 nm. Daiguji *et al.*[40] demonstrated that the maximum efficiency for electro-chemo-mechanical energy conversion can be obtained when the channel height is about twice the Debye length of the solution; however, even under this condition, power efficiencies smaller than 4% were achievable. Such a limitation strongly hinders the broader implementation of these technologies.

The application of photoelectric conversion to convert light energy to electric energy is another energy harvesting technique that has attracted intense attention in the past years. Photoelectric conversion systems consist of smart gating nanochannels that act as ion pumps and move ions against a concentration gradient to create osmotic potential. While substantial number of studies were devoted to synthetic proton-to-gradient conversion,[41–45] the biological light-driven ion pump systems have proven to be of much greater efficiency. Tian and Jiang[46] studied a photoelectric system that uses solar energy as the only driving force for cross-membrane proton mobility and generates a diffusion potential and a consequent photocurrent that can be utilized as an electrical energy source. This bio-inspired setup consists of three main sections, as shown in **Fig. 1E**. Part I is exposed to light irradiations, while other sections are covered. An anion-exchange membrane is placed between part I and part III; and two pieces of membranes with proton-driven nanochannels

are placed between part I and part II, and between part II and part III. The generated protons can move between part I and II, resulting in a charge imbalance between opposite sides of the membrane. Under irradiation, the photochemical reactions take place which results in the generation of a diffusion potential and a photocurrent flowing through an external circuit. This system represents a simple and environmentally friendly photoelectric conversion; however, the obtained photoelectric conversion performance was lower than that of conventional solid photovoltaic devices. In a recent study, Xiao *et al.*[47] fabricated an artificial light-driven ion pump system based on carbon nitride nanotube that uses illumination to move ions forward through thermodynamical uphills and against up to 5000-fold concentration gradient. They coated the cylindrical nanochannels of a commercial membrane with carbon nitride to form nanotubes needed for the ion pump system (**Fig. 1F**). The transmembrane potential created by separation of electrons and holes in the carbon nitride nanotube membrane is believed to be the foundation for pumping phenomena, primarily due to the strong light adsorption properties of carbon nitride material. The results indicated that an open circuit voltage of 550 mV and a current density of 2.4 $\mu Acm^{-2}$ is achievable through application of this setup. The ion pump system showed a strong dependence on the light wavelength, where between two monochromatic light with same power densities, blue light created the largest power while yellow light had almost no effect. An important feature of this simple and inexpensive artificial ion pump system is its universality *i.e.*, it can work in different salt, acid and alkali solutions to harvest solar energy.

Temperature gradient can be utilized to induce mass transport and generate electrical energy, as well. In fact, energy can be extracted from low-grade heat through thermo-osmosis energy conversion process; where a sustained vapor heat flux from the warmer side is utilized to pressurize the flow in the cooler side and drive a turbine. To this end, a hydrophobic porous membrane is

placed between the warm and the cold liquid streams. The hydrophobic walls of the pores inhibit liquid penetration into the membrane and air gaps will be formed inside the membrane pores, as shown in **Fig. 1G**. Mass transfer across the vapor-gap region takes place as the liquid evaporates from one meniscus, transports across the gap and condenses on the opposing meniscus; however, the higher equilibrium vapor pressure of the warm stream results in a net vapor flux toward the cold stream. Considering the partially restricted volume increase, this liquid condensation into the cold stream generates a hydraulic pressure. Continued liquid condensation onto the cold meniscus, pressurizes the flow that can be directed into a hydro-turbine to generate electricity. The obtainable energy will be a function of temperature difference (across the membrane), operating pressure and the choice of liquid; while the latter is rarely discussed since water is often chosen. Higher energy conversion efficiencies can also be obtained by increasing the temperature difference between the streams and/or increasing the operating pressure. An exemplary work was done by Straub *et al.*[48] who employed a 77% porous PTFE membrane with a nominal pore diameter of 20 nm as the separator between the cold and the warm streams and achieved a maximum power density of 3.5 $\mathrm{W/m^2}$ with a $40 C^{\circ}$ cross-membrane temperature difference and at 10 bar. They further incorporated this membrane modulus into a proposed full-scale power generation system. As depicted in **Fig. 1H**, a heat exchanger was also employed to recover the latent heat of vaporization and conductive heat transferred across the membrane. By directing the pressurized stream through a turbine, they estimated to be able to harvest energy with efficiencies as high as 7%. These calculations demonstrate that energy conversion systems can achieve higher thermal efficiencies when operating on thermal-osmosis process compared to thermo-electrochemical process.

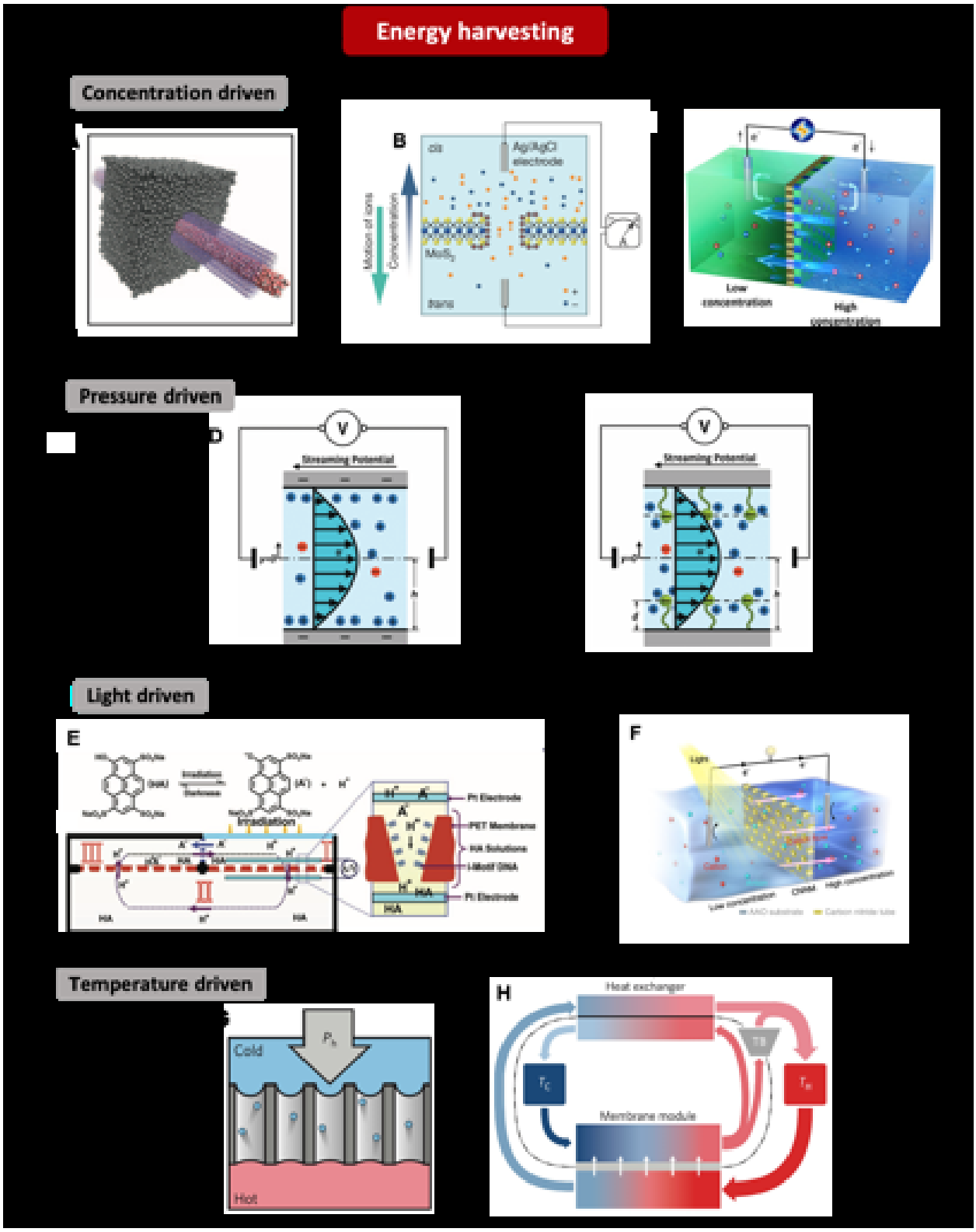


**Figure 1**. Applications of nanofluidics in energy harvesting can be categorized based on their driving forces. **Concentration-driven**: salinity gradient in two reservoirs (fluid systems) causes

ions and fluid to move across nanochannels, and thus converts energy to the form of electrical power. **(A)** Single boron nitride nanotube connecting two reservoirs with different concentration generates electric current with power density of 4 $kWm^{-2}$ .Adapted with permission from ref [34] Copyright 2013 Springer Nature. **(B)** Concentration gradient across a single-layer $MoS_2$ nanopore induces huge current leading to $10^3$ $kWm^{-2}$ power density. This large amount of power is mostly ascribed to the ultra-small (atomic scale) thickness of the $MoS_2$. Adapted with permission from ref [35] Copyright 2016 Springer Nature. **(C)** Ultra-thin (500 nm) nanofluidic power generator is made from separation of two block copolymers. This macroscopic-scale device can provide approximately 2.1 $Wm^{-2}$ power density which is one order of magnitude higher than previous reports. Reproduced with permission from ref [37] Copyright 2017 American Chemical Society. **Pressure-driven:** in electromechanical energy conversion, electric current is produced by pressure driven transport of liquid in nanofluidics. **(D)** Streaming potential in nanochannels grafted with end-charged polyelectrolyte brushes. Adapted with permission from ref [38] Copyright 2005 Royal Society of Chemistry. **Light-driven:** in photoelectric energy conversion, light irradiation to nanofluidic system generates ion pumps or electric current. **(E)** Bio-inspired photoelectric system constructed using a photoelectrochemical cell consisting of three main parts, where part I receives the light irradiation and the consequent photochemical reaction leads to generation of a photocurrent flowing through an external circuit. Adapted with permission from ref [46] Copyright 2011 Springer Nature. **(F)** Harvesting solar energy through carbon nitride nanotubes membrane. Light illumination causes ions motion against a concentration gradient leading to light-induced ion pumps. Adapted from ref [47] Copyright 2019 Springer Nature. **Temperature-driven:** in thermo-osmosis energy conversion, electric current is generated by utilizing pressurized flow obtained from vapor-phase mass transport across a hydrophobic membrane. **(G)** Schematic of the air gap

created between the cold and hot streams and the resulting vapor-phase mass transport. Adapted with permission from ref [48] Copyright 2016 Springer Nature. **(H)** Proposed full-scale power generation system based on thermo-osmosis energy conversion. Adapted with permission from ref [48] Copyright 2016 Springer Nature.

## Chemical reaction

Nanochannels can modify the chemical properties of the confined species and facilitate chemical reactions especially by enhancing the catalytic activities. Catalyst nanoparticles dispersed inside nanoscopic confinements such as nanotubes and mesoporous media demonstrate improved performance. In fact, the nanoconfinements act as very small reactors that immobilize (encapsulate) catalysts, and thus confine chemical reactions.[49,50] As shown in **Fig. 2A**, Zhang *et al.*[51] reported that the tubular channels of CNTs enable a homogenous distribution of Fe-Co alloy nanoparticle catalysts inside them. In another study, Zhang *et al.*[52] used diffusion-limited atomic layer deposition to coat metal oxides near the entrance of nanochannels inside mesoporous media (**Fig. 2B**), that resulted in successful encapsulation of Co and Ti complexes inside the nanoconfinements and led to excellent catalytic activity. Levin *et al.*[53] designed a nanofluidic device that enables studying nanoparticles catalytic activity in liquid solutions. The device was comprised of isolated nanofluidic channels, as shown in **Fig. 2C**, where nanoparticle catalysts were encapsulated in their own channels and examined under different controlled reaction conditions. These examples underscore the broad range of nano/molecular size confinements that can be utilized as nano-reactors and their importance for different types of chemical reactions.

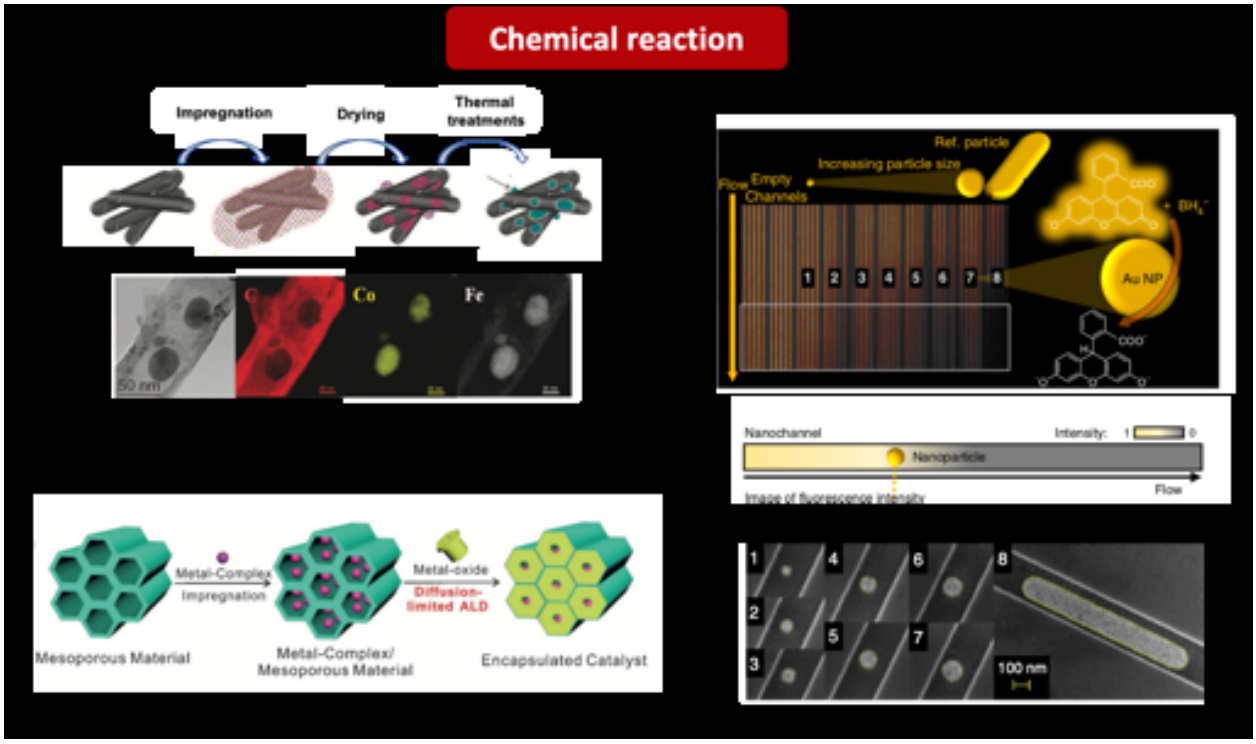


**Figure 2.** Application of nanoconfinement in chemical reactions. Nanochannels are great candidates for nanoreactors since they can immobilize (encapsulate) catalyst, and thus confine chemical reactions.[49,50] **(A)** Nanoconfined characteristic of carbon nanotubes leads to homogenous distribution of catalyst (Fe-Co) nanoparticles inside tubular CNTs. Reproduced with permission from ref [51] Copyright 2008 American Chemical Society. **(B)** Nanochannels are used to capsulate the metal complex through atomic layer deposition of metal oxide at the pore entrance. Adapted with permission from ref [52] Copyright 2017 John Wiley and Sons. **(C)** Nanofluidic device enables examination of nanoparticle catalytic activity in a liquid phase. Single Au nanoparticle (catalyst) is placed in the center of individual nanochannels, then reactant reaches the catalyst through laminar flow and fluorescence microscopy is used to visualize the reaction progress. As shown, fluorescence intensity reduces along the nanochannel length as catalytic reaction occurs. Catalytic activity of Au nanoparticle is explored based on its size for (1) 64 nm, (2) 82 nm, (3) 91 nm, (4)

102 nm, (5) 113 nm, (6) 121 nm, (7) 128 nm, and (8) patch of 139 × 1138 nm. Adapted from ref [53] Copyright 2019 Springer Nature.

## Separation

Nanochannel-based membranes have demonstrated great potentials for separation applications by regulating the permeation of substance passing through their porous structure. Carbon nanotubes and nanosheets, boron nitride nanotubes and nanoporous graphene are few examples of membranes that have been utilized for such purposes.[54–56] Moreover, exploring mass/ion transport across materials with nanoscopic conduits helps understand the fundamentals of separation mechanisms, and thus design and develop more efficient nanofiltration membranes for application in a variety of fields *e.g.*, water desalination, drug delivery and gas filtration. Hence, separation properties of nanochannel-based materials are of great importance and will be discussed in this section.

Mimicking natural phenomena is, arguably, the most important incentive for development of nanochannel-based material. Scientist have been inspired by biological channels existing in natural organisms to create artificial nanochannels that can separate water from hydrate ions and small gas molecules. So far, different material such as carbon nanotubes, graphene nanomesh, block copolymers and metal organic frameworks with various geometries have been successfully used to develop artificial membranes for nanofiltration applications;[57–59] membranes that are reverse engineered from biological channels *e.g.*, water channels, ion channels. Ion channels, for example, can reject gaseous phases while conducting water and are good candidates for application in catalysis or $CO_2$ conversion. Recently, Li *et al.*[60] reported *in Situ* water removal through gas-impeding water-conducting nanochannels composed of NaA zeolite crystals, **Fig. 3A**. To fabricate zeolitic nanochannels, they assembled zeolite crystals into a continuous separation membrane;

where a porous ceramic support was dip coated by 50-200 nm NaA nanocrystals, and then thermally annealed to the membrane to form a chemical bond between physically loaded nanocrystals and the surface of the support. The possibility of simultaneous water-conduction and gas-rejection through fabricated membrane arises from gating effect of sodium ion in NaA zeolite crystal structure. The structure of NaA zeolite with a channel diameter of ~4.2 Å, consists of 8-oxygen ring and sodium ion ($Na^+$) located in the aperture of zeolite nano-cavity to neutralize the negative charge of the framework. Therefore, this positively charged ion can affect the passage of small molecules not only by reducing the effective channel size but also based on their electric charge. Hence, it enhances the transport of water molecules due to their small size and polarity; while, it does not allow larger and less polar molecules such as $CO_2$ or $H_2$ to pass. The capability of $Na^+$ gated zeolite nanochannels to separate water molecules from other gas species is especially useful to boost $CO_2$ conversion to liquid fuel such as methanol; where water is the major byproduct of the reaction restricting the product (methanol) yields. To investigate the performance of the NaA zeolite membrane on methanol production efficiency, they made a reactor in which the membrane was sandwiched between catalyst layer (copper-zinc-alumina) and porous support, as shown in **Fig. 3A**. The observations showed that $CO_2$ conversion in reactor containing the membrane was 2.6-3 times higher than that in similar reactor without membrane layer. This significant enhancement in efficiency is attributed to the effective *in Situ,* water removal by NaA zeolite nanochannels membrane. The sieving concept has also been utilized as the foundation for development of synthetic nano-slit membranes with angstrom-size channels that are permeable to water but block all ions (except for protons).[61–63]

Nanoconfined gas bubbles can act as osmotic membranes for separation applications, as well. In fact, as shown in **Fig. 3B**, liquids such as water can cross the gas barrier *i.e.*, a bubble trapped

inside a channel through evaporation/condensation; however, the bubble remains impermeable to ionic solutes. The main advantage of gas bubble-based semi-permeable membranes is that the sub-nanometer pores needed for separation *via* liquid-phase transport-based membranes is no longer necessary and membranes with pores as large as tens of nanometer can be used. Lee *et al.*[64] used a hydrophobic coating to selectively functionalize the entrance of the pores in a 50 $\mu m$ thick alumina membrane, and thus, created a nanoporous composite membrane with a hydrophilic core and a short hydrophobic entrance that traps a gas bubble when the membrane is immersed in water solutions. This configuration enabled them to verify and systematically study the vapor-phase transport of water across opposing liquid menisci. The experiments were conducted at different temperatures, osmotic pressures and pore aspect ratios. The results indicated that the existence of a mass transport regime is determined by the resistance of the liquid/vapor interface that in turn depends on the transmission probability of water molecules across the nanopores and on the condensation probability of a water molecule incident on the liquid surface. While this setup seems a very promising design to advance separation technology, there are still a few challenges that need to be overcome before it can declare itself as a viable technology in the market. Bocquet[65] lists topics such as the long-term mechanical and chemical stability of the nanobubbles, the resistance of the membrane to pollution and fouling and the feasibility of design for reverse osmosis as the main fields that require careful investigations.

Mi *et al.*[66] developed a nanoporous membrane with three-phase interface that mimics the mechanism in lung airways. This bioinspired nanoporous membrane (BNM) was developed as a 5-layer porous media *i.e.,* poly-D-lysine/Au nano-particles/n-dodecanethiol/Au/porous anodic alumina (PAA), from bottom to top. The top side of the porous anodic alumina (PAA) membrane was in contact with the medium for cell culture, and the bottom side contacted the gas phase

directly for gas exposure. As depicted in **Fig. 3C**, this BNM acts as a one-way valve: while, the gas molecules, stored in a container connected to the bottom side, can pass through the hydrophobic nanochannel and contact with the alveolar cell resting on the top side of membrane, the channels remain impenetrable in the opposite direction. The developed BNM lung airway model is a simple device that provides a very appropriate environment for cell cultivation and can be used for *in Vitro* assays of lung inflammation analysis, drug screening, and identification of environmental toxins.

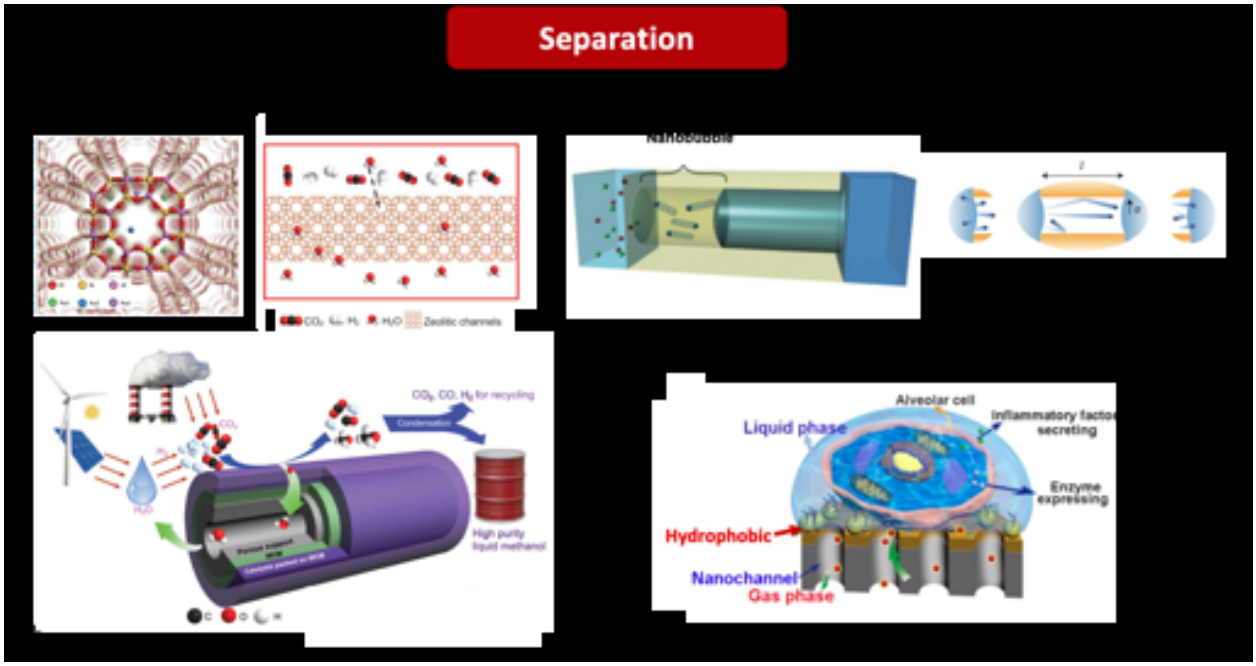


**Figure 3.** Application of nanochannels in separation. **(A)** Water conducting nanochannels made of NaA Zeolite crystals allow permeation of water molecules while rejecting small gas molecules such as $H_2$. The separation characteristic of these nanochannels could enhance $CO_2$ conversion to liquid fuels. Adapted with permission from ref [60] Copyright 2020 The American Association for the Advancement of Science. **(B)** A nanobubble trapped in the hydrophobic section of the nanochannels acts as a separation membrane for sea water desalination. In fact, it rejects ions and allows permeation of water through liquid-vapor transformation (*i.e.* evaporation and

condensation). Adapted with permission from ref [64] Copyright 2014 Springer Nature. **(C)** Bioinspired nonporous membrane composed of anodic alumina nanochannels mimics the lung air way with three-phase interface. Reproduced with permission from ref [66] Copyright 2019 American Chemical Society.

## Drug delivery

Drug delivery is one of the most needed technologies that can significantly benefit from nanofluidics. Drug delivery technologies are developed for targeted delivery of medicine with rapid and simple adjustment of drug doses. Additional capabilities such as the sensing capability that enables the release, adjustment or interruption of drug release by sending physical or biological signals, the ability to continuously control the drug release process that is especially useful in treating chronic diseases as well as the remote communication and control capabilities, make the drug delivery technology very desirable. Different nanoengineered devices with tunable pores have been developed for drug delivery applications.[67–69] Trani *et al.*[70] used semiconductor fabrication techniques and developed a silicon carbide (SiC)-coated membrane with a buried doped polysilicon electrode extended under the surface of a set of densely packed nanochannels. A schematic of this device is shown in **Fig. 4A**. In this way, they were able to fabricate a membrane with adjustable permeability. This innovative nanofluidic membrane actuator utilizes electrostatic gating to control the release of drug.

Controlled release of drugs is beneficial for cancer prevention therapies, as well. Ballerini *et al.* [71] developed a nanochannel delivery system (nDS), for controlled and sustained release of Tamoxifen (a FDA approved drug) in mammary tissue for breast cancer prevention. *In Vitro* evaluations on 9-week old rats showed that nDS implant enables sustained low dose drug delivery over several month. Also, since the nDS was placed next to the target organ, whole-body exposure

and associated side effects were minimized, while the treatment efficiency in reducing the mammary gland aggregates was improved compared to alternative common treatment methods. Nonetheless, improved drug solubility is still imperative to achieve a longer and more constant release needed for treating larger animals and humans.

In addition, nanochannel arrays can be used for controlled drug release required for visual impairments. Trani *et al.*[72] built the so-called nanofluidic vitreal system for therapeutic administration (nViSTA) that operates using a nanochannel membrane and does not require any pump, actuation or medical intervention. This intravitreal implant is only $700\times700\times800\ \mu m$ in dimensions and contains nanochannels with heights of only 20 nm. The dimension of the nanochannels are particularly tailored to enable optimal utilization of electrostatic, steric and hydrodynamic effects to achieve and maintain hindered diffusion across the membrane. As depicted in **Fig. 4B**, the drug is loaded in powder form into microchannels and is later dissolved into fluid driven by capillary forces. The concentration gradient in the fluid across the nanochannel membrane leads to drug diffusion. A major advantage of the nViSTA implant is that unlike most of the currently available intraocular implants, it offers flexibility in drug choice allowing for delivery of different types of medications from the same platform.

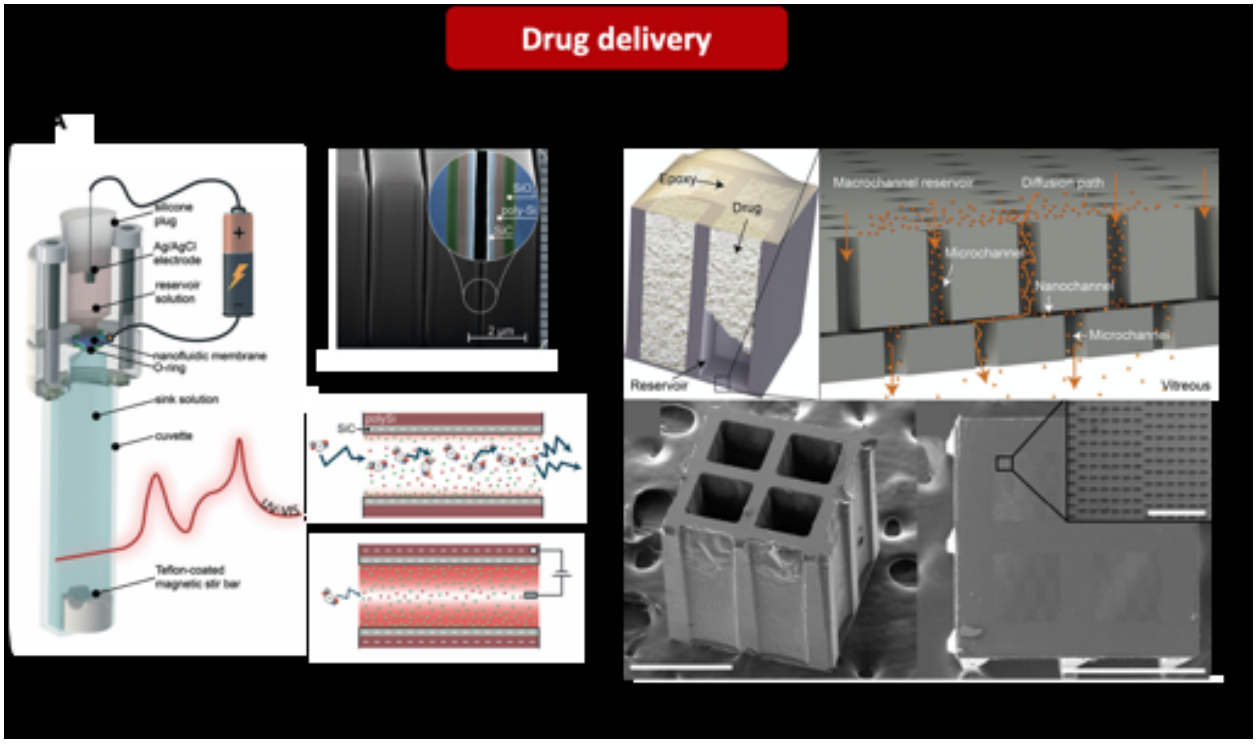


**Figure 4**. Application of nanochannels in drug delivery. **(A)** Demonstration of a tunable drug delivery system composed of nanofluidic membrane coated with silicon carbide layer. This layer protects the vertical nanochannels from chemical degradation. In such system, drug release and delivery can be controlled by electrostatically gating characteristic of nanochannels. In fact, the negative surface charge increases when negative voltage is applied which leads to negatively charged ion-impeding. Adapted from ref [70] Copyright 2020 Royal Society of Chemistry. (**B)** Nanochannels membrane system is designed to sustain zero-order drug release for vision impairment treatment. The side view image shows the drug diffusion path. Also, the scanning electron microscopy (SEM) image of a diced nanochannel as well as the SEM bottom view of membrane microchannels are shown. Scale bar in SEM images represent 400 $\mu m$. Scale bar in inset is 25 $\mu m$. Adapted with permission from ref [72] Copyright 2019 Elsevier.

## Nanoconfinement for nanofabrication

Nanoconfinements are of great importance in developing structures with nanoscopic features. The incorporation of these nanostructures leads to enhanced operation of the fabricated systems in a variety of applications such as sensing and detection,[73] photonics[74] and energy conversion.[75,76] For example, template wetting technique can be used to fabricate ordered arrays of both high aspect ratio and low aspect ratio one-dimensional (1D) nanostructures. Garcia-Gutierrez *et al.*[74] used a wetting nano-porous anodic aluminum oxide (AAO) template with polymer solution and were able to produce arrays of isolated poly(vinylidene fluoride) (PVDF) nanorods that are strongly desirable for applications in photonics, electronics, and mechanical and biomedical devices (See **Fig. 5A**). The fabricated high aspect ratio 1D nanostructures are also suitable for studying size-dependent processes such as phase separation in block copolymers, or crystalline textures. This fabrication technique is based on phase transition in PVDF confined within nanopores and its interaction with the walls of the AAO membrane. The nano-template confinement can be utilized for polymeric nanowire fabrication, as well. Cauda *et al.*[75] studied the properties of arrays of nanowires prepared *via* template wetting of PVDF and poly(vinylidene fluoride-trifluoroethylene), PVTF, into AAO membranes. As expected, the confinements in nano-geometries of the AAO membrane led to preferential orientation of semi-crystalline polymers and formed needle-like crystals stacked perpendicularly to the long axis of the PVTF nanowires, as shown in **Fig. 5B**. They also applied a triangular voltage stimulus to these polymeric nanowires and investigated its piezoelectric properties such as the ferroelectric hysteresis loops, the current switch peaks in the I−V characteristics, and the displacement butterfly loops. In particular, a piezoelectric behavior was observed for the PVDF templated nanowires, whereas this property was completely absent in the thin film of the same material. This observation underscores the crucial role of nanoconfinement in the enhancement of the piezoelectric features of the templated nanowires.

Another example that highlights the significant role of nanochannels in nanofabrication, is their application for lithium metal batteries stabilization. Lithium metal batteries are notorious for their safety issues related to potential short circuit between the opposite electrodes caused by dendrite growth on lithium metal and the consequent firing. Liu *et al.*[76] reported a strategy to stop the dendrite growth on the anode where a polyimide coating layer with vertical nanoscale channels of high aspect ratio was used to deposit the lithium metal (**Fig. 5C**). In fact, when the nanochannel coating is introduced into the electrode geometry, the ionic flux streamlines are seen to be more uniformly distributed within the columnar pores compared to the regular filamentary lithium anodes where regions of increased Li cation flux (also known as hot spots) that lead to dendrite growth are observed; hence, the introduction of nanoscale features proves to help inhibit the dendrite growth.

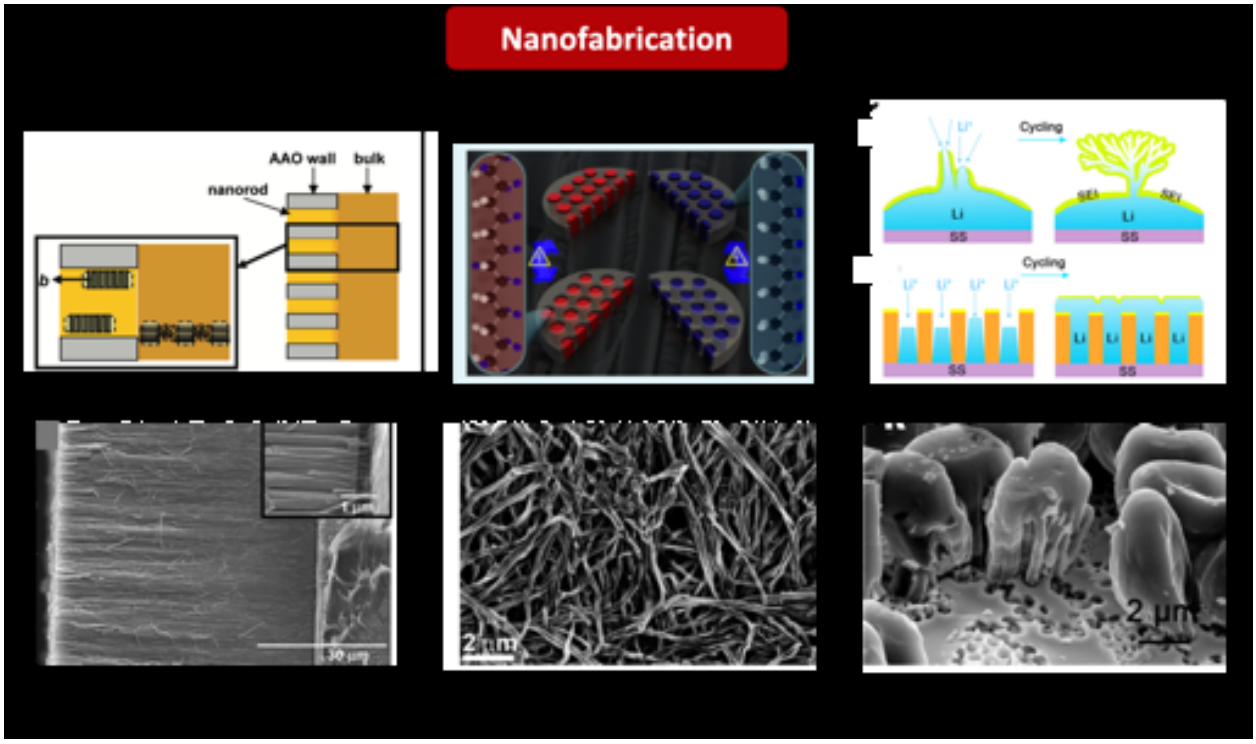

**Figure 5**. Application of nanochannels in nanofabrication. **(A)** Anodized aluminum oxide nanochannel is used as the template to fabricate high aspect ratio arrays of polymer nanorod through solution template wetting method. The nanoconfinement causes alteration in polymer crystal orientation from a residual film to the nanorod arrays. Reproduced with permission from ref [74] Copyright 2010 American Chemical Society. **(B)** Fabrication of polymeric nanowire materials with nano-template confinement method results in enhanced piezoelectric properties of PVDF due to oriented crystallization. Reproduced with permission from ref [75] Copyright 2013 American Chemical Society. (**C)** High aspect ratio nanochannels can overcome the dendrite growth problem in lithium metals anodes since the confinement effect provides consistent distribution of Li-ion flux. Reproduced with permission from ref [76] Copyright 2016 American Chemical Society.

## Mass/ion transport metrology

### Experimental techniques

It is well known that fluid behavior at nanometer length scale deviates from that in the bulk. Sophisticated instruments and techniques are essential to explore the mechanics of fluid and transport phenomena at such small scale. Various methods such as optical and fluorescence microscopy, electrical conductance measurement, scanning and transition electron microscopy, mass spectroscopy and surface characterization technique such as AFM have been utilized to probe the transport properties and nature of fluid at nanofluidic devices. In this section, we briefly review the most important approaches and existing challenges in recent experimental studies.

Optical microscopy has been frequently used as the prevalent method to visualize the fluid dynamics inside transparent channels,[77–82] as depicted in **Fig. 6A**. However, the optical contrast

between liquid and vapor phase becomes negligible as the height of the channels drops to nanometer and sub-nanometer scale; where the optical path across the channel is too short to distinguish between liquid and vapor phases. Nonetheless, this situation can be improved by introducing an optical enhancement layer. Li *et al.*[83], studied fluid flow in sub-10 nm channels *via* direct visualization that was only possible after the deposition of silicon nitride on the bottom of the channels as the enhancement layer. They examined the capillary flow of six different liquids including hydrocarbons and water. The results indicated that Lucas-Washburn (LW) equation holds for both polar and non-polar liquids even at sub-10 nm scale, while two additional coefficients were introduced to the original LW equation to account for the liquid/wall interactions at those scales. In a later study by Nazari *et al.*,[84] analogous results were reported for capillary flow of a binary mixture of ethanol/water (0.20/0.80) in 10 nm high channels, where the modified LW equation was satisfied. However, they also reported the breakdown of capillary flow (and LW-like behavior) in sub-10 nm channels for pure ethanol and isopropanol. Their observation revealed that for liquids with low surface tension, the capillary imbibition was completely inhibited and mass transport along the channel was limited to vapor diffusion. The results were confirmed using several other techniques besides optical microscopy. They also studied the capillary flow of isopropanol and ethanol through channels with heights of 40, 20 nm, as well, where both liquids penetrated the channels with a rate agreeing to that predicted by the modified LW equation.

Fluorescence microscopy is an alternative technique to probe the fluid behavior in nanoconfinements. Fluorescence imaging functions as a fluorescence dye dissolved in the liquid becomes excited and emits light within a specific wavelength. This technique is specifically useful for biological and physical research in nanofluidics due to its high signal-to-noise ratio and single-molecules sensitivity. It also overcomes the limitations caused by small fluid volume characteristic

of these systems. For instance, Zhong *et al.*[85] applied fluorescence microscopy to monitor fluid behavior at sub-10 nm nanochannels, **Fig. 6B**. However, the intensity of the emitted light was very weak due to the small number of fluorescence molecules confined in the nanochannels. Hence, they also employed silicon nitride layer to build a Fabry–Pérot resonator that enhances both excitation and emission lights. Although many researchers have employed optical and fluorescence microscopy techniques to study fluid behavior at nanoconfinements, these methods are insufficient when the confinement size shrinks to less than 5 nm. To the best of our knowledge, there is no report regarding the direct observation of liquid at sub-5 nm scale.

Environmental scanning electron microscopy (ESEM) is a promising approach that can be used for *in Situ* studying of liquid transport at small scales. Unlike conventional scanning electron microscopy (SEM), this technique allows for imaging of hydrated material and does not require vacuum condition. In fact, imaging is carried out under pressures up to 20 Torr, maintained by circulating a gas (typically water vapor or nitrogen) inside the ESEM chamber. Also, ESEM chamber accommodates a Peltier plate which makes temperature and pressure adjustments possible. Rossi *et al*.[86] utilized ESEM to study the filling and displacement of water inside CNTs with diameters between 200-300 nm and walls of 10-15 nm thickness. The ability of ESEM to see through the CNT walls was used to explore water evaporation and condensation inside CNTs, as well. Authors fabricated the CNTs through chemical vapor deposition of carbon in alumina membrane. The developed CNTs demonstrated strong hydrophilicity with water contact angles between 5 to 20 degrees, as shown in **Fig. 6C**.

While ESEM can provide useful information about fluid dynamics, transport and phase change properties inside relatively larger CNTs, its spatial resolution is not sufficiently high to visualize liquid structure within nanoscale confinements. Transmission electron microscopy (TEM), on the

other hand, enjoys higher, sub-nanometer spatial resolution. Notwithstanding, the ultra-high vacuum required for TEM operation, leads to fast evaporation of most fluids, making the study of nanoconfined liquid limited to closed cap CNTs or liquid cells, wherein a larger pressure can be maintained. The observations of Tomo *et al.*,[87] however, suggested that a thin layer of water remains stable on the walls of open hydrophilized CNT, as shown in **Fig. 6D**, and does not evaporate even under the extremely low pressures maintained during TEM visualization. The stability of this 1-7 nm liquid layer inside CNTs with diameters of tens of nanometer was attributed to a combination of curvature, nanoscale surface roughness, and confinement resulting in a lower vapor pressure for water, hence inhibiting its vaporization.

Another innovative approach to analyze the properties of nanoconfined liquids is through the application of atomic force microscopy (AFM). Whereas, AFM commonly serves as an apparatus to characterize solid surfaces topographical properties *e.g.*, roughness, alternative applications have taken advantage of this technology, as well. For example, Fumagalli *et al*.[88] employed AFM for dielectric imaging of nanochannels. They investigated the properties of water inside nanochannels fabricated *via* van der Waals assembly[89] of atomically flat crystals of graphite and h-BN; where graphite was used as a bottom layer for the assembly as well as the ground electrode in capacitance measurements. A h-BN crystal served as the top layer that was separated from the graphite by a spacer layer of h-BN in the form of parallel stripes. This striped h-BN layer formed the channels and determined their heights. As shown in **Fig. 6E**, AFM was utilized to scan over the channels and detect the electrostatic forces between the graphite layer and the AFM tip that served as the second electrode. **Fig. 6E** demonstrates that the water filled nanochannels are easily distinguishable from channel walls made from h-BN. It was observed that the out of plane dielectric constant of confined water was almost identical to its bulk value in channels with heights

larger than 100 nm, but it dropped drastically to values as small as 2 for few nanometer tall channels.

Scanning electrochemical microscopy (SECM) is a powerful tool to study molecular transport across ionic channels and has been successfully used to determine the permeability of artificial and biological nanoporous membranes. SECM is a very useful technique to characterize the relationship between membrane structure and molecular transport behavior, because in addition to measuring the molecular transport rate across the membrane, it resolves the spatial distribution of molecules at the membrane surface. Yao *et al.*[90] employed SECM to study the dynamics of molecular transport across ultrathin silica nanoporous membranes consisting of sub-3 nm diameter perpendicular channels. **Fig. 6F** depicts the schematic of the setup as well as an example 2-D current image obtained by scanning over four pores of the silica nanochannel membrane. The observations suggested that the membrane with negatively charged surface have permselectivity to anionic molecule and the transport rate of anionic redox probe depends strongly on the overlap of EDL; a lower electrolyte concentration resulted in a stronger overlap of EDL, which in turn led to a slower transport of the redox probe.

Alternative innovative instruments and techniques have also been developed for mass transport analysis. For example, Radha *et al.*[91] used van der Waals assembly method to fabricate graphitic channels with heights ranging from one to a few tens of atomic planes with atomic scale precision; where atomically flat top and bottom graphite crystals were separated by an array of spacers made from few-layer graphene. Precision gravimetry was used to explore the kinetics of water transport through these hydrophilic channels (contact angle ~55°-85°): the nanocapillary device was inserted into a Si nitride chip and mounted on top of a miniature container partially filled with deionized water, as shown in **Fig. 6G**. The variations in container mass by time was monitored for

nanocapillary devices with different channel heights from which water transport rates were extracted. **Fig. 6G** shows sample experimental data from weight measurement, where the container mass decreases linearly by time due the ongoing water evaporation and transport through the capillaries. The observations revealed unexpectedly fast transport of water through nanochannels (with velocities up to 1 m/s) that was attributed to high capillary pressures (ca. 1000 bar) and substantial flow slippage.

Gas transport through nano/molecular scale channels is another phenomenon that its accurate characterization is imperative owing to the its omnipresence in nature and technology.[92–94] Mass spectrometry can be employed to precisely quantify the gas flow rate through channels with such small dimensions. Keerthi *et al.*[95] developed a setup, schematically depicted in **Fig. 6H**, that helps determine gas flow rates through channels as small as 6.7 Å. In this setup, the nanochannel device (a tri-crystal van der Waals assembly) covers an aperture in a silicon nitride membrane prepared on top of a silicon wafer. The wafer separated two containers, one of which had a gas under adjustable pressure whereas the other was a vacuum chamber equipped with a mass spectrometer. Also shown in **Fig. 6H**, are the measured flow rates as a function of pressure for permeation of helium through nanochannels made from different material *i.e.*, graphite, h-BN and $MoS_2$. Helium transport through these 2-D channels demonstrated strong dependence on channel material; where permeation through h-BN and graphite channels turned out to be two orders of magnitude faster than that for $MoS_2$, for identical channel geometry.

Electric current (I) against voltage (V) measurements can be used to examine mass transport in nanochannels, as well. In these experiments, the nanochannel connects two micro-reservoirs at its opposite ends, as shown in **Fig. 6H**. Once the reservoirs and the channel are filled with liquid, two electrodes are placed inside reservoirs and I-V curves are obtained. Nazari *et al.*[84] used this method

and calculated the electrical conductivity for different liquids and for channels with different heights (**Fig. 6H**). The smaller conductivity observed for 10 nm channels compared to channels with 20 and 40 nm heights, was attributed to the presence of an electrically insulting phase (vapor) inside these channels. Hence, spontaneous capillary wicking was shown to break down for 10 nm channels. Increasing the surface tension of the liquid, however, resulted in recovery of the electrical conductivity *i.e.*, complete filling of the channels with liquid. This phenomenon was exploited to introduce the concept of surface tension nanogates.

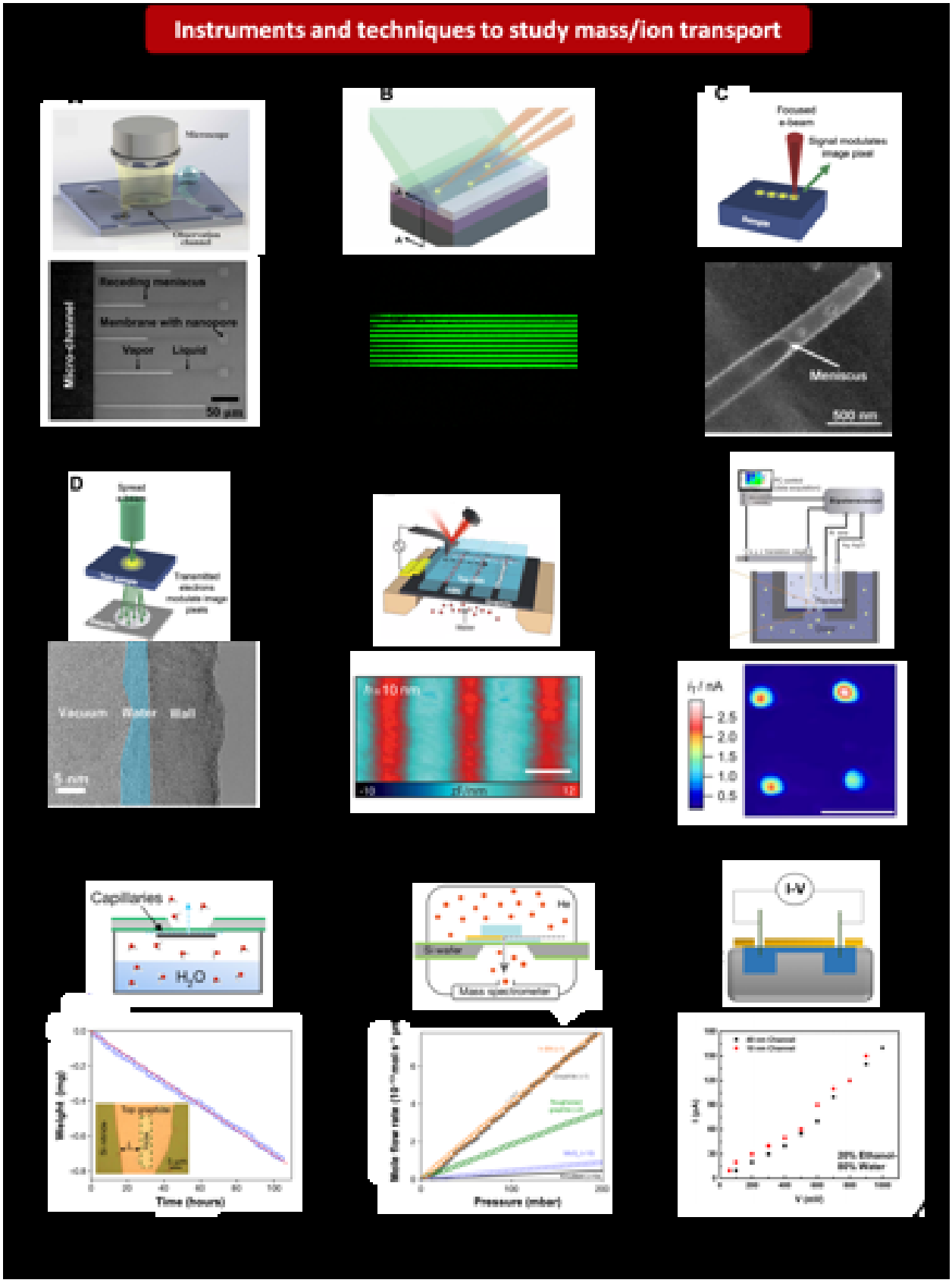
Instruments and techniques to study mass/ion transport
Receding meniscus
Membrane with nanopore
Vapor
Liquid
Micro-channel
50 μm
B
C
Focused e-beam
Signal modulates image pixel
Meniscus
500 nm
D
Transmitted electrons modulate image pixels
Vacuum
Water
Wall
5 nm
Capillaries
$H_2O$
He
Si wafer
Mass spectrometer
I-V
Time (hours)
Pressure (mbar)
V (volt)

**Figure 6.** Instruments and techniques for studying fluid/ion transport in nanoconfinement. **(A)** Direct observation of liquid motion in silicon based nanochannels through optical microscopy. Adapted with permission from ref [77,78] Copyright 2016 Springer Nature and Copyright 2019 American Chemical Society. (**B)** Schematic of fluorescence dye stimulation in nanochannels and confocal microscopy image of 10 nm nanochannels filled with fluorescence sensitive solution. Adapted with permission from ref [84,85] Copyright 2018 Royal Society of Chemistry and Copyright 2020 American Chemical Society. (**C)** Schematic of environmental scanning electron microscopy Adapted with permission from ref [96] Copyright 2016 Elsevier; and ESEM image of a water meniscus within a carbon nanotube. Reproduced with permission from ref [86] Copyright 2004 American Chemical Society. (**D)** Schematic of transmission electron microscopy. Adapted with permission from ref [96] Copyright 2016 Elsevier; and TEM image of ultrathin water film absorbed on the inner wall of carbon nanotube. Reproduced with permission from ref [87] Copyright 2018 American Chemical Society. **(E)** Schematic of atomic force microscopy system used to probe the dielectric constant of the confined water in nanochannels made of 2-D materials, and the corresponding AFM image. Adapted with permission from ref [88] Copyright 2018 The American Association for the Advancement of Science. (**F)** Schematic of scanning electromechanical microscopy setup to explore mass transport in sub-3nm silica nanochannels and the corresponding 2-D image. Reproduced with permission from ref [90] Copyright 2019 American chemical Society. **(G)** Schematic of a weight measurement method used to investigate capillary evaporation in graphene nanochannels. Adapted with permission from ref [91] Copyright 2016 Springer Nature. **(H)** Schematic of a mass spectrometer setup to probe gas transport within atomic scale confinement. Adapted with permission from ref [95] Copyright 2018 Springer Nature. **(I)** Schematic of the electrical measurement setup and the corresponding I-V characteristic results used to explore

nanoscale fluid behavior. Reproduced with permission from ref [84] Copyright 2020 American Chemical Society.

## Molecular simulations

When nanochannels height approaches a few nanometers, molecular simulation becomes an indispensable tool to study the fluid properties and elucidate the physics of flow within the channel in addition to the experimental techniques. Simulations not only help explain experimental observations, but also are crucial in studying phenomena at the molecular level, especially in close proximity of the liquid/wall interface, where experimental investigation is extremely challenging. Such phenomena include wall-induced molecular restructuring, apparent viscosity, slip behavior, wall friction, energy dissipation, *etc.* In this section, we first briefly introduce molecular simulation techniques used for studying nanofluidics. Then, we survey the advancements in the understanding of nanofluidics aided by molecular simulations.

### Molecular simulation methods

Molecular Dynamics (MD) and Monte Carlo (MC) are the two main techniques used to study fluid behavior in nanochannels. The main difference between these two methods is the way they step forward and generate the next configuration of the modeled molecular system. In MD, the equations of motion are numerically integrated as a function of time to generate the next state; thus it can provide dynamics of the molecular movement, which is essential for studying transport properties (*e.g.*, diffusivity, viscosity, thermal conductivity and slip conditions), as well as static properties such as liquid layering near channel wall and radial distribution function. For example, Huang *et al.*[97] used MD simulations to show that by modifying the surface chemistry of a

nanochannel using self-assembled monolayer (SAM), slip conditions could be widely tuned from negative slip to no-slip and to positive slip depending on phenomena such as the liquid layering and variations in surface friction and local viscosity that in turn depend on SAM hydrophobicity.

MC, on the other hand, generates the next configuration state based on the present configuration using a probabilistic rule and repeats the process to generate a sequence of states that have no time correlation. Since there is no time involved, MC can only provide static information such as the structural and thermodynamic properties (*e.g.*, free energy, density profile), rather than transport properties. However, MC can be a very valuable tool to prepare reasonable molecular systems for subsequent MD simulations (**Fig. 7A**). For example, prior to application of MD to study the transport of water in carbon nanotube (CNT), Striolo *et al.* [98] and Wei *et al.*[99] used Grand Canonical MC (GCMC) to fill the CNT with the equilibrium number of water molecules under a given thermodynamic condition (*e.g.*, 1 atm and 300K). Without this GCMC simulation, MD simulation may not yield reasonable results since the packing order of water molecules and transport properties can be strongly impacted by the density.

Popular MD simulation packages such as LAMMPS,[100] GROMACS,[101] AMBER[102] are all appropriate for simulations of fluid flow in nanochannels. LAMMPS provides the additional advantage that GCMC can be performed in the same package. To calculate transport properties, two methods can be used in MD simulations. One is the non-equilibrium molecular dynamics (NEMD) method, which allows for direct measurement of target properties analogous to that in experiments. For example, a shear force can be established by translating a wall with respect to another for viscosity calculation (**Fig. 7B**). Additional experiment-inspired phenomena such as viscous flow in nanochannel,[103,104] *in Situ* nanoindentation and stress test[105] can also be easily simulated using NEMD. The obtained results often demonstrate close agreements with the

experimental data. In addition, NEMD is relatively straightforward and generally produces robust results. However, given the mismatch between computational and real experimental time and length scales, the non-equilibrium conditions applied in NEMD can be unrealistically large (*e.g.*, >100 m/s for shear velocity, $10^7$ K/m in temperature gradient),[106,107] and thus it is common to test the calculated properties as a function of the applied non-equilibrium gradient to either see a convergence or perform extrapolation to realistic gradients.[108–110] The other method is the equilibrium molecular dynamics (EMD), which calculates transport properties based on the linear response theory.[111] EMD can be considered advantageous as it does not require applying unrealistic non-equilibrium conditions (*e.g.*, high shear rate or temperature gradient). For example, as long as the sought after property is a transport property such as diffusion,[112] shear viscosity/friction coefficient,[99,113] and thermal conductivity,[114–116] EMD is recommended. However, one usually needs to run many independent simulations in order to overcome the convergence problem related to the incomplete sampling of the phase space or insufficient replicas.[116,117]

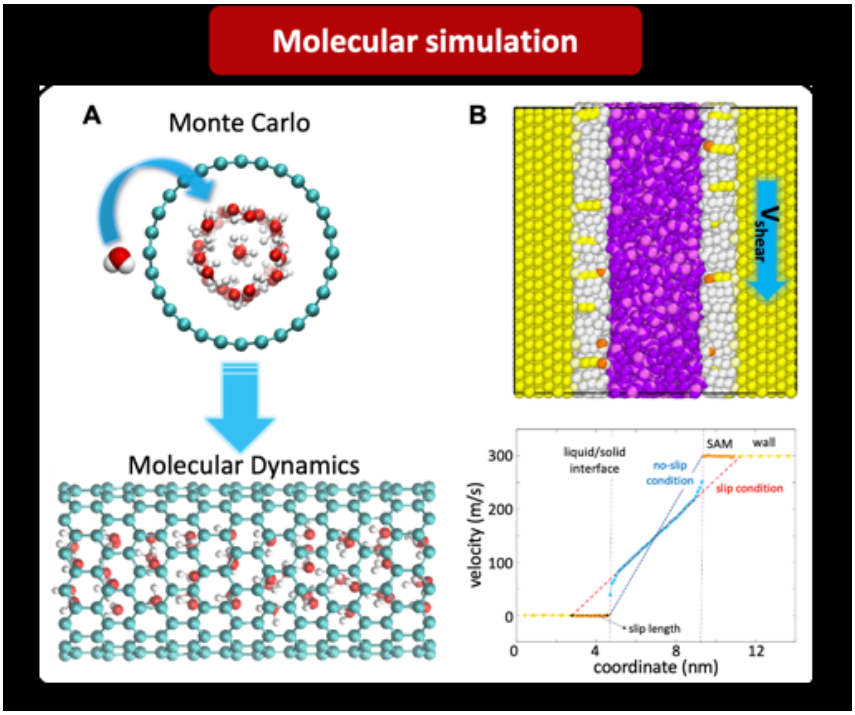


**Figure 7**. Molecular simulation techniques play an important role in studying behavior of nanoconfined fluids. **(A)** In molecular simulations of fluid flow in nanochannels, a hybrid MC/MD is usually used; where MC estimates the equilibrium molecule density in the channels and MD simulation utilizes the MC-produced molecular configuration as the input to predict transport properties. Reproduced with permission from ref [99] Copyright 2018 American Chemical Society. **(B)** A typical NEMD setup and steady state velocity profile to calculate viscosity and study slip conditions. Reproduced with permission from ref [97] Copyright 2019 American Chemical Society.

**Molecular simulation for nanofluidics**

Most unconventional behaviors of fluid in nanochannels originate from the nanoscale size effect. The small channel size makes the ratio between the wall/liquid interface area and the liquid volume very large, making the fluid flow in such channels dominated by the interfacial interaction, especially when the channel sizes are only a few nanometers. If we consider an interatomic interaction cutoff of 1 nm, then the ratio of the numbers of the surface atoms (the ones within the

interaction range from wall) and the total atoms is roughly $(x^2 - (x-2)^2)/x^2$ in a nanochannel with a square cross-section with a side of $x$. When $x$=10 nm, this ratio is 36%, and it becomes 64% when $x$=5 nm. A key influence from the wall is directly from its interaction with liquid molecules, making the surface atoms experiencing a different bonding environment than those in the bulk. Liquid/wall interaction mainly consists of van der Waals and electrostatic interaction, both of which are physical interactions. Chemical bonds can form when chemical reaction with the wall happens, but such bonded molecules become a part of the wall and can serve as surface functionalization, such as SAM. Such functionalization is an effective way of tuning the liquid/wall interaction.[97,106,118–121] When the liquid/wall interaction is strong, it can lead to the formation of ultra-thin stagnant liquid layers on the surface which can reduce the effective size of the channel and results in increased flow resistance. From a boundary condition point of view, this is the no-slip boundary (**Fig. 7B**). However, these molecular-level, sub-nanometer features pose significant challenges for experimental characterization, where molecular simulations come up to be an indispensable tool.

For example, Lane *et al.*[122] used MD to show that surface functionalization *via* SAM can confine the orientation of water molecules in a nanochannel, forming special structures, and such a confinement depends on the nanoscale size of the channel. Despite the nanoconfinement, the MD simulation found that there was always liquid diffusion inside the channel. Similar liquid molecular re-structuring phenomena near the nanochannel wall have been widely seen in recent molecular simulation studies.[97,106,123,124] Nanoconfinement can also induce or work with other mechanisms to influence the fluid behavior in the nanochannels. For example, the electro-viscous effects,[125–127] formation of gas nanobubbles,[128,129] presence of stagnant liquid layer adjacent to the walls[130–136] are some of the proposed causes for the flow slowdown in nanochannels. Molecular

simulations have played important roles in understanding these mechanisms. The electro-viscous effect is caused by the presence of the EDL near the wall/liquid interface, which is essentially the result of the electrostatic interaction between the wall and polar liquid molecules (*e.g.*, water). Such an effect is proposed to be responsible for ionic transport behavior within nanochannels and to generate a streaming potential that results in an electro-osmotic counter flow and an increase in the apparent dynamic viscosity.[137] Zhang *et al.*[124] conducted MD simulations of electro-osmotic flow in nanochannels and showed that the electrostatic interactions between the ions and the charged wall were dominant in the EDL region rather than the van der Waals interactions. Lee *et al.*[138] used MD simulations to model the EDL and found excellent agreement for various qualitative and quantitative assessments on mass density profiles, charge density, electric potential profiles and capacitance trends with the constrained density functional method, providing the molecular details that cannot be easily characterized in experiments.

Slip boundary condition is another phenomena that has been extensively studied using molecular simulations.[139–146] Since the surface effect plays a dominant role at nanoscale channels, the interfacial fluidic behavior is more important in nanochannels than in their micro or macroscale counterparts. Ewen *et al.*[147] conducted tribological experiments and NEMD simulations to investigate the effect of confined fluid molecular structure on nonequilibrium phase behavior and friction. The simulations showed that the friction coefficient of lubricants (that are broadly linear molecules) increases as a function of strain rate and pressure; results that agreed well with those obtained from the experiments. Priezjev *et al.*[144,146] have shown that by changing the polymer melt/wall interaction, the slip behavior of the fluid and the structure of the fluid could be changed. Similar NEMD studies has also been extensively performed for different liquids and surface conditions.[140,142,143,145] Huang *et al.*[97] performed MD simulations to study the slip behavior of water

confined between different SAM-functionalized surfaces and found positive and negative slip lengths for hydrophobic and hydrophilic SAM functionalization, respectively; a transition that can be explained by the strength of the interfacial interactions between water molecules and the SAM surface. The smaller relaxation time of the interfacial water and the more pronounced water trapping inside the SAM layer which impede the water slip were also the result of the stronger interaction.

One of the most widely studied nanochannels with a few nanometer sizes are CNTs. The fast water transport in CNT is the most prominent behavior observed both through computer simulations[148–150] and experiments.[151–153] Falk *et al.*[154] studied the interfacial friction of water at graphitic interfaces with various topologies and found the friction coefficient curvature dependence is mainly associated with a curvature-induced incommensurability between the water and carbon structures. Bahu *et al.*[155] discovered that the degree of confinement and curvature effects had greater impact on the liquid/solid interfacial friction in the case of confined water molecules in CNTs. Ma *et al.*[156] performed MD studies of water transport in CNT with flow velocities comparable to experimental values and observed previously undetected oscillations in the friction force between water and CNTs, showing that these oscillations resulted from the coupling between confined water molecules and the longitudinal phonon modes of the nanotube. Suk *et al.*[157] modeled the water flow rate through CNTs while taking the entrance/exit effects into consideration and proposed a water flow model that covers various lengths and radii of CNTs. Walther *et al.*[158] performed large scale MD simulations to simulate micrometer thick CNT-based membranes commonly used in experiments but found flow rates far below experimental values, suggesting the reported superfast transport rates could not be attributed to interactions of water with pristine CNTs alone.

The fast water transport in CNTs is typically attributed to breakdown of no-slip boundary conditions. Slippage of water molecules at the interface of CNT has been discussed in a range of studies,[153,154,159,160] and the reported slip length varies between 25-100 nm depending on the diameter. [161] An important benefit of MD simulation is that, unlike experiments, one can easily conduct parametric studies in MD. For example, Ma *et al.*[162] showed the relationship between the CNT wall/water interfacial friction stress and slip velocity follows a transition-state-theory-based inverse hyperbolic sine function and this was found universally valid regardless of wetting properties. Under nano-confinement, water can be more susceptible to electrostatic interactions from the confining walls. Wei *et al.*[99] performed a systematic parametric study of the charges of the carbon atoms on CNT, which helped revealing why boron-nitride nanotube (BNNT) had such different water transport than CNT. This MD study also showed that water molecules experience a drastically different potential landscape in a CNT than in a boron-nitride nanotube, where the two material differ only by the electrostatic interactions due to the charged boron and nitrogen atoms. Brog and Reese[163] showed that CNTs had higher flow enhancement factor compared to BNNTs and silicon carbide nanotubes (SiCNTs) with identical length. They also concluded that experimental results suffered from very large uncertainties and would require many independent replications, whereas MD simulations can be alternatively used to provide meaningful guidance. Thomas *et al.*[141] also modeled the transport of water through CNTs using MD and observed an enhanced transport of water in CNTs. They argued that the frictionless surfaces and depletion layers formed near the walls due to the electrically and mechanically smooth surfaces of CNTs were responsible for the fast water diffusion. On the other hand, for water transport across membranes made of armchair (8, 8) BNNTs and armchair (8, 8) CNTs, MD simulations predicted similar fluxes,[3] indicating similar friction coefficients for water transport.

There is also a wide range of parametric studies about other relevant factors, *e.g.*, CNT diameter,[148,164–167] chirality[168–172] and charge,[99,158,173,174] which have helped further clarify the role of these parameters in water transport through CNTs. Similar parametric studies have also been conducted in MD simulations to investigate the influence of the surface effects on the nanoconfined liquid not restricted to those in CNTs.[175,176] For example, Dai *et al.*[177] conducted MD simulations to show that the water flow rate in graphene oxide (GO) nanochannels was slow and the confined water structure became more disordered and loose when the GO nanochannels was more corrugated. As we move to scales on the order of molecular length, the transport characteristics in nanochannels become more intriguing as chain-like transport can occur,[61,148] and MD simulation was used to aid the understanding of such chain-like transport.[178]

MD has been found extremely useful to investigate a broad range of problems especially in nano/molecular scale, where elaborate experimental setups are required, however, definition of boundary conditions is essential to obtain reliable results. For example, seemingly contradictory results have been reported for water transport through hydrophobic nanoconfinements. Whereas, the majority of studies have demonstrated enhanced water diffusion through nanochannels with hydrophobic walls, nanoconduits with water diffusivities close to or even smaller than bulk value have been reported, as well. For example, MD simulations conducted by Liu *et al.*[179] showed that water diffusion rate in nanopores and nanoslits was markedly lower than the bulk value. This in sharp contrast to results reported elsewhere, such as Zaragoza *et al.*;[180] where the nanoconfinement was shown to expedite the flow. The unconventional behavior reported by Liu *et al.* stems from their boundary condition definition, where they ignored atomistic interactions at the liquid/wall interface and assumed that molecules rebound from the hydrophobic surface. Surface roughness could have been another potential cause of flow slowdown, while it is typically neglected in

molecular simulation studies. Indeed, one of the reasons for the ultra-fast water transport through CNTs is their inherent smoothness, that may be absent in other nanoconduits. In an intriguing study, Daejoong *et al.*[181] conducted both equilibrium and nonequilibrium MD simulations of electro-osmotic flow of water and found that the diffusion of water along the flow direction in a charged nanochannel is similar to the bulk value; a result that was primarily attributed to the walls surface roughness.

Molecular simulations have proven to be a very useful method not only to verify experimental results, but also to expand the investigations of fluid transport properties to the extents that are not experimentally feasible. Notwithstanding, challenges can be encountered when applying these techniques. Molecular simulations are infamous for their inability to model large systems for long times, since the computational times can increase unreasonably. In addition, MD simulations rely on high fidelity force fields to correctly model the dynamics of the molecular system, but existing force fields can be inaccurate or even missing for certain interactions. Kannam *et al.*,[182] also, pointed out a few shortcomings of NEMD simulation method, such as the very small velocity gradient of water inside CNTs, the fact that the magnitude of the average velocity is significantly larger than the thermal velocity of water (*e.g.*, 10-100 m/s and ~ 340 m/s, respectively, at 300 K), and the limitation of the model size. Since NEMD simulation requires a very careful analysis of the velocity profile, they suggested EMD as a more reliable method. Potential solutions are in development to address the current issues with molecular simulation techniques that will be discussed in chapter 6. It must be noted that despite the mentioned problems, molecular simulations remain a vital contributor to the study of flow behavior and fluid properties at the nano/molecular scale.

## Transport phenomena in nanochannels

### Liquid transport

Understanding the underlying physics of flow of liquids confined in nanoscale geometries is essential to address many common challenges existing in science and engineering applications such as nanomedicine,[66,68,69] energy storage and conversion,[34,36,47,183–188] water purification,[3,189–191] and electronic cooling.[192–196] As the confinement dimensions shrink, the role of liquid/wall interactions becomes more significant. These interactions result in the properties and behavior of the confined liquid to deviate considerably from those of the bulk liquid,[77,83,197] so that the classical theories no longer hold.[29] Nomura *et al.*,[198] for example, demonstrated that both low density and high density states of water can exist inside an isolated CNT with a 1.25 nm diameter at temperatures close to room temperature; whereas, this metastable co-existence state is predicted to be feasible only at temperatures below 230 K for bulk water.

The observed departure in nanoconfined fluids properties from the bulk are mainly due to the contributions of physical phenomena such as flow slippage[151–153,199–201] and apparent viscosity[113,133,159,202,203] that were negligible at larger scales. Liquid transport phenomena in nanoscopic confinement has been investigated both by MD simulations and experiments. In some cases, the results show slower flow in nanoconduits compared to the predictions from classical theories, whereas, sometimes the flow rate of the confined liquid exceeds the theoretical predictions.[77,159,204] These apparently contradicting results for flow behavior in nanochannels are, in fact, due to different types and strengths of the liquid/wall interactions. These interactions that play a crucial role at small scales can be categorized according to the degree of affinity between the liquid and the wall surface. Hydrophobic and hydrophilic are two broad categories that surfaces with weak and strong affinity with water fall into, respectively. Therefore, there can be a significant

difference in properties and transport behavior of water in nanochannels with hydrophobic walls and those with hydrophilic wall surfaces.[205] In hydrophobic confinements, water molecules can slip on walls, and consequently, the classical assumption of no-slip boundary condition is no longer valid.[148–150,206] In fact, the weak liquid/wall interactions lead to formation of a depletion layer near the wall surfaces wherein the liquid viscosity is substantially less than bulk viscosity. This phenomenon results in higher mobility of water molecules and can be characterized in terms of true slip length.[207] However, the situation in hydrophilic confinements, where liquid molecules undergo a notable epitaxial ordering, is quite different. That is, the strong liquid/wall interactions immobilize a very thin liquid layer adjacent to the walls leading to a significant increase in local and average viscosity; that in turn, slows the fluid flow. This phenomenon, known as multilayer sticking, has been reported in several studies.[208–211] One might intuitively assume that stronger liquid/wall interactions (better liquid/wall wetting) always imply greater friction. However, an interesting study carried out by Rajan *et al.*[212] argued against this statement. They observed an increasing trend in friction coefficient between h-BN walls and different liquids while the liquid/wall affinity decreased. The observations were explained by highlighting the point that the electrostatic component of liquid/wall interactions play the main role in determining the liquid/wall friction coefficient, while the wettability shows a strong dependence on the dispersion component. More details on liquid/wall interactions effects on liquid flow through nanochannels is provided in the following.

**Expedited liquid transport**

The slippage of polar liquids on hydrophobic surfaces as well as the decrease in their viscosity near such surfaces leads to a significant increase in the average liquid flow velocity in nanofluidic systems made from such material. Slip length has been defined as a parameter to quantify the

degree of flow slippage and the extent of change in properties (such as viscosity) of liquid confined within nanochannels with hydrophobic walls. As shown in **Fig. 8A**, Wu *et al.*[207] defined effective slip (length) as the linear sum of true slip and apparent slip raising due to water/wall slippage and varying viscosity near the walls, respectively. The slip length denotes the distance between the channel height and the height of a hypothetical channel where the liquid velocity would become zero at the walls. **Fig. 8C** shows the MD simulations results obtained by Huang *et al.*[213] depicting the relationship between the true slip length and water/wall contact angle for a variety of organic and inorganic surfaces. Interestingly, slip lengths on different surfaces collapse nearly onto a single curve as a function of the static contact angle characterizing the surface wettability, thereby suggesting a quasi-universal relationship. They also discredited the classical assumption of existence of a linear relationship between slip length and depletion layer thickness. **Fig. 8D** shows the measurements for the slip length *versus* the depletion width for three extremely smooth diamond surfaces, where instead of the simple linear relationship, the slip length seems to scale with forth power of the depletion width. Results obtained from molecular dynamics simulation and experiments have demonstrated that surface wettability, wall roughness, operation conditions and liquid viscosity are the parameters affecting the slip length.

An ultra-fast water transport in hydrophobic nanoconfinements has been reported in many experimental studies.[91] Among them, CNTs[152,214] are of special interest as they allow the study of mass transport through channels with nanoscopic diameters and atomically smooth walls and seem very promising to serve as membranes, as well as for application in nanofluidic systems, desalination, energy harvesting and nano-filtration. Majumder *et al.*,[152] for instance, studied liquid transport through multiwall carbon nanotubes with an inner diameter of 7 nm at 1 bar. The observations indicated a substantial deviation in liquid velocity from the classical Hagen-Poiseuille

theory where the liquid flew four to five orders of magnitudes faster compared to the predictions. This improvement in liquid flow rate was attributed to slip phenomenon. In fact, the weak molecular interactions between water and CNT walls lead to formation of a molecularly thin depletion layer near the liquid/wall interface that increases the flow velocity by eliminating the frictions and associated viscous dissipations between water and CNT walls surface. The degree of flow slippage was also characterized in terms of slip length with values in the range of 3-70 μm. They measured the flow rate of a variety of solvents such as Ethanol, Isopropanol, Hexane and Decane, as well. The results indicated a decrease in the slip length as the solvent became more hydrophilic *i.e.*, its affinity carbon nanotubes walls increased, that is reasonable since boundary slippage is based on weak liquid/wall interactions. Both computer simulations[148–150] and experiments[151–153] have recognized the breakdown of no-slip boundary condition responsible for the fast water transport in CNTs. Slippage of water molecules at the interface of CNT is discussed in a range of studies[153,154,159,160] and the reported slip length[161] varies in the range 25-100 nm depending on the diameter. Secchi *et al.*[153] conducted further investigations, where they measured the pressure driven flow of water through individual CNTs and boron nitride nanotube (BNN)s. The obtained experimental data, plotted in **Fig. 8B**, reveal substantial water slippage on CNT walls that decreases drastically for CNTs with larger radii. However, no water slippage was observed in BNNs, regardless of the tube dimensions. This result is of great importance considering the fact that MD simulations using semi-empirical interfacial parameters predict similar flow behavior through CNTs and BNNTs.[215,216] Albeit more recent simulations results predict that water friction on CNT surface is lower than that on BNNT,[217] however, the projected difference in flow rates is significantly smaller than the experimental observations by Secchi *et al.* Since CNT and BNNT have identical crystallography, this unexpected difference in slippage properties was attributed to

their electronic structure: CNTs are semi-metallic while BNNTs are insulators. These findings highlight that even subtle differences in atomic-scale details of solid-liquid interfaces can substantially impact the hydrodynamics of flow in nanofluidic systems.

Unlike the systematic variations in slip length by channel size reported in previous studies, Xie *et al.*[218] observed a wide range of relatively scattered values of slip length for water flow through graphitic nanoconduits. To experimentally measure the slip length, they used MEMS fabrication techniques and developed hybrid silica/graphene nanochannels, where a silica and a graphene nanochannel with identical cross-sectional dimensions were connected. The slip length of water on graphene was determined by measuring the hydraulic resistance in the channels. They monitored the meniscus location movement inside the graphene and the silica nanochannels through an optical microscope. The obtained data for slip length in channels with heights varying between 20 and 125 nm does not show any specific trend; instead a random distribution of values between 0 and 200 nm with a statistical median of 16 nm is observed. Differences in functional groups and charges on graphene surface as well as the interaction between graphene and its silica substrate were postulated to be responsible for these variations in graphene slip length.

Despite the promising fast liquid transport demonstrated for CNTs, their integration into macroscopic devices has remained extremely challenging, limiting their applications. On the other hand, graphene has also attracted considerable attention as a potential core material for nanoconduit fabrication. Several studies on gas, liquid, ion and DNA transport through graphene pores have been conducted. However, fabrication process of artificial graphene capillaries with precisely controlled dimensions at nanometer scale appears challenging and requires further investigations to overcome challenges such as those associated with surface roughness. Recently, Radha *et al.*[214] reported an innovative technique for fabrication of narrow and atomically smooth

graphene nanochannels. This structure is produced through van der Waals assembly of exfoliated graphene sheets separated by a two-dimensional crystal spacer. Using this fabrication method, they developed nanofluidic devices containing 200 nanochannels with widths of 130 nm and lengths between 2-10 μm. They were able to control the channels height between 0.7 to 10 nm by changing the number of 2-D crystal stripe spacers. They used precision gravimetric to explore water permeation through the nanofluidic device and analyze the capillary flow in graphene nanochannels. The extremely fast water transport observed in nanochannels was attributed to water slippage on the channel walls. They also measured the capillary flow rate in channels with different heights ranging from 10 nm to several angstroms: the liquid flow rate reduced by decreasing the channels height, but an unexpectedly fast flow was observed in channels with heights smaller than 2 nm. In addition, the highest measured liquid flow velocity of approximately 1 $m.s^{-1}$ occurred in channels that accommodated only a few layers of water. This unexpected behavior was attributed to an increased structural order in nanoconfined water. Molecular dynamics simulations showed a slip length of ca. 60 nm and a viscosity increased by a factor of two compared to bulk for water flow in very shallow nanochannels. Nonetheless, these results may need further verification through experimental investigations. This work can significantly impact the nanofluidics field by introducing an additional technique to fabricate capillaries with sub-nanometer size and providing a wide choice of atomically flat materials such as h-BN and $MoS_2$ for channels wall. Despite high transport kinetic in these nanopores, these channels cannot match the fluxes and selectivity of biological porins.[219,220] Marbach *et al.*[221] suggested surface wiggling through enhanced diffusion and entropic trapping governs the mass transport in these biological porins. This explains the higher performance of biological pores compared to the synthetic membranes.[222]

As the channel height moves toward single-digit nanometer and molecular scales, the transport characteristics becomes more interesting as the chain-like transport phenomenon can occur in these scales;[61,148] where the extreme confinement forces the liquid to form single-file chain within the channel. **Fig. 8E** shows the enhancement factor (the ratio of actual flow rate to that predicted from Hagen-Poiseuille equation) for different channel/tube characteristic lengths, where data are extracted from different experimental and simulation studies.[223] A noticeable increase in transport rate observed at sub-10 nm scales is followed by an even more drastic increase at molecular scales. Tunuguntla *et al.*[224] reported an order of magnitude higher permeance through sub-nanometer CNT (0.8 nm) compared to 1.5 nm CNT, **Fig. 8F**. Water permeability in these angstrom-size CNT porins exceeded that in biological channels *e.g.*, aquaporins by an order of magnitude, as well. These observations underscore the importance of this form of expedited liquid transport in molecular size channels. Furthermore, chain-like transport in nanomembrane with sub-nanometer pores provides a route for high mass flux membranes.[178] On the other hand, transport characteristic observed only in sub-10 nm channels display substantial proton transport enhancements and ion mobility. This increased transport is realized by the dominance of surface charge effects at these scales.[225,226]

In must be noted that similar to chain-like transport that only takes place in molecular (sub-nanometer) channels, additional properties distinguish the transport in molecular channel from that in nanochannels. Firstly, the liquid/wall interactions play a significantly more dominant role in molecular channels. An example of this was evidenced by the drastic change in water transport behavior in nanometer-scale and molecular-scale CNTs, mentioned earlier. Moreover, since the diameter of hydrated ions is comparable to angstrom-size confinements, molecular channels can act as geometrical confinements for steric exclusion of specific ions. These gating features will be discussed in detail in section 4.3.

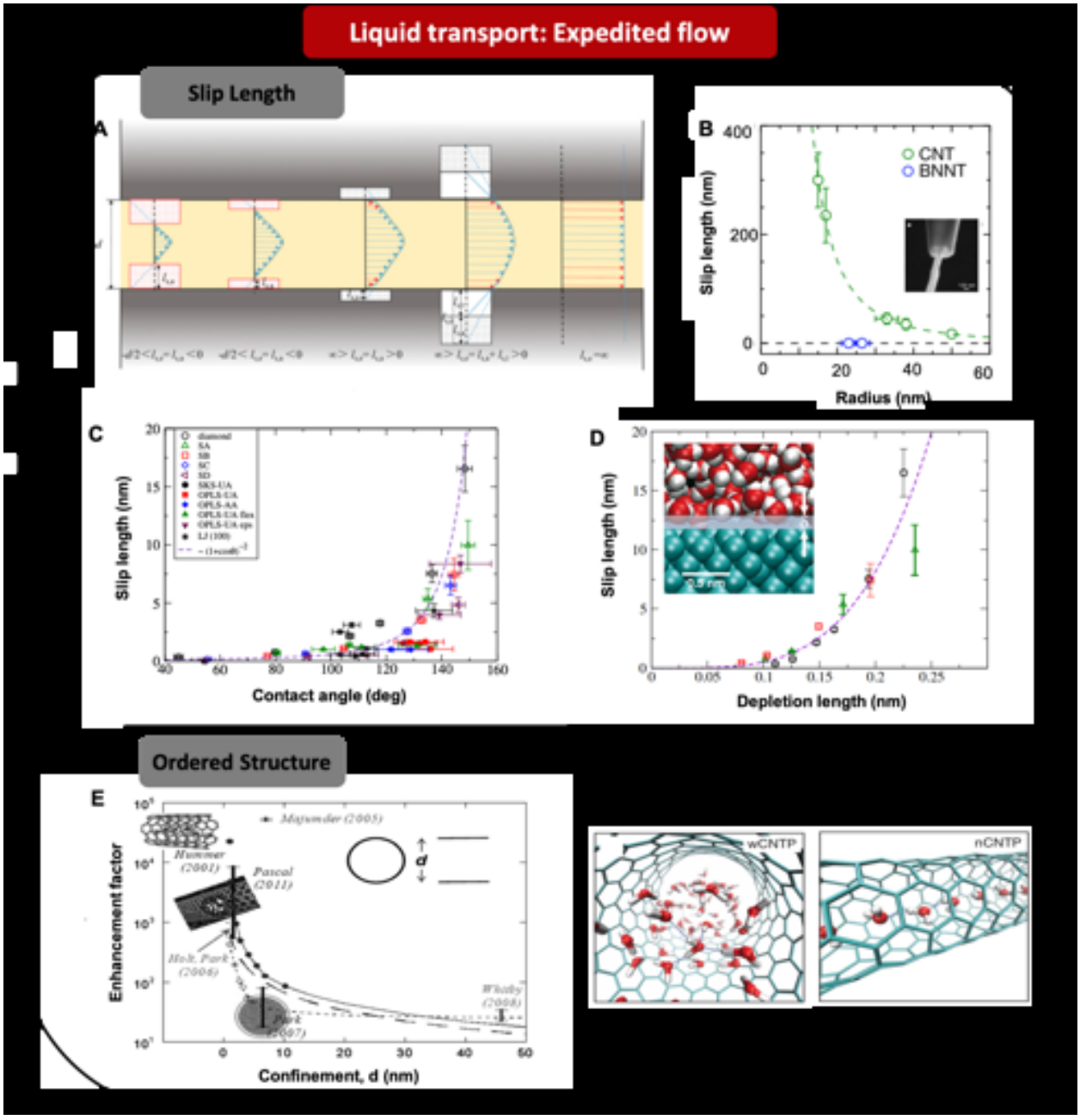


**Figure 8.** Flow enhancement in nanoconfined geometry occurs due to fluid slippage on the confinement wall. **(A)** Schematic of the liquid velocity profile in nanoconfinement based on liquid-wall interaction (contact angel) demonstrates the concept of slip length. From left to right, the strength of liquid-wall interaction reduces and thus contact angel increase. Adapted with

permission from ref [227] Copyright 2016 Society of Petroleum Engineers. (**B)** Experimentally measured water slip length within carbon nanotube and boron nitride nanotube as a function of nanotube radius. Adapted with permission from ref [153] Copyright 2016 Springer Nature. **(C)** Water slippage as a function of contact angel for different hydrophobic surfaces is obtained by molecular dynamic simulation of an atomistic water model. Adapted with permission from ref [213] Copyright 2008 American Physical Society. (**D)** Dependence of water slip length on depletion length for diamond surfaces. Adapted with permission from ref [213] Copyright 2008 American Physical Society. In addition to slippage, ultra-small nanoscale confinement causes ordered structure of liquid within the conduit leading to extremely fast fluid transport. (**E)** Flow enhancement factor as a function of carbon nanotube diameter based on the result obtained by different models and experiments. As demonstrated, the enhancement factor increases exponentially as confinement size decreases arising from 1-D ordered structure effect of water. Adapted with permission from ref [223] Copyright 2014 Royal Society of Chemistry. (**F)** First principle MD simulation of water molecules in CNTPs. The left figure shows water molecules diffusion, which behaves like bulk, in carbon nanotube with 1.5 nm diameter, while the right one presents 1-D molecular ordering of water in 0.8 nm diameter. Adapted with permission from ref [224] Copyright 2017 The American Association for Advancement of Science.

**Impeded liquid transport**

Unlike water flow within hydrophobic confinements, the transport of water through hydrophilic nanoconduits is slower than the theoretical predictions from classical flow rate equations. The electro-viscous effects,[125–127] formation of gas nanobubbles,[128,129] liquid/wall interactions and presence of stagnant liquid layer adjacent to the walls[130–136] are the proposed causes for the flow slowdown in nanochannels. The electro-viscous effect is caused by the presence of the electric

double layer near the wall/liquid interface. The electro-viscous effect can increase the apparent dynamic viscosity due to the electro-osmotic counter flow induced by a streaming potential. The interfacial charged properties, such as electric double layers and Stern layer, are also important for ionic transport behavior within nanochannels.[226] However, it has been shown that in nanochannels with a height of less than 200 nm, the contribution of the electro-viscous effect to the apparent viscosity is insignificant.[228] Formation of nanobubbles in front of the advancing meniscus can slow down the imbibition by increasing the viscous resistance, but its effect on capillary flow rate seems negligible in sub-100 nm channels.[129] Hence, the strong liquid/wall affinity *i.e.*, the considerable long-range interactions between liquid molecules and the surface of the walls leads to an apparent increase in the liquid viscosity near the walls that is to blame for the slow flow rate.[229] Kelly *et al.*[230] used reflected differential interference contrast microscopy to visualize the imbibition of isopropanol (IPA) in siliceous 2-D nanochannels. Their observations yielded that IPA permeation into these nanochannels under ambient conditions was consistently at least 5 times slower than the Lucas-Washburn equation prediction. They attributed this slower flow to the formation of a relatively thick quasi-crystalline layer (10-25 nm) near the walls, wherein molecules are strongly organized and structured. As shown schematically in **Fig. 9A**, the velocity profile inside the channels is highly affected by these layers that results in a decrease in overall flow rate. Alibakhshi *et al.*[77] designed a hybrid nanochannel device for precise measurement of water transport through 2-D hydrophilic silica nanochannels. They measured the hydrodynamic resistance against the flow and compared it against the resistance predicted from classical LW equation. The variation in ratio of the actual resistance to the theoretical resistance for different nanochannel heights is shown in **Fig. 9B**; where for larger channels no significant deviation from predictions is observed. However, the difference increases with decreasing channel height and reaches 45% in the case of 7 nm

channels. Formation of a stagnant layer of water (hydration layer) on the silica surface with the thickness up to 7 Å is believed to explain the increased resistance.

Li *et al.*[83] fabricated nanochannels with height of only 8 nm and used high contrast optical microscopy to directly visualize the real-time fluid dynamics of capillary filling for different polar and non-polar liquids through silica nanochannels. **Fig. 9C** shows their obtained data for displacement of the meniscus position by time for filling of hexane, octane and hexadecane as well as the theoretical predictions from modified LW equation. The results indicate that while the filling rate is consistently smaller than predictions from the original LW equation, it still follows the square root relationship suggested by LW equation. In addition, the modified LW was shown to successfully predict the experimental results.

To characterize the overall effect of the liquid/wall interactions on flow rate, an interfacial layer in close proximity of the channel walls can be defined within which the liquid viscosity is greater than the bulk viscosity.[113] Experimental observations confirm the existence of such a layer, as well. For example, Tomo *et al.*[87] reported the formation of super-stable ultra-thin water film on hydrophilized CNT walls observed *via* transition electron microscopy. These films with thicknesses of 1-7 nm, were surprisingly stable even under vacuum conditions. The wall roughness and the strong liquid/wall adhesion were identified as the key parameters for the stability of the ultrathin water films. Recent investigation by Nazari *et al.*[113] provided additional information about the properties of the interfacial layer developed near nanochannel walls such as the layer thickness and liquid viscosity within this layer for different liquids. The results obtained from both experiments and simulations suggested an interfacial viscosity three times larger than its bulk counterpart for both ethanol and IPA. The effective viscosity observed in nanochannels is, in fact,

determined by the contributions from both the interfacial viscosity (applicable to the interfacial region) and bulk viscosity (applicable outside the interfacial region).

The increased viscosity within the interfacial region is primarily due to reorientation and structuring of liquid molecules in response to long-range forces exerted from the walls. Hence, the interfacial viscosity highly depends on liquid/wall affinity as it determines the strength of the interactions. Wu *et al.*[207] also highlighted that water viscosity within interfacial region (0.7 nm thick) strongly depends on the contact angle, since contact angle represents the strength of the liquid/wall interactions. They proposed a linear relationship between the ratio of interfacial viscosity to bulk viscosity and the liquid/wall contact angle; an assumption that was supported by experimental and simulation data from previous studies,[161,210,230–239] as shown in **Fig. 9D**. Shaat and Zhang[229] used a hybrid continuum-molecular mechanics (HCMM) technique to study the variations of viscosity and velocity across nanotubes cross section. As shown in **Fig. 9E**, a clear peak in viscosity profile was observed near the wall. This is because a solid phase of water (ice) with viscosity multiple times higher than the one of bulk water was observed at the first water layer. They calculated the interfacial water viscosity for different values of water/wall interactions strength: the viscosity increased to ~10 times the bulk water viscosity when water/wall interaction strength was increased from 0.1 to 10 kJ/mol. They also demonstrated that velocity profile for water flow in nanotubes is neither parabolic nor plug-like. A study by Wu *et al.*[240] showed that temperature can be used as a stimulus to manipulate liquid fluidity in nanoconfinements. They experimented both hydrophobic and hydrophilic nanopores. The temperature increase appeared to restrain water fluidity in hydrophilic confinements, but it improved water transport by at least four orders of magnitude in hydrophobic confinements. These observations can be explained as the affinity between water and hydrophilic wall strengthens at higher temperatures, whereas an

increase in temperature adversely affects the interactions between water and hydrophobic walls. In fact, interfacial resistance and viscous resistance are the main forces slowing water transport. It is shown argued that interfacial resistance plays the main role in determining the water flow behavior in water/hydrophobic nanopore systems, while the viscous resistance dominates in water/hydrophilic systems.

The electrostatic effects rising from interactions between liquid and charged walls can impact the transport properties, as well. Geng *et al.*[241] used MD simulations to investigate the combined effect of surface charge and wettability on flow in nanoconfinement. They modeled water flow between two oppositely charged solid planar surfaces for different values of surface charge density and solid/liquid interaction energy (wettability). They used a positively charged upper surface and a lower surface with negative charge. As expected, the slip length decreased for larger solid/liquid interaction energies (more wettable surfaces). But, interestingly, at the largest surface charge density, the slip length became nearly independent of the water/solid interaction energy. Increasing the surface charge density also resulted in shrinkage of the slip length and increased molecular structuring near the walls. However, the impacts from positively and negatively charged surfaces on water structuring within the interfacial layer and slip length was different: at small surface charge densities, the positively charged surface induces less ordering structure and larger slip than that by the negatively charged surface; whereas, for large surface charge densities, the opposite correlation was observed. These differences can also be seen in **Fig. 9F**, a representative density profile of water under different surface charge densities and water/solid wettabilities. Note that the first peak in density profiles near the walls is closely related to the magnitude of slip length; it also, increases for larger surface densities.

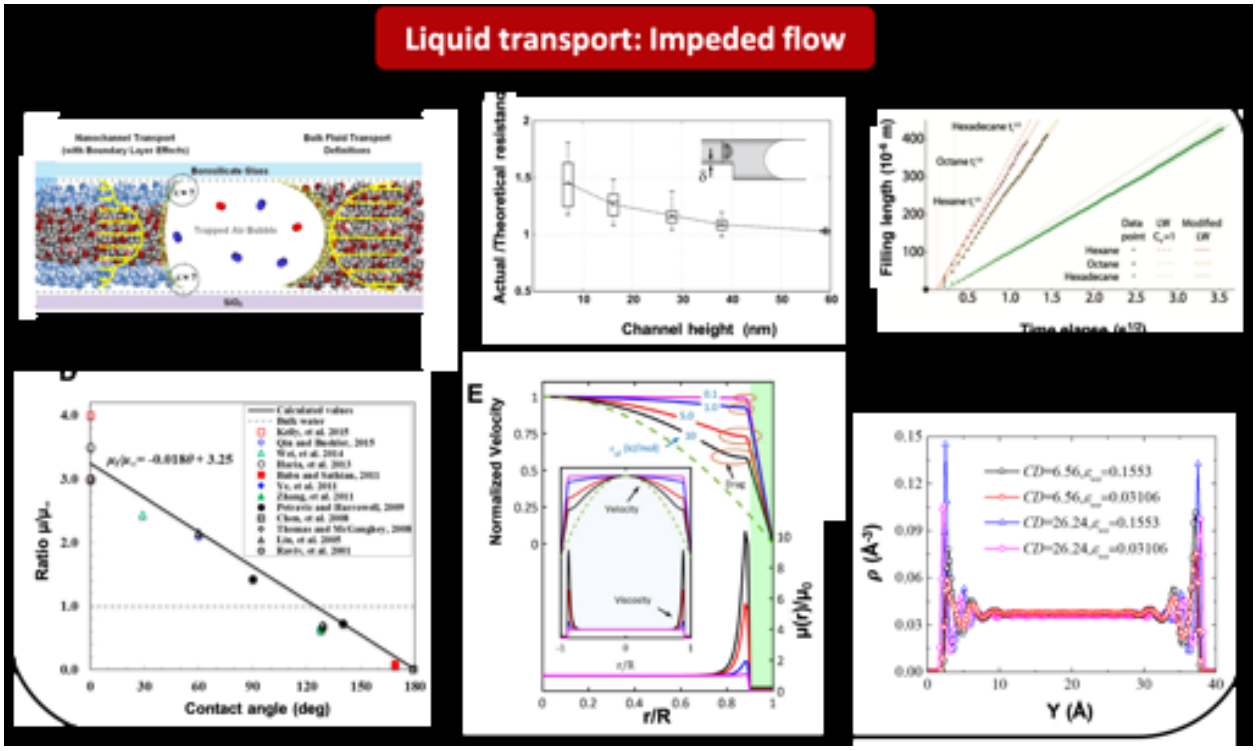


**Figure 9.** Flow inhibition in nanoconfinement arises from high strength of liquid-wall interactions. (**A)** Organic liquid (IPA) transport in nanochannels deviates from bulk due to nucleation of structured boundary layer and increased viscosity. Reproduced with permission from ref [230] Copyright 2015 American Chemical Society. (**B)** The ratio of the actual flow resistance in silica nanochannels to theoretical resistance as a function of channels height is shown. The rise of flow resistance at the nanoconfinement is attributed to the formation of immobile water layer on the channel wall. Adapted with permission from ref [77] Copyright 2016 Springer Nature. (**C)** Capillary filling of polar and non-polar liquids in sub-10 nm channels indicate deviation from classic Lucas–Washburn equation. Adapted with permission from ref [83] Copyright 2008 Royal Society of Chemistry. (**D)** Interfacial viscosity of water increases as contact angle reduces. In fact, strong affinity between liquid and wall (smaller contact angle) causes dense hydrogen bonding network and ordered structure in the interfacial region resulting in increased viscosity. Adapted with permission from ref [227] Copyright 2016 Society of Petroleum Engineers. (**E)** Velocity profile

and distribution of water viscosity within 5 nm nanotubes for various water-wall interaction is shown. Adapted from ref [229] Copyright 2019 Springer Nature. (**F)** The density profile of water flowing between two walls with oppositely charged surfaces. Adapted from ref [241] Copyright 2019 Springer Nature.

## Gas transport

Gas transport through nanoconfinement is a of great significance in nature and technology and emerges in a variety of applications *e.g.*, gas filtration in chemical plants and natural gas extraction from nonporous shale rocks, where gas molecules have to transport through tight spaces. At sufficiently small confinements, the mean free path of gas molecules becomes larger than the channel dimension and molecular flow regime controls the transport. Knudsen theory provides a universal description for this regime, in which gas molecules predominantly collide with confining walls rather than one another. This classical theory is based on diffuse reflection *i.e.*, it assumes that gas molecules rebound from confining walls in all directions with random angles. However, several studies have revealed that gas flow rates through CNTs and graphene membranes exceed the Knudsen theory limit.[21,152] For instance, K. Holt *et al.*[152] reported gas fluxes through vertically aligned CNT membranes that are one to two order of magnitude greater than those predicted by Knudsen theory. The observed gas flow rates through CNT-based membranes were also several orders of magnitude larger than those in commercial polycarbonate membranes, despite having pore sizes an order of magnitude smaller. This flow rate increase can be attributed to the intrinsic smoothness of the graphitic surfaces. Indeed, surface smoothness significantly affects the gas/wall collisions. Under atomically smooth surface condition, the angle of incidence of gas molecules to the surface is the same as the angle of reflection, and thus gas molecules experience specular reflection from the channel walls rather than diffusion reflection. Consequently, the enhanced flow

in graphitic nanoconduits can be attributed to the combination of specular and diffusion reflections. Notably, in the case of pure specular reflection at the gas/wall interface, a frictionless gas transport through the channels can take place.[152] A specular reflection dominant collision can be achieved by making the wall surfaces extremely flat. Keerthi *et al.*[95] achieved complete specular reflection in nanochannels made by van der Waals assembly of 2-D materials.[95] Exfoliated graphite, h-BN and $MoS_2$ with thicknesses of about a single layer of atoms are common 2-D materials that have been utilized to fabricate sub-nanometer scale channels with atomically flat surfaces. Investigations have shown that the transport of low-pressure helium gas through graphite or h-BN nanochannels enjoys a ten to several hundred-time enhancement in flow rate compared to Knudsen theory predictions (see the enhancement factors shown in **Fig. 10A**). It is also found that the gas permeability of graphite nanochannels is independent of channels length *i.e.*, no momentum loss happens for gas molecules, confirming the frictionless gas transport through the channels. In contrast to h-BN and graphite nanochannels, the gas permeability through channels made by $MoS_2$ follows the Knudsen theory predictions (diffusion reflection). The observed dissimilar gas transport behavior in channels with identical geometry but different materials arises from differences in their surface roughness. In other words, the $MoS_2$ surface is rougher than graphite and therefore, specular reflection of gas molecules cannot take place in the $MoS_2$ nanochannels. This can be seen in **Fig. 10A** that compares the intrinsic roughness of graphene and $MoS_2$ (grey curves). Keerthi *et al.*[95] also investigated the dependence of gas permeability on the channels size for frictionless channels *i.e.*, h-BN and graphene-based conduits. Interestingly, the results showed a less significant increase in flow rates for larger channels. The authors explained this observation by referring to the increased surface roughness of larger channels due to the adsorbed hydrocarbon molecules on their walls. However, the wall surfaces in smaller channels remain smooth as they

are protected from adsorption of the large hydrocarbon molecules due to their smaller "capture zone".

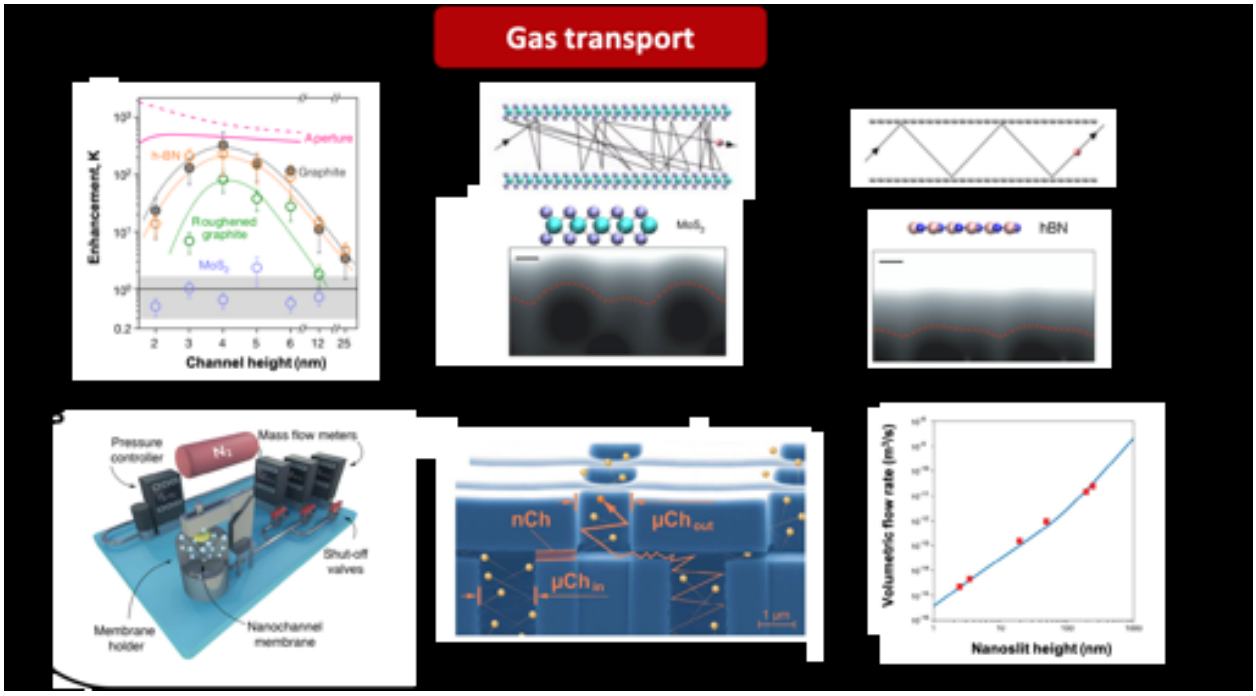


**Figure 10.** (**A**) Enhancement factor of gas flow inside the atomically smooth nanochannels made of 2-D materials as a function of channel height. Adapted with permission from ref [95] Copyright 2018 Springer Nature. The significant higher flux in h-BN nanochannels compared to $MoS_2$ arises from its atomically smooth surface which leads to ballistic transport. (**B**) Schematic of the mass flow measurement set-up, nanofluidic membrane system and volumetric gas flow as a function of nanochannel heights. Reproduced with permission from ref [242] Copyright 2018 American Chemical Society.

The mean free path of gas molecules, which is affected by particle/particle and particle/wall collisions, strongly depends on geometry of the confinement. Although a variety of applied materials such as CNTs and Zeolites have been utilized to study the gas flow at nanoscale

confinement, advanced nanofluidic structures are needed to precisely characterize the effect of geometry and size of the conduit on the gas transport. Scorrano *et al.*[242] investigated the gas flow through a controllable nanofluidic structure fabricated *via* sacrificial layer method. The researchers employed physical vapor deposition to fabricate channels with precise dimensions and heights as small as 2.5 nm by adjusting the thickness of the sacrificial layer (Tungsten film). As shown in **Fig. 10B**, the structure of the fluidics device is arranged in form of a membrane where rectangular shape nanochannels are connected to the membrane inlet and outlet through microchannels. The authors measured gas flow rate across the membrane using the experimental setup shown in **Fig. 10B** and carried out finite element simulations to verify that the parallel sets of nanochannels control the gas flow within the membrane rather than the array of microchannels. In addition, they developed a numerical model to calculate the geometry-dependent mean free path of gas molecules and predicted the volumetric gas flow rate within nanochannels of various heights (ranging from 2.5 to 250 nm) that was in close agreement with their experimental results.

## Ion transport

Ion transport can be a critical component in a considerable portion of applications associated with nanochannels; hence, understanding its potential contributions is of great importance. Electrostatic forces *e.g.*, the surface charges play the major role in ion transport phenomena. A fundamental concept of electrostatic contribution in ion transport is explained in the context of EDL which is defined as the region where the surface charge is balanced by the opposite ion cloud.[243] The EDL width is denoted by Debby length and is inversely proportional to the ionic concentration of the confined solvent.[244] At low ionic concentrations, Debye length becomes comparable to the nanometer dimension of the confinement and as a result, surface charge will

control the ion transport. Surface-charged governed regime of ion transport mostly happens in hydrophilic nanochannels, such as silicon or glass, where the surface is negatively charged. Vermesh *et al.*[245] investigated the transport of potassium chloride (KCl) solution through hydrophilic silica nanochannels, where the solution concentration was sufficiently small for Debye length to exceed the channel height. They demonstrated that during the surface-charged governed regime, there is a threshold voltage beyond which sharp and non-linear enhancement of ion transport occurs, **Fig. 11A**. This non-linear behavior arises from the variation in the ionic characteristic transport in EDL: the electric field overcomes the attractive electrostatic force between the cations and the negatively charged surface causing the movement of cations along the surface. The motion of ions pulls water on the surface and leads to breakdown of the zero-slip boundary condition. Therefore, a promising method to enhance ion transport properties in nanofluidic systems is triggering water slippage over the surface which can be achieved either by applying electric field or utilizing hydrophobic surfaces. Xie *et al.*[246] studied the effect of liquid/wall affinity in ion transport enhancement by comparing the ion transport in silica (hydrophilic) and graphene coated (hydrophobic) nanochannels with the same geometry. Graphene nanochannels were developed through wet transfer of monolayer graphene onto silica nanochannels followed by glass anodic bonding, where three sides of the channels were covered with graphene. They reported that the graphene channels exhibit higher ionic conductance than silica nanochannels in the surface-charged-governed regime, although the difference fades at high ionic concentration, **Fig 11B**. The enhanced ionic conductance of graphene nanochannels at low ionic concentration should be attributed to improved electro-kinetic transport of ions. In other words, the higher surface charge and the large slip length on graphene surface leads to higher ionic conductance compared to silica. Jung *et al.*[247] studied the effect of ionic concentration on ion

transport properties in graphene and silica nanochannels in channels with different heights (3.6, 10 and 50 nm). Analogous to the previous study, the graphene nanochannels demonstrated faster ion transport compared to silica nanochannels specially at low ionic concentrations, **Fig. 11C**. That is because at low ionic concentrations, the surface-charged regime which is strongly affected by flow slippage becomes the dominant mechanism of ion transport in nanochannels, resulting in enhanced ion transport in graphene nanochannels with significantly larger slip lengths compared to silica. In addition, the highest flow enhancement factor obtained at low ionic concentration was observed for the smallest channel (3.6 nm height). This observation can be also explained in the context of surface-charged-governed regime; as the channel height decreases, there is a higher chance for the EDLs extending from different walls to overlap and make surface-charge regime dominant across the entire channel.

Esfandiar *et al.*[61] studied ion transport through angstrom-scale slits with atomically flat surfaces. Three types of channels were fabricated by mechanical exfoliation: crystals of graphite, h-BN or $MoS_2$ were placed on top of each other, separated by stripes of bilayer graphite or monolayer $MoS_2$. Analysis of the surface charge of the fabricated channels indicated surface charge densities that were three to four orders of magnitude smaller than typical those reported for CNT, h-BN and silica nanopores; a special feature that enabled the authors to investigate the role of more subtle phenomena such as steric effects, precisely. It was found that ions with hydrated diameters larger than the slit size can still permeate through the channels. They also reported that in graphene and h-BN slits, anions have lower mobility compared to cations of the same size; primarily due to their stronger interactions with the walls. **Fig. 11D** compares the conductance of slit devices made from graphite, h-BN, and $MoS_2$, separated by graphene spacers. It can be seen that the models for all three different walls converge at higher salt concentrations.

The role of hydrophobic walls in fast ion transport was further underscored by Jung *et al.*[247] who realized that for a deionized water solution under electric field, a 3.6 nm high graphene nanochannel conducts ions up to 115 times faster than a nanochannel without graphene. To cover all channel walls with graphene, they developed a graphene-based nanochannel fabrication technique: graphene was transferred onto both glass and nanochannel-patterned silica/Si substrates and was bonded using physical pressure, high temperature, and voltage under a vacuum of 10 mTorr, as shown schematically in **Fig. 11E**. They measured the ionic conductance for channels with heights varying from 3.6 nm to 50 nm and solutions with 0 to 0.2 M concentration of NaCl. **Fig. 11E** shows that nanochannels with larger heights and/or solutions with higher salt concentrations lead to greater ionic currents. The enhancement factor *i.e.*, the ratio of the ionic conductance of graphene nanochannels to the bare silica nanochannels hit its maximum of 113 for 3.6 nm channels, but it decreased to much smaller values of 5.12 and 1.4 for channels with heights of 10 and 50 nm, respectively. The considerable change in ion conductivity observed for the small nanochannels can be attributed to the highly enhanced electroosmotic ion transport in these ultra-small hydrophobic graphene nanochannels.

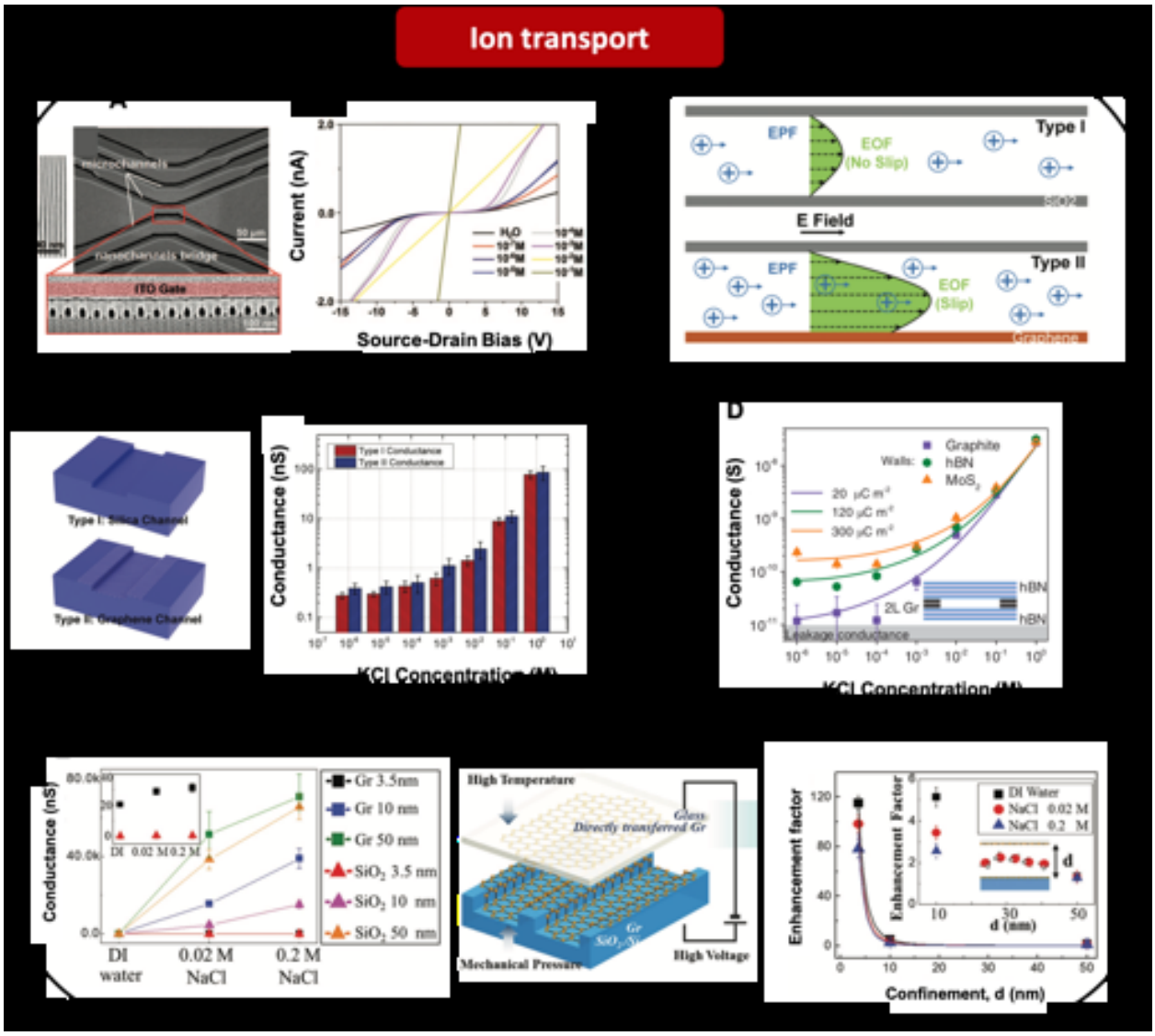


**Figure 11.** Ion transport in nanochannels. (**A)** Exploring ion transport within 20 nm hydrophilic ($SiO_2$) nanochannels. Non-linear ion transport at the surface charged regime happens due to break-down of zero-slip condition caused by high applied voltage. Reproduced with permission from ref [245] Copyright 2009 American Chemical Society. (**B)** Physics of ion transport in hydrophilic and hydrophobic nanoconduits. Adapted with permission from ref [246] Copyright 2008 Royal Society of Chemistry. (**C)** Comparison of ionic conductance in Silica and graphene nanochannels. Adapted with permission from ref [246] Copyright 2008 Royal Society of Chemistry. **(D)** Ionic conductance

dependence of ultra-small nanoconfinements made by assembling of 2-D materials on KCl concentration. Adapted with permission from ref [61] Copyright 2017 The American Association for Advancement of Science. (**E)** Ionic conductance of fully covered (all four channels wall) graphene nanochannels and Silica nanochannels as a function of concentration. Adapted with permission from ref [247] Copyright 2017 John Wiley and Sons.

Ion transport properties of channels can change when the dimension of the fluidics system approaches the size of fluid molecules and ions. Here, we highlight some important characteristic of ion transport in the context of channel size. As discussed earlier, the dominant mechanism of ion transport in nanochannels depends on the ionic concentration of the solvent. At high ionic concentrations, nanochannels geometry and bulk ionic concentration control the conductance regime. However, at low ionic concentration, the transport characteristic is mainly determined by the surface charges. Since, the surface of hydrophilic nanochannels such as Si or glass, are negatively charged, an approximately 1 nm thick hydration layer typically forms adjacent to the wall surface. In other words, water molecules bond to hydrophilic channel surfaces *via* hydrogen bonding. Water molecules within the hydration layer assume an organized structure enforced by hydrogen bonding network.[123] This network of hydrogen bonded water molecules can induce extremely high proton mobility originating from proton hopping (or diffusion of protons), also known as Grotthuss mechanism.[248] Duan *et al.*[226] studied the ion transport in hydrophilic nanochannels with a height of 2 nm where the two hydration layers overlapped. The results indicated high proton mobility due to Grotthuss mechanism. The silicon nanochannels were fabricated through standard photolithography and reactive ion etching and sealed with glass on top *via* anodic bonding. They explored the ionic conductance in the nanochannels for several solutions,

including sodium chloride (NaCl), potassium chloride (KCl) and hydrochloric acid (HCl), under the surface charge-governed regime. The critical ionic concentration below which surface charge governs the ion transport process, was determined as 100 mM for nanochannels with a height of 2 nm. The results indicated that at very low ion concentration (*i.e.* 0.1 mM), the conductances of all solutions are very close to one another and similar to DI water, implying that in all solutions, proton is the dominant cation in driving the ion transport. The ratio of proton mobility in 2 nm deep nanochannels to the corresponding bulk values shows a four-fold enhancement at low concentrations, **Fig. 12A**. In addition, the ion mobility in 2 nm deep nanochannels was faster than that in 25 nm deep nanochannels. These differences in ion mobility can be attributed to the confinement induced structuring and the consequent formation of one-dimensional ordered water chains inside the 2 nm deep channels. Hence, the liquid structuring phenomenon appears to enhance ion transport in nanochannels. However, more investigation of this phenomenon and its impacts on proton transport properties in hydrophobic nanoconfined geometries is still required. In fact, all the detail information about the structure-enhanced properties of confined water is presented based on molecular dynamics simulations, and direct observation and experimental studies are lacking. Recently, advancements in synthetic techniques have led to development of materials such as metal-organic frameworks (MOFs) which can form hydrophilic/hydrophobic nanochannels in their structure. The most important aspects of this material are the richness in structural degrees of freedom and the relative ease of structural characterization. Therefore, crystallographic techniques, such as XRD, can be utilized to characterize the structure of water confined in MOF-based nanochannels, and thus provide direct information about it.

In addition to inorganic solutions, the transport of organic anions and cations is also important due to their significant role in drug delivery applications of nanofluidic systems. In a systematic

study, Bruno *et al.*[249] investigated the transport of charged and neutral organic molecules through silicon nanochannels, **Fig. 12E** . An unexpected transport regime took place in which the neutral molecules behaved similar to charged molecules. In other words, in this regime all molecules seem to have either actual or effective electric charge which happens due to the emergence of the surface tension role at such small scale. They also demonstrated that by decreasing the channel height to sub-10 nm, the transport of all type of molecules undergoes a dramatic slowdown, regardless of their electric charge. Nevertheless, this behavior is complicated and cannot be explained by the existing theories such as electrostatic, hard sphere, and hydrodynamic interactions.

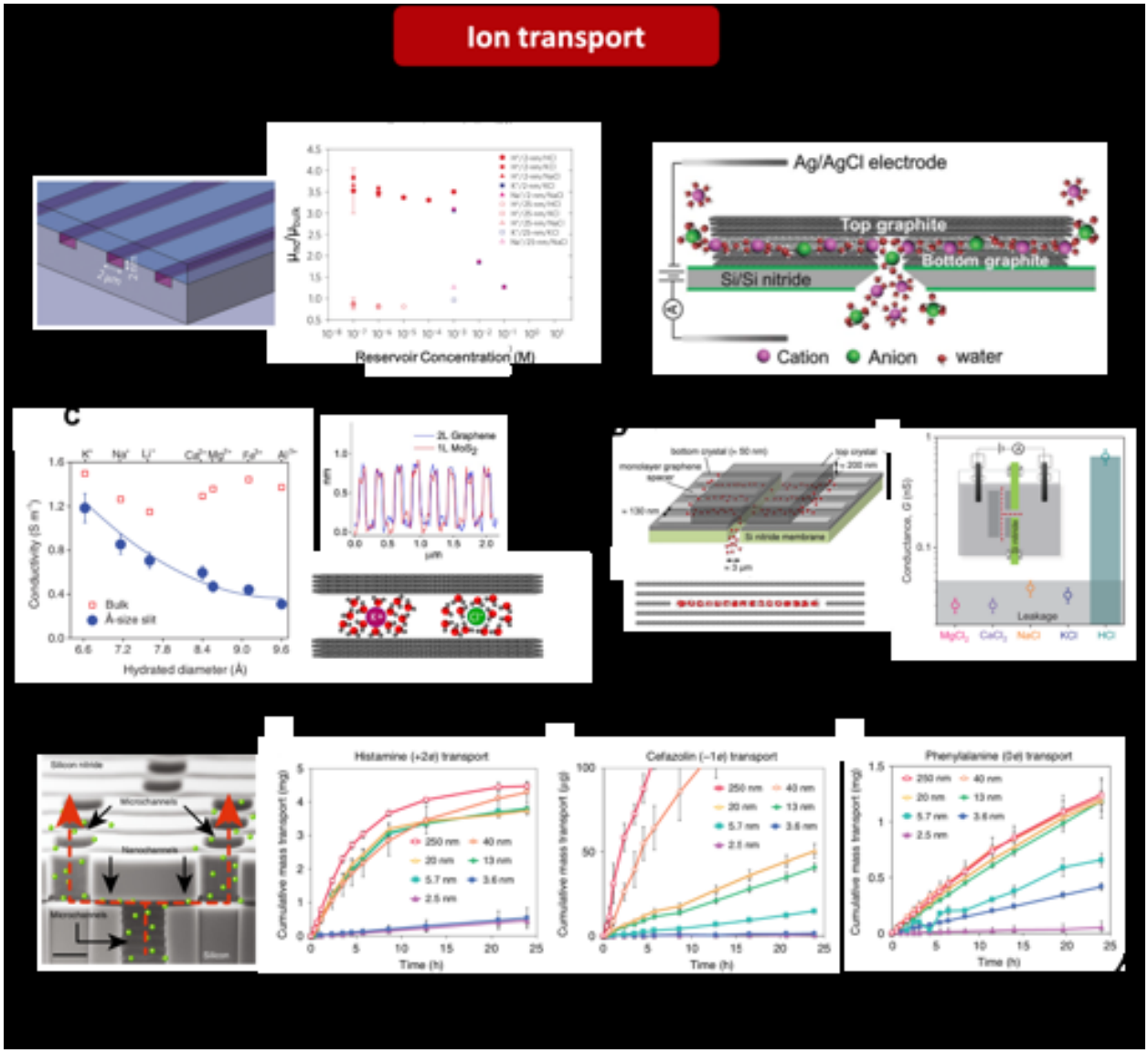


**Figure 12.** Ion transport in nanochannels**. (A)** Dependence of ionic mobility in 2 nm silica nanochannels on reservoir concentration. Adapted with permission from ref [226] Copyright 2010 Springer Nature. **(B)** Schematic of ion transport under angstrom-scale channels made by van der Waals assembling of 2-D materials. Adapted with permission from ref [61] Copyright 2017 The American Association for Advancement of Science. **(C)** Ionic conductivity in sub-nanometer channels as a function of hydrated diameter, height profile of the bilayer graphene spacers, and schematic of water molecules surrounding anions and cations in narrow slits. Adapted with permission from ref [61] Copyright 2017 The American Association for Advancement of Science.

(**D)** Schematic of the nanofluidic device which has the cavity space for only one monolayer of water (shown by molecular simulation) and its ionic conductance for different solutions. Adapted with permission from ref [63] Copyright 2019 The American Association for Advancement of Science. (**E)** SEM image of nanochannels membrane used to study ionic and molecular passage and the corresponding results for neutral, positively and negatively charged species. Adapted from ref [249] Copyright 2018 Springer Nature.

To better understand the physics of ion transport at sub-10 nm scale, one can go even further to angstrom-size dimensions where the channel size is comparable with the hydration diameter of ions. The nanochannels with atomically smooth walls fabricated by van der Waals assembly of 2-D materials *e.g.*, graphene and h-BN, provide such ultra-small confinements with heights of 6.6-6.7 Å,[61] as shown in **Fig. 12B**. The confinements fabricated from mechanically exfoliated 2-D materials exhibited three to four order of magnitude smaller surface charge density compared to those reported for silica and even CNTs. The small value of surface charge for these channels is due to their extremely clean surfaces and the absence of any surface defects. Consequently, these channels can operate as geometrical confinements while having the slightest chemical interaction with the ions. To explore the steric exclusion of angstrom-size channels, several chloride solutions with cation hydration diameter in the range of 6.6-12.5 Å were examined. As shown in **Fig. 12C**, all cations were able to transport through the channels, although the hydration diameters of cations exceeded the channel height. In fact, this is possible since under such strong confinements, ions do not act as hard spheres, but instead flatten their hydration shells and penetrate these small channels. Therefore, the steric rejection of ions can be avoided to some extent despite the hydrate diameters of ions being larger than the channel height. Nevertheless, further reduction in channel height can bring ion permeation to a complete halt. Gopinadhan *et al.*[63] reported a complete

blocking of ions in capillaries made with the same technique as in Esfandiar's work[61] but with a height close to the thickness of only one atomic plane of 2-D materials (ca. 3.4 Å). This extremely small dimension of the confinement is almost half the size of the smallest hydrated ions while still larger than effective size of water molecules (2.6 Å). The ion conductance measurement for various chloride solutions in 1M concentration showed that in contrast to the channels with a height of 6.7 Å, no conductance was observed for any of the salts in these sub-nanometer scale channel (**Fig. 12-D**).[61] Thus, it can be concluded that the steric exclusion of ions can be suppressed as long as the confinement dimensions remain larger than at least half the size of the hydrated ion diameter. On the downside, it also implies that geometrical confinement is unlikely to provide satisfactory selectivity between small ions and additional considerations such as electrically charging the channels may be required. It must be noted that while the observations showed no salt conductance through the atomic-size channels, ion transport took place when HCl was used, as can be seen in **Fig. 12-D**. In fact, in this case the protons did not diffuse through the channels in form of hydrated ions, but instead, they permeated the capillaries through hopping between the monolayer of hydrogen-bonded water molecules excising there, as indicated in Grotthuss mechanism.

**Gating behavior**

Gating is another important phenomenon that plays a critical role in different natural and industrial applications *e.g.*, molecular and ionic fluxes for metabolic and signaling purposes, semi-conductor industry *etc.* A variety of smart gating membranes inspired by biological channels, has been developed.[250–255] While these synthetic membranes have similar functionalities, they are made from different material, their activation requires different stimuli, and are designed for different applications. Different stimuli that can trigger the gating mechanism can be categorized

as physical, chemical and physicochemical. Smirnov *et al.*[256] demonstrated an example of application of physical stimulus to induce gating. In their work, they mimicked the functioning of biological voltage-gated channels by applying voltage across membranes with hydrophobic nanopores. In fact, the transition between wetting/non-wetting states in nanopores acts as the switch between open and close modes of the membrane. **Figure 13A**, depicts two possible mechanisms to induce wetting in hydrophobic pores *i.e.*, electrowetting and meniscus overlap. Hou *et al.*[257] designed a liquid-based gating mechanism, where a capillary-stabilized liquid as a reversible, reconfigurable gate that fills and seals pores in the closed state, and creates a non-fouling, liquid-lined pore in the open state (**Fig. 13B**). These types of gates are very versatile and the absolute and relative pressures for gases or liquids to pass through can be tuned by using membranes with different materials and/or pore sizes. The gates feature a combination of differential tunability and reversible opening and closing that enables fast and repeatable control over multiphase flows in both micro/macro-fluidic systems by simply adjusting the system pressure.

Chemical stimuli can be used to trigger gating mechanisms, as well. Cheng *et al.*[23] produced nanochannels with gating capability by controlling the wettability of the inner surface of nanochannels of mesoporous silica nanoparticles, **Fig. 13C**. The nanochannels constitute a biomimetic on demand delivery system analogous to the aquaporins in nature, where the transport of water and ions is controlled by regulating channel wettability, which results from the transition between the intrinsic hydrophobic state and the stimulus-induced hydration state. Xu *et al.*[258] also employed chemical stimulus for gating mechanism activation. They achieved active gating through the self-assembled stimulus-responsive polymeric brushes that were planted inside nanochannels to act as valves, as shown in **Fig. 13D**. In this case, poly(N-isopropylacrylamide)

(PNIPAM) that is a thermo-responsive polymer, *i.e.*, it exhibits a reversible phase transition at its lower critical solution temperature (LCST) was used. When heated above LCST, the hydrated extended PNIPAM chains instantaneously convert into dehydrated compact aggregates. A quick valving performance in respond to temperature change was observed owing to the sharp phase transition temperature of PNIPAM brushes. The results revealed that the nanoscale PNIPAM brushes locally self-assembled in the nanofluidic channels can act as active valves to regulate femtoliter-scale fluids with quickly responding to the external temperature change.

Xie *et al.*[259] designed functionalized hydrophobic nanopores using azobenzene-derivatives-modified polymer and employed light and electric field to control wettability and regulate mass transport. In fact, nanopore surface wetting was adjusted to switch between conducting and non-conducting phases. Mass and ion transport were regulated by applying ultraviolet (UV)/visible light and different voltages. They found a threshold voltage beyond which the hydrophobic Azo-modified nanopores can be wetted by the electrolyte solution *i.e.*, become completely open for transmembrane transport. As shown in **Fig. 13E**, when exposed to visible light, the hydrophilic reaction products cover the hydrophobic surface of the nanopores allowing for transport across the membrane. Xiao *et al.*[260] used electrostatic charge and electric field to trigger gating mechanism for water transport, **Fig. 13F**. They successfully regulated the surface charge density and external electric field through a process involving alternating capillary evaporation and capillary condensation to enable switching between open (conductive) and closed (non-conductive) states.

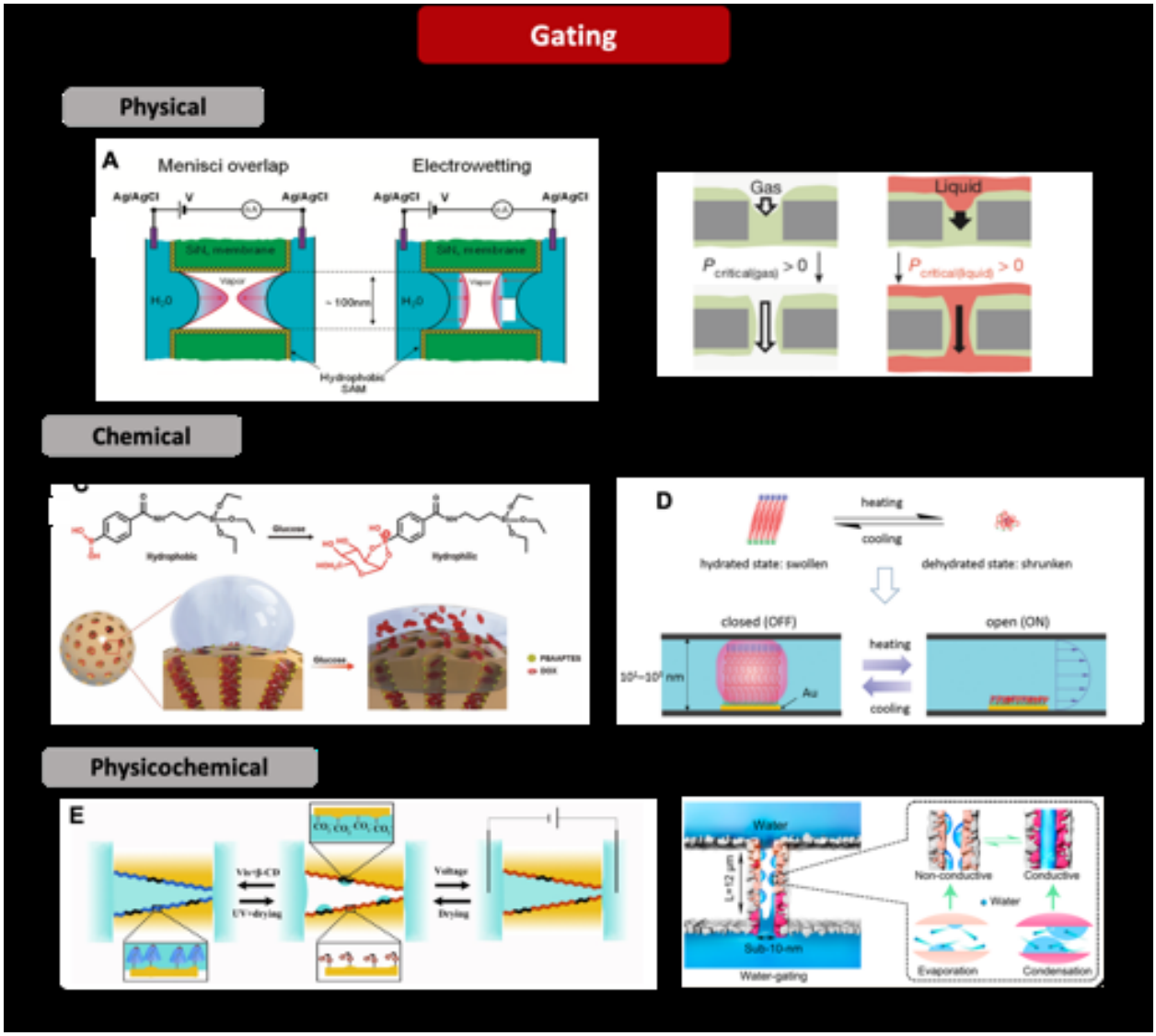


**Figure 13.** Transport of ions and liquid in nanochannels can be controlled by various gating mechanism. Gating behavior in nanochannels is achieved by physical, chemical or physical-chemical regulations. **Physical stimuli: (A)** Transition between wetting and non-wetting state in the hydrophobic nanochannel is achieved by applying a voltage across them. Two possible mechanism of electro-wetting is schematically shown. The left figure depicts the movement of the contact line, while the right one indicates a decrease in the contact angle. Reproduced with permission from ref [256] Copyright 2011 American Chemical Society. **(B)** Demonstration of liquid-based gating channels. The channel is filled with the liquid (green color) in the closed state. To

achieve open state, which enables the transport of other liquids or gases, the pressure of transporting fluid should overcome the capillary pressure at the liquid-gas or liquid-liquid interface. Adapted with permission from ref [257] Copyright 2015 Springer Nature. **Chemical stimuli: (C)** Schematic of changing inner surface wettability of mesoporous silica nanochannels. Reversible conversion of intrinsic hydrophobic state to stimulus-induced hydrophilic state is obtained by regulating surface functional molecules. Adapted with permission from ref [23] Copyright 2012 Royal Society of Chemistry. **(D)** Local flow in nanofluidic channel is controlled by regulation of well-tailored thermoresponsive polymers. Adapted with permission from ref [258] Copyright 2016 John Wiley and Sons. **Physicochemical stimuli:** (**E)** Wetting behavior in hydrophobic nanochannels is controlled by light emission due to photoresponsive molecules existing on the channels surface. In addition, applied electric field across the nanochannel can result in transition from non-conductive to water conductive state. Reproduced with permission from ref [259] Copyright 2018 American Chemical Society. (**F)** The sub-10 nm hydrophobic PET nanochannels is transferred from non-conductive to water conductive state by electrostatic charge variation as well as applied electric field. Reproduced with permission from ref [260] Copyright 2016 American Chemical Society.

As discussed, physical stimuli such as pressure and voltage can be utilized to turn on/off the molecular and ionic transports across nanochannels. Mouterde *et al.*[62] examined ion and water transport inside angstrom-scale channels. In both graphite and h-BN channels, gating effect was observed, albeit with marked material-dependent differences. They developed an experimental setup for ionic current measurement, shown in **Fig. 14A**, in which the voltage across the nanochannels could be controlled *via* a patch-clamp amplifier and the required pressures were applied through a pump connected to a reservoir. This setup allowed for measurement of the

pressure driven component of the ionic current (often referred to it as the streaming current) which provides an indirect measure of water flow under confinement. To explore how the coupling between the pressure-induced current and the electric forces at molecular scales, pressure driven streaming currents were measured under different applied voltage biases. **Fig. 14B** demonstrates the time response of the streaming current when pressure gradient and voltage bias are applied, simultaneously. The data reveal a considerable coupling between pressure and voltage, since the current at a voltage of 50 mV jumps to more than double of its value at zero bias. The crystal structure and atomic flatness of graphene and h-BN are similar and so was the pressure gradient effect on them, where the streaming current changed linearly with pressure for both of them. But a significant difference was observed in their ion mobility properties. **Fig. 14C** shows the normalized ion mobility for graphite and h-BN channels: mobility variations against electric bias in graphite channels follows a quadratic relationship, whereas it is essentially linear for h-BN. The authors argued that the different material response observed in **Fig. 13C** for channels made from h-BN and graphite can be traced back to the difference of molecular friction of water and ions on these two materials.

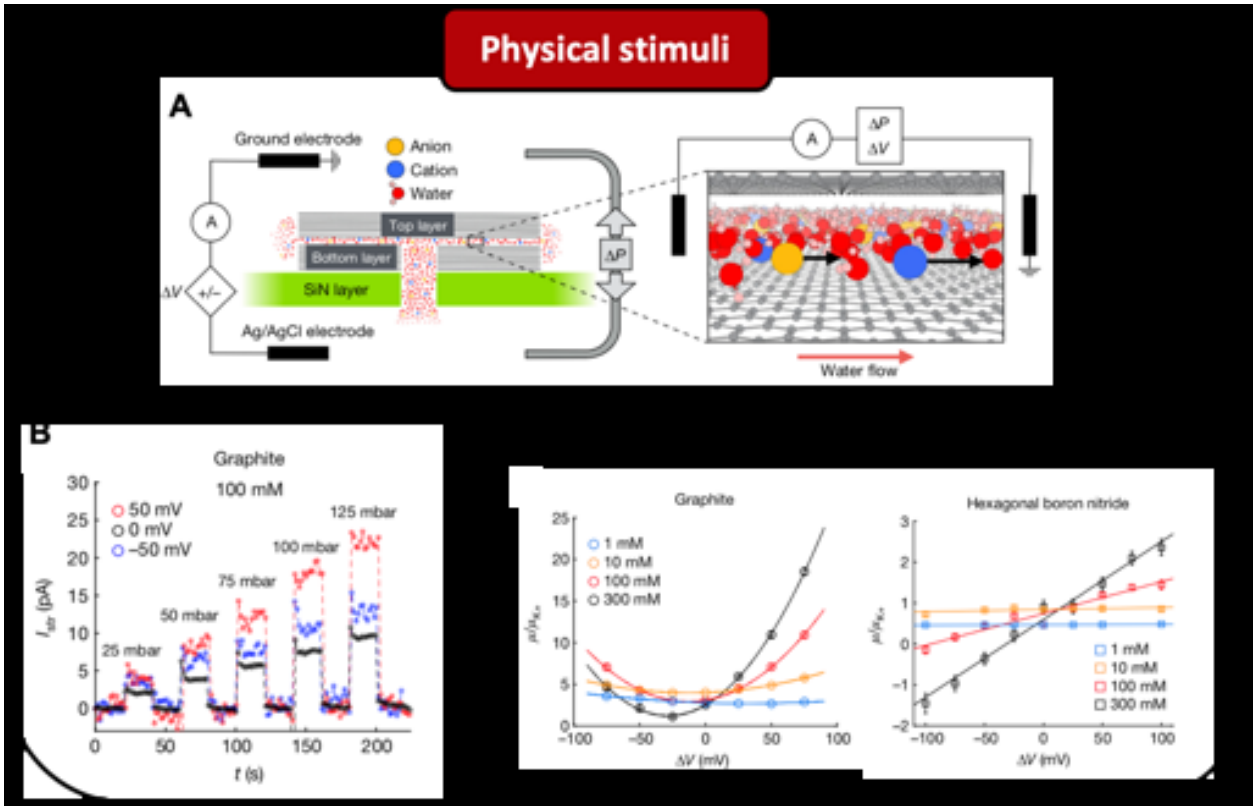


**Figure 14**. (**A)** Schematic of the experimental set-up to explore the gating behavior of angstrom-scale channels with applied pressure and voltage as external stimuli. Adapted with permission from ref [62] Copyright 2019 Springer Nature. **(B)** Pressure and voltage driven current as a function of time clearly demonstrates the gating behavior of those channels. Adapted with permission from ref [62] Copyright 2019 Springer Nature. **(C)** Ion mobility as a function of applied voltage is shown for graphene and h-BN channels. Adapted with permission from ref [62] Copyright 2019 Springer Nature.

**Ionic diodes**

One of the important synthetic nanofluidic structures with asymmetric ion transport properties are the nanofluidic diodes that rectify the ionic current inside nanochannels under oscillating voltage bias. Nanofluidic diodes are essential for a variety of applications including biomimetic energy conversion systems[261–264] and nanofluidic sensing systems.[265,266] The charge selectivity and

preferential transport direction observed in these diodes that results in ionic current control and accumulation/depletion of ions at the junction, is due to the nanochannel height being comparable to the Debye length. Therefore, the channels typically possess at least one length scale with sub-10 nm size. It is argued that ion transport in nanochannels with heights greater than 5 nm is governed by electrostatic forces, while steric interactions and hydration play the main role in ion transport within sub-5 nm channels.[267] The ion rectification that occurs as a result of an enhancement in concentration of counter-ions and a decrease in that of co-ions is observed due to the electrostatic interactions between the ions and the charged channel walls. Hence, high surface charge density along with small critical dimensions of the channel and low ionic concentration of the bulk solution are needed to create a high counter-ion to co-ion ratio and so, play critical roles in operation of ionic diodes. Channels with asymmetric geometry (*e.g.*, conical), channels with asymmetric bath concentration at the opposite ends, or channels with asymmetric surface charge distribution along the walls are most commonly employed to generate a nanofluidic diode,[268] as demonstrated in **Fig. 15A**. Other strategies such as creating a wettability gradient along the channel,[269,270] applying asymmetric metal coating,[271–273] asymmetric surface chemical modification with organic molecules[27,274,275] and inducing pH gradient across the channel[276] have been used to produce ion rectifying channels or enhance the rectification ratio of current diodes, as well. Different studies have demonstrated the application of a conical pore as an ionic diode, where the pore tip size is comparable to the Debye length whereas the tip base can be several hundred nanometers.[277–282] As shown in **Fig. 15B**, these devices show diode-like properties under symmetric electrolyte concentration and can pump ions against concentration gradients when harmonic electric-field oscillation is applied. On the other hand, homogenous channels (with flat parallel walls) can also demonstrate diode-like behavior, provided that a concentration gradient

exists at the opposite ends.[283] In such circumstances, only at one side of the channel (*i.e.* the one with lower electrolyte concentration), the EDLs will overlap (**Fig. 15C**). Hence, the charged walls will differently impact the ions on both sides of the channel and result in ion rectification. Another way for creating channels with diode-like behavior is through asymmetric charge distribution on the walls, for example, by developing a channel with opposite surface charges on either half of it.[284,285] This type of nanofluidic diodes are very similar to bipolar membranes used in electro-chemistry while having much smaller sizes. One of the main challenges for this type of ion diodes is the processing required to generate channels with heterogenous surface charge distribution. Different techniques have been utilized to develop such channels. While most of these techniques rely on surface chemical modifications (*e.g.* diffusion limited pattering, carboxyl/amino groups coating),[285,286] heterogenous channels made from solid oxide material with different isoelectric points can also be used to generate channels with mixed positive and negative surface charges.[287] Nanofluidic diodes can also be prepared in a protein ion channel such as bacteria porins.[288,289] Sub-nanometer size CNT porins are yet another candidate for ionic diode development. It has been shown that these extremely small channels completely block anion transport even at salinities that exceed seawater levels.[224] Additionally, their ion selectivity can be tuned to configure them into switchable ionic diodes.

The rectification ratio of the discussed nanofluidic diodes are constant and depend on their geometry and charge distribution *etc.* and cannot be altered once the device is fabricated. However, nanofluidic diodes with tunable rectification degree have been developed, as well; where external chemical stimuli such as pH,[288,290,291] enzymes[292] and polyvalent cations[293] are typically used for ionic flow regulation. Nonetheless, Guan *et al.*[294] developed a reconfigurable ionic diode with a single asymmetrically placed gate or dual-split gate on top of the nanochannel that can modulate

the predefined ionic properties without introducing any external chemical stimuli. The schematic and the obtained results plotted in **Fig. 15D**, show that the linear I-V curve of the nanofluidic device can switch to one with diode-like behavior simply by moving the gate voltage.

The same technology utilized for nanofluidic diodes can be further expanded to generate nanofluidic triodes composed of two nanofluidic diodes and a npn diac that can be used as a switch to regulate the ion flow with very large rectification factors.[287]

In addition to ion diodes that can be used for electric current control, fluid flow can also be controlled through nanofluidic devices such as osmotic diodes.[295] Picallo *et al.*[295] demonstrated that asymmetric charge distribution on nanochannel walls leads to nonlinear coupling between water flow and ion dynamics and enables water flow rectification; where the reversal of the osmotic driving force generates diode-like behavior in such nanofluidic systems, **Fig. 15E**. In fact, the osmotic pressure was found to be a nonlinear function of salt concentration difference and voltage drop across the nanochannel, leading to rectified osmotic response. Similar electro-osmosis rectifying effect can be achieved by using asymmetric (conical) nanochannels.[296] An important feature of such devices is that the rectifying character of the diode allows for water flow against the osmotic gradient under an oscillating electric field.

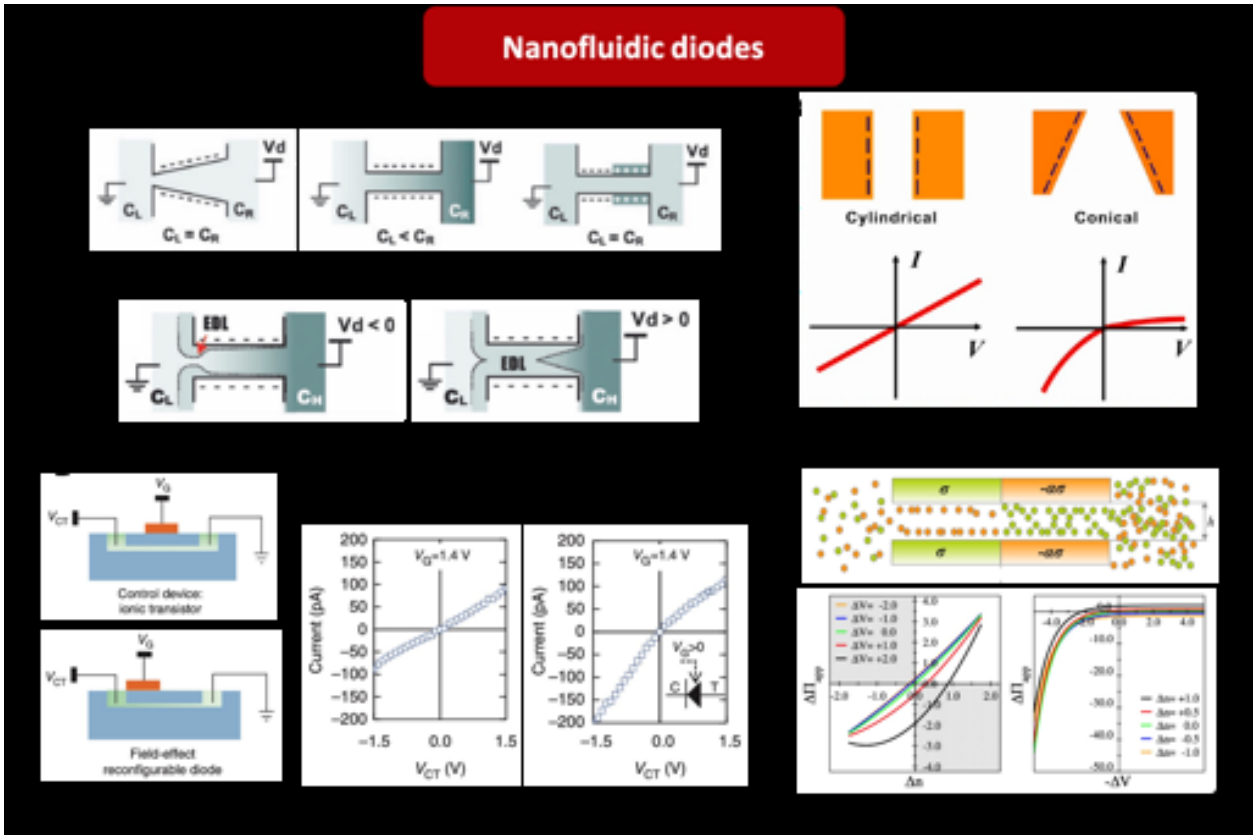


**Fig. 15. (A)** Schematic of three main configurations for nanofluidic ionic diode development. Adapted with permission from ref [268] Copyright 2010 Royal Society of Chemistry. **(B)** A simple way to achieve diode-like behavior is to use conical channels: the linear I-V curve for homogenous channels shows no signs of ion rectification while diode-like behavior in conical channel is clear. Reproduced with permission from ref [297] Copyright 2013 American Chemical Society. **(C)** The formation of a thicker EDL layer at the low concentration end of the nanochannels; the EDLs may or may not overlap depending on the concentration, voltage bias and channel height. Reproduced with permission from ref [283] Copyright 2007 American Chemical Society. **(D)** Schematics of reconfigurable nanofluidic device that switches between transistor state and diode state and corresponding I-V curves, where an apparent gate voltage-controlled rectifying effect demonstrates the diode-like behavior. Adapted with permission from ref [294] Copyright 2011 Springer Nature. **(E)** Sketch of a nanochannel with asymmetric surface charge and different salt

concentrations in the left and right reservoirs leading to development of nanofluidic osmotic diode and plots of variation in osmotic pressure build-up *versus* salinity gradient and applied voltage. Adapted with permission from ref [295] Copyright 2013 American Physical Society.

## Fabrication

### Silicon/glass-based materials

Nanochannels are the core component in many nanofluidic devices and their fabrication is of great importance as it directly impacts the operation of the system. The methods for fabrication of nanochannels are strongly material-dependent and a universal method cannot be envisioned. Initially, nanochannels were mostly made from silicon using the well-established fabrication techniques for microelectronics devices. In the past years, different techniques compatible with glass (fused-silica glass) substrate were developed for nanochannels fabrication.[298–303] Since then, glass has become one of the most promising materials for development of nanofluidic devices, mainly due to its superior optical transparency, thermal stability, chemical/biological inertness, mechanical robustness and hydrophilic nature that are of great interest in chemical and biological applications.

The standard procedure for fabrication of silicon-based nanochannels with planar walls is straightforward. Typically, a thick silica layer is deposited through plasma enhanced chemical vapor deposition (PECVD), then photoresist film and HF etching along with standard photolithography techniques are used to define the desired nanochannel pattern. Once the nanochannel bases are complete and cleaned, anodic bonding is used to attach the top wall of the channels. Additional steps may be incorporated for specific purposes; for example, Li *et al.*[83]

deposited a layer of $Si_3N_4$ on the original silicon wafer to enhance the visualization of liquids in sub-10 nm high channels, **Fig. 16A**.

Nam *et al.*[304] proposed a 1-D patterning technology for nanofabrication purposes. In this technique, controlled propagation of a crack initiated with a simple manually generated indentation creates the channels. Besides its simplicity, this method also obviates the need for sophisticated equipment and required experimental environment that is necessary for the standard technique, such as high vacuum, clean room *etc.* The platform required for nanochannel fabrication is prepared by depositing a layer of $Si_3N_4$ on a single crystal silicon wafer. The crack initiated in the substrate by using an indenter, has a tendency to grow in a specific direction (<100> direction, as shown in **Fig. 16B**) due to the crystallographic anisotropy of the substrate. The crack is arrested either by an encounter with a discontinuity in the film or through the interposition of a crack-stop structure. The width of the crack and its propagation speed can be adjusted by changing the thickness of the $Si_3N_4$ layer; thicker films result in wider cracks and higher growth rates. This technique can produce channels with dimensions as small as 10 nm.

Wong *et al.*[305] introduced a self-sealing technique for fabrication of glass-based nanotubes. It can provide channels with circular cross-sections and diameters ranging from 30 to 2000 nm. First, a thick layer of silicate glass (USG) was PECVD deposited on a silicon wafer. Standard deep UV lithography was used to pattern trenches on the USG film that were subsequently ion etched. Nonconformal phospho silicate glass (PSG) or BPSG deposition by low pressure PECVD was used to create self-sealing nano/microchannels with triangular cross-sectional areas within the oxide trenches. A glass substrate was anodically bonded to complete the channels. A thermal reflow process was carried out during which the molten PSG squeezes into the voids. The softened PSG, also, rounds up its sharp features and minimizes its surface energy by transforming to a

circular cross-section and creating a smooth and curved interface. A schematic representation of this procedure is presented in **Fig. 16C**.

Xu and Matsumoto[306] employed focused ion beam (FIB) technology to fabricate nanochannels with high aspect ratios and nanopillar array nanochannels in fused silica substrates. Prior to milling with FIB, a thin layer of gold was deposited onto the (insulating) fused silica substrate to avoid charge accumulation on the surface during the process (**Fig. 16D**). Scanning the FIB over the substrate, channels with different heights could be obtained depending on the dwell time of the beam. In addition to dwell time, ion beam parameters such as aperture size, beam diameter, beam current, and current density are critical parameters to generate high aspect ratio channels in fused silica. The method would be especially useful for developing integrated nanofluidic devices with high throughput.

Despite its advantages, the high costs of glass substrates in addition to the expensive nanofabrication technologies required for development of glass-based nanochannels such as e-beam lithography, plasma dry etching, focused ion beam lithography and many other delicate, sophisticated, and time-consuming processes conducted in high-class clean rooms, restrict the application of glass-based nanofluidic devices to only a few research groups. Therefore, there is an urgent need for alternative materials and methods for fast, efficient and economical fabrication of nanochannels for nanofluidic systems.

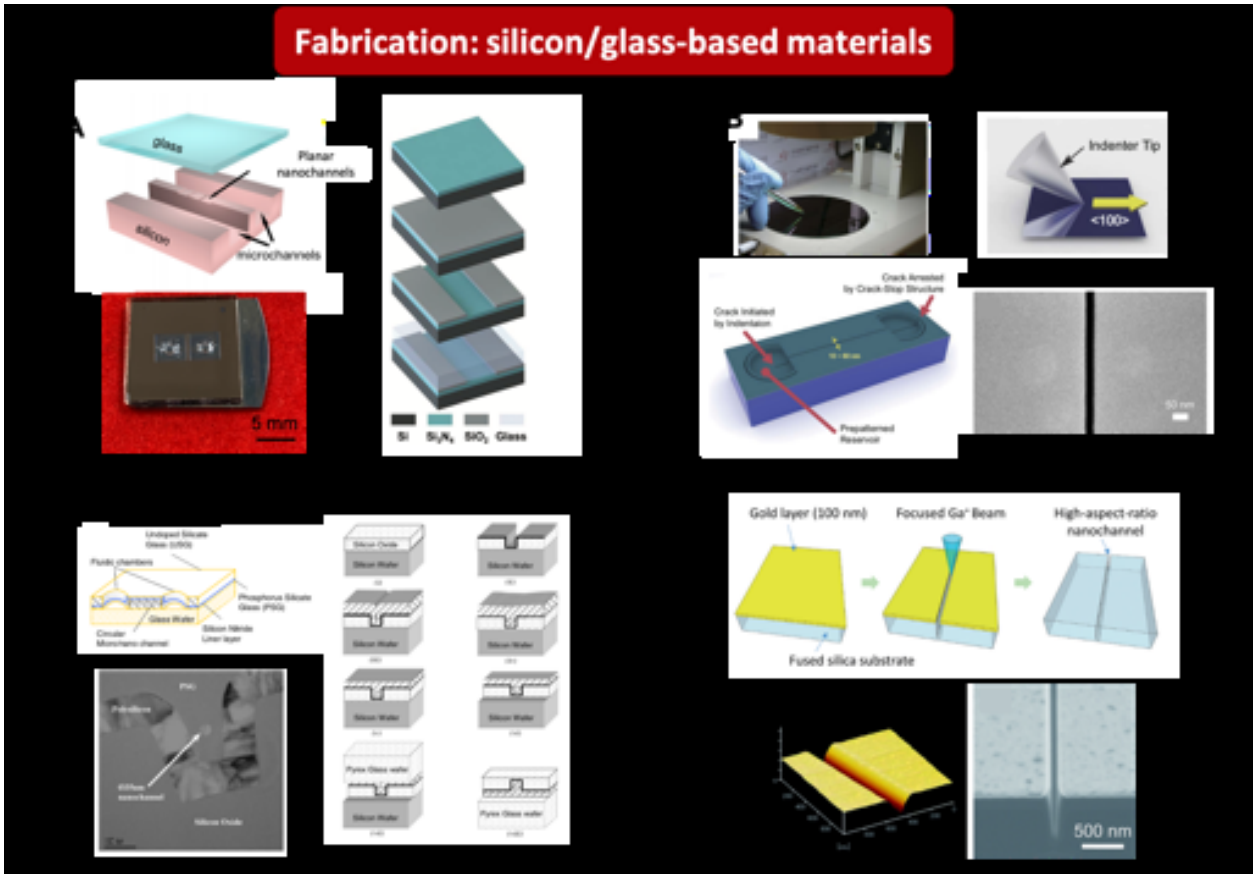


**Figure 16**. Fabrication of silicon/glass based nanochannels. (**A)** Fabrication process of planar nanochannels in silicon wafer involves standard photolithography, reactive ion etching, and anodic bonding. The borosilicate glass on top provides direct observation of liquid motion inside the channels through optical microscopy methods. Adapted with permission from ref [83,307] Copyright 2017 Royal Society of Chemistry and Copyright 2010 Royal Society of Chemistry. As shown in the lower left subfigure, two holes are created in the glass to assist liquid introduction to the device. (**B)** Nanochannels are fabricated in a silicon wafer through natural crack propagation induced by indentation. Cracking is controlled by manual manipulation of a hard-indenting tool. This method can create nanochannels as narrow as 10 nm with high aspect ratio and infinite length. Adapted from ref [304] Copyright 2016 Springer Nature. (**C)** Fabrication of self-sealed circular nanochannels in glass substrate. First, silicon oxide is deposited on a silicon wafer, then nanotrench is crated on

the deposited layer through etching. Afterward, the trench is sealed by plasma enhanced chemical vapor deposition (PECVD) of glass (PSG). Subsequently, the device is transferred to the borosilicate glass through anodic bonding method. Adapted with permission from ref [305] Copyright 2007 IOP Publishing. (**D)** Fabrication of high aspect ratio nanochannels in fused silica substrate through focused ion beam technique. Since fused silica is insulator, 100 nm gold layer is deposited to overcome the charging problem. Also, AFM and scanning ion microscopy (SIM) images of a 500nm×100nm nanochannel are shown. Adapted from ref [306] Copyright 2015 Royal Society of Chemistry.

## Polymer-based materials

Polymer-based materials are an attractive option for nanochannel fabrication mainly owing to their low cost, flexible processing and potential for high throughput production. A variety of standard and non-traditional approaches suggested for precise fabrication of polymeric nanochannels with sub-100 nm heights are discussed here.

Fanzio *et al.*[308] used the standard procedure of microfabrication coupled to Focused Ion Beam (FIB) nanofabrication to fabricate a silicon master, which was then replicated in a polymeric material by soft lithography to produce polymeric nanochannels for DNA detection. Cheng *et al.*[309] combined the sidewall lithography technique with hot embossing approach to create low-cost 2-D polymer nanochannels. To this end, they first developed a 2-D silicon nano-mold. Hot embossing technique was, subsequently, used to directly replicate the pattern of the 2-D nano-mold into a polyethylene terephthalate (PET) substrate. **Fig. 17A** shows the schematic illustration of this fabrication technique.

Unwanted roof-collapse phenomenon, commonly occurred when sealing the polymeric nanochannels, is not desired as it can impair the functionality of the channels. Pezzuoli *et al.*[310]

proposed a fabrication technique that inhibits roof-collapse without increasing the chance of deep crack formation. First, FIB is used to pattern the nanostructure onto a silicon wafer. The PDMS cast is then poured on the silicon master. It was followed by slowly dispensing a drop of hard PDMS on the region of the negative replica with the nanostructure. After 30 minutes of curing another layer of PDMS was poured all over the negative replica. The fabrication of channels with this focused drop-casting technique was completed by sealing the channels with a glass coverslip. These fabrication steps are depicted in **Fig. 17B**.

Developing nanochannels using the crack growth phenomenon is a promising approach with low cost potentially high throughputs that has been proposed in several studies.[311–313] But this method typically suffers from lack of controllability. Artificial defects made on the surface of polymers can be used to create nanochannels with controllable size and location. In a work by Peng and Li,[314] controlled and repeatable nano-crack arrays were developed to serve as nanochannels. They first, used an indenter tip to mark artificial defects on polystyrene surface that positions the nano-crack. Nano-cracks were then generated using the solvent-induced method; where the shrinkage resulted from absorption and vaporization of a chemical reagent creates the nano-crack, **Fig. 17C**. Nanochannel molds were also produced by replicating the generated nano-crack onto a photoresist. Kim *et al.*[315] also introduced a crack-photolithography technique for creating channels with mixed-scale patterns; where they used micro-notch structures on the surface to specify the channel ends. In this two-layered thin film technique, the tensile stresses induced in the elastic layer due to a swelling in the viscoelastic layer drives the cracking process and forms the desired channels (**Fig. 17E**). This technique offers features such as perfect 2-D patterning, simultaneous micro/nanopatterning, complete suppression of unwanted crack growth that distinguishes it from relevant alternatives.

Park *et al.*[316] proposed a fabrication technique based on the controlled collapse of microchannel structures. As shown schematically in **Fig. 17D**, in this roof-collapse technique, a thin layer of photoresist or evaporated metal is deposited on a silicon wafer substrate and lithographically pattered to the desired channel layout. The channel size, in this technique, depends on the height of the master and low resolutions can be used to pattern the channels. Patterning different thicknesses allows interfacing of different channel size. After patterning, the PDMS solution is cast onto the master. Eventually, the PDMS mold is removed and bonded to a plain substrate.

Park *et al.*[317] suggested another technique, where they used sacrificial mold to fabricate PDMS nanochannels with circular cross-sections. Near-field electrospinning method was used to directly and continuously deposit the water-soluble sacrificial material (nanofibers) from a polymer droplet onto a substrate using an appropriate electric field. Hard PDMS was then poured and partially cured, followed by curing of soft PDMS. Finally, the PDMS is demolded and the nanofibers are dissolved (**Fig. 17F**). This technique can be used to fabricate channels with controlled dimensions, positions and high precision and reproducibility.

While polymer-based materials have been widely used to fabricate commercial microfluidic devices, their use in nanofluidic devices is still relatively rare, mostly due to issues confronted during fabrication process. For example, unwanted deformation during the replication of nanochannel structures is a critical problem met when working with polymer-based material. Several studies have attempted to alleviate these issues. van Kan *et al.*[318] demonstrated a rapid prototyping technique for fabrication of PDMS nanochannels for disposable nanofluidic lab-on-a-chip devices. The nanofluidic devices are replicated with masters that can be used up to 200 times, prepared with proton beam writing in hydrogen silsequioxane. This allows for high throughput production, which is necessary for studying single DNA molecules, where ideally, a fresh device

should be used for each experiment. Wu *et al.*[319] also used a polymeric stamp made from a UV-curable resin that retains its structure without undergoing unwanted deformations due to sequential imprinting of nanofluidic devices. Chantiwas *et al.*[320] produced mixed-scale structures on thermoplastic polymers (*e.g.*, poly(methyl methacrylate), PMMA, cyclic olefin copolymer, COC, and polycarbonate, PC) using a PDMS mold. Combination of hot embossing and nanoimprinting was used to replicate the desired micro and nano structures onto the substrate. Application of oxygen plasma treatment for both the substrate and coverslip was shown to substantially reduce the thermally induced structural deformations during assembly.

A non-traditional lithography technique for PDMS structuring was proposed by Thangawng *et al.*[321] They used the so-called bond-detach lithography (BDL) method for direct patterning of thin PDMS films; where the patterned PDMS film can be used either as a structure or as a mask to transfer the pattern to another substrate in conjunction with other microfabrication processes. As the name implies, the basis for the BDL technique is the bonding of thin PDMS film and the patterned stamp, where the master is made by patterning the desired features with standard photoresist. The mold is brought into complete contact with the PDMS film and allowed to bond without applying pressure. Placing a drop of ethanol on the membrane or the structure is found to be an effective means of ensuring good contact and bonding. The two parts become bonded after the ethanol evaporates from the surface. Finally, within a few minutes of bonding the two PDMS parts, the stamp is carefully peeled from the base substrate. Hybrid mask-mold (HMM) lithography coupled with thermal bonding is another procedure for fabrication of polymeric nanofluidic devices, presented by Li *et al.*[322]

As another innovative fabrication method, Wu *et al.*[323] presented a simple process for the fabrication of all-transparent and encapsulated polymeric nanofluidic devices using nano-

indentation lithography. In this technique, a nanomechanical probe is used to 'scratch' nanoscale channels on PMMA substrates with sufficiently high hardness. PDMS substrate is subsequently used to duplicate the nanochannels onto PDMS substrates from the 'nano-scratched' PMMA substrates. Takei[324] demonstrated that step and flash nano imprint lithography process, a common type of ultraviolet (UV) nano imprint lithography technique, can be successfully applied to fluorinated silicon-based resist materials that can enhance the nanochannel fabrication process.

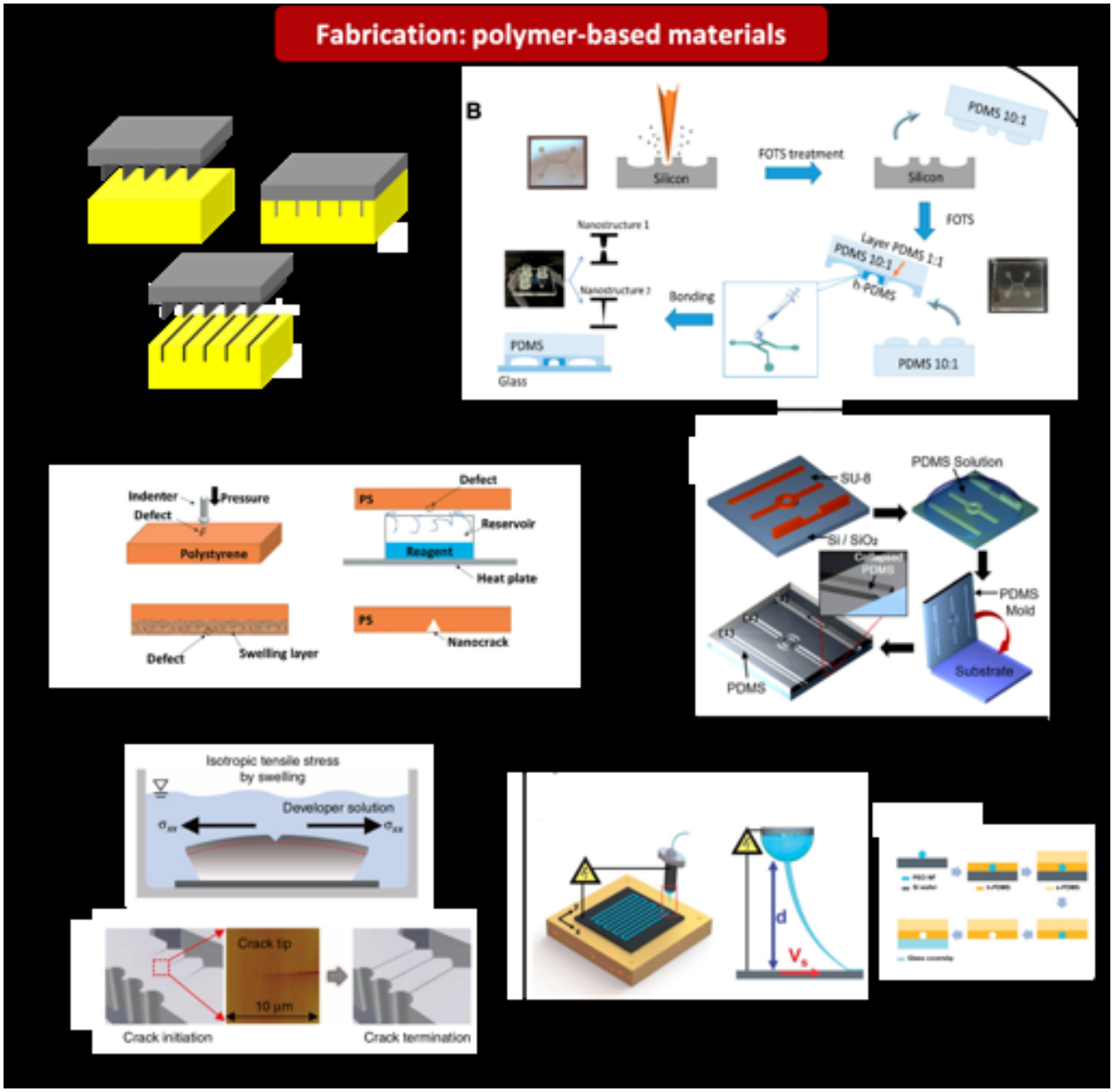


**Figure 17.** Fabrication of polymer based nanochannels. **(A)** Nano-mold is used to replicate the nanochannels pattern into PET polymer substrate through hot embossing method. **(B)** Fabrication of sub-100 nm channels with focused drop-casting of hard PDMS on nanostructured silicon master. This method can overcome the roof collapse problem of shallow channels as well as deep crack formation due to the peel-off step. Adapted from ref [310] Copyright 2019 MDPI. **(C)** Nanocracks are created on a polystyrene substrate by using artificial defects. The size and spacing of the nanochannels is controlled through solvent-induced method. Adapted with permission from

ref [314] Copyright 2000 Royal Society of Chemistry. (**D)** Fabrication of complex polymer nanofluidic device by elastomeric collapse method. As shown, the PDMS solution is casted onto the silicon master, then after curing, the PDMS mold is removed to be bonded to another plane substrate. Adapted with permission from ref [316] Copyright 2009 National Academy of Sciences. (**E)** The nanochannels is created through cracking-assisted method. Two layers including viscoelastic and elastic layers are designed to cause a tensile stress in the elastic layer which leads to crack formation at the notch. Adapted with permission from ref [315] Copyright 2015 Springer Nature. (**F)** Circular nanochannels are fabricated through low-cost non-lithographic method. In this approach, a near-field electrospinning method is used to print a nanofiber on the substrate which acts as a sacrificial mold to create nanochannels. Adapted from ref [317] Copyright 2018 Royal Society of Chemistry.

## Carbon nanotubes

The advancements in nanomaterials and nanofabrication techniques made the production of reliable nanofluidic devices more reachable. For instance, CNTs have emerged as intriguing materials for studying unusual transport phenomena with length scales corresponding to molecular dimensions, primarily because they can be directly employed as nanofluidic channels without complicated lithography processes. In the early times, however, the difficulties associated with fabricating a CNT-based nanofluidic device, limited researchers to use simulation (*e.g.*, MD) as a more accessible tool to study fluid characteristics in CNTs. Over the past few years, the increased availability of CNT membranes for experimental investigations, resulted in a significantly improved understanding of transport properties of these material and their potential utilization for a variety of applications.[325–328] For example, Cong *et al.*[329] developed a CNT membrane for ion and protein transportation with temperature and magnetic driven gating capability. To this end,

they used surface-initiated atom transfer radical polymerization (SI-ATRP) method to graft thermal-sensitive poly(N-isopropylacrylamide) (PNIPAM) and $Fe_3O_4$ nanoparticles ($Fe_3O_4$ -NPs) on the open ends of pre-aligned CNTs with a diameter around 15 nm. The inner cavity of the modified CNTs that is designed to be the only path for ion and protein transport has an effective diameter that can be reversibly tuned between 5.7 and 12.4 nm by adjusting the temperature and magnetic field. As shown in **Fig. 18A**, to develop such membranes, chemical vapor deposition was used to grow arrays of vertical CNTs on the substrate. Epoxy embedment followed by microtome cutting was employed to prepare the CNT/epoxy nanoporous membrane which was later functionalized by grafting PNIPAM onto the open ends of its CNTs. It must be mentioned that these vertically aligned nanotube membranes derived from the chemical-vapor-deposited CNTs are exceedingly hard to make, and nanotube size homogeneity and geometry in this technique is very difficult to control.

Tunuguntla *et al.*[330] developed nanoporous membranes using carbon nanotube porins (CNTPs). In this technique, to cut the typically long CNTs to lengths comparable to the thickness of a lipid bilayer, sonication-assisted cutting[331] was used. The sonication was performed in the presence of lipid molecules that stabilize the cut CNTs in the solution. As shown in **Fig. 18C**, ultracentrifugation of the resulting solution was carried out to separate the uncut long CNTs from the lipid-stabilized CNTP suspension. These developed CNTPs can be inserted into phospholipid membranes to form nanometer-scale-diameter pores that approximate the geometry and many key transport characteristics of biological membrane channels.

It must be noted that the observed transport phenomena in CNT membranes are averaged across numerous nanochannels in these materials and may not reflect the properties of individual CNTs. Realization of this fact has resulted in a recent trend to experimentally study the transport

phenomena in isolated single CNTs to unveil the detailed fluidic characteristics in CNTs.[332,333] Some groups have built single-CNT nanofluidic platforms by overcoming the great challenge to embed single CNTs in micro/nano devices *via* various approaches. These platforms offer great potentials to utilize CNTs as building blocks to flexibly build devices with complex nanofluidic networks in future. For example, Choi *et al.*[333] studied the ion transport inside individual single-walled carbon nanotubes (SWNTs) with diameters ranging from 0.94 to 2.1 nm. To this end, a nanofluidic device was developed as follows: aligned SWNTs were grown on a silicon wafer, identified with a marker and diameter characterized with Raman spectroscopy. Then, all except one or a few of the SWNTs were removed with a razor blade. The wafer was then covered by an epoxy structure constructed with two reservoirs and a 1-mm barrier region perpendicular to the SWNT alignment. Eventually, the exposed ends of the SWNT were removed using oxygen plasma leaving open SWNTs that spanned the epoxy barrier. **Fig. 18B**, illustrates the fabrication process, schematically.

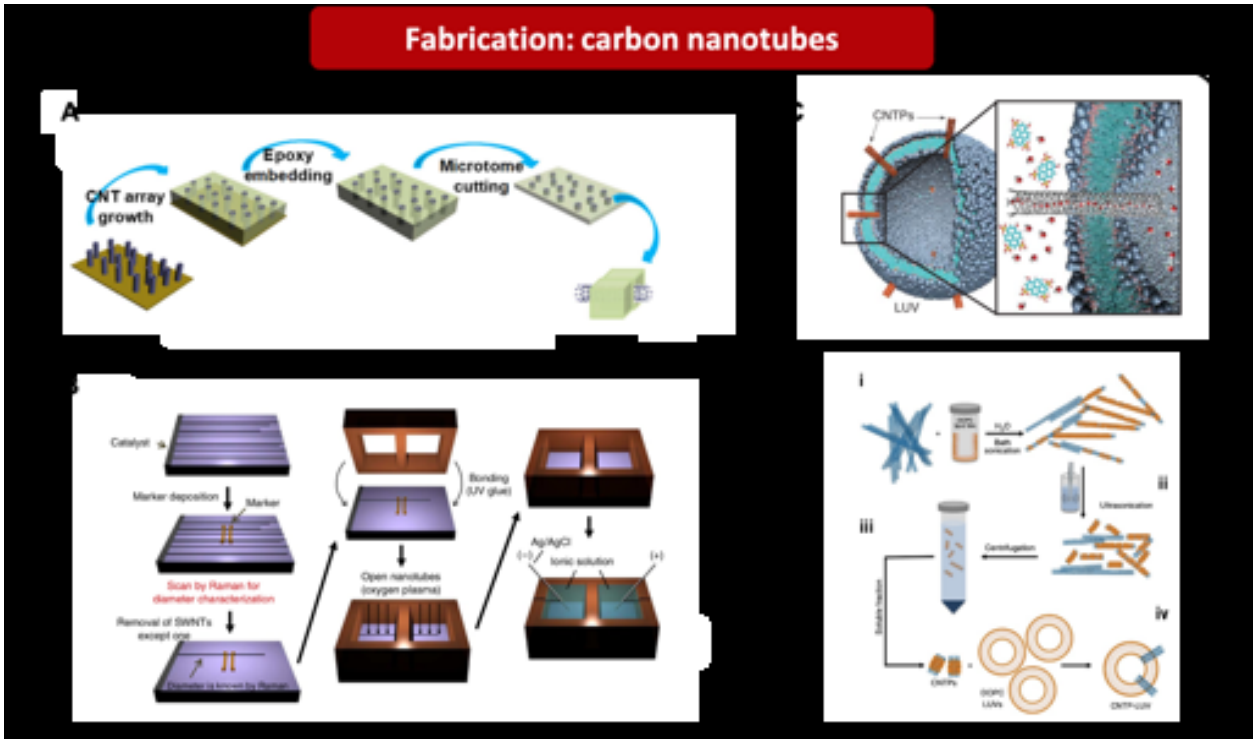


**Figure 18.** Carbon nanotubes: **(A)** Fabrication process of vertically aligned carbon nanotubes embedded in a crack-free matrix. The obtained membrane provides ions and water transport only through carbon nanotubes. Adapted from ref [329] Copyright 2016 Springer Nature. (**B)** Fabrication flow of a nanofluidic device made of single carbon nanotubes connecting two micro-reservoirs. First, aligned single carbon nanotubes is grown on a silicon wafer, then they were identified with a marker. Afterward, Laser blade was used to remove few SWCNT and the reservoirs plane is bonded to the Si wafer. Finally, two ends of carbon nanotubes are opened by Oxygen plasma etching to study ion transport through carbon nanotubes. Adapted with permission from ref [333] Copyright 2013 Springer Nature. (**C)** Bio-inspired carbon nanotubes porins are formed through spontaneous insertion of 10 nm-long CNT into a lipid membrane. Adapted with permission from ref [224] Copyright 2017 The American Association for Advancement of Science. The schematic of the synthesis steps is demonstrated. Adapted with permission from ref [330] Copyright 2016 Springer Nature.

## 2-D Materials

Two-dimensional (2-D) materials, made of carbon, boron nitride and $MoS_2$, are currently under investigation for their fluids and ion transport properties. These materials have attracted substantial attention due to their crystallographic nature and electronic properties. The so-called MXenes, made from transition metal carbides or nitrides (2-D materials) and graphene oxide and clay as (multilayer materials) are some examples. Nanoporous devices can be fabricated using these materials, as well. For example, by drilling 2-D material layers with ion or electron irradiation, and exploiting the existence of intrinsic defects, 2-D membranes with well-defined nanopores can be fabricated. The pores are tunable with diameters that can vary from tens of nanometers to a few angstroms.

Van der Waals assembly is another intriguing technique to fabricate 2-D channels with well-controlled heights and confinement dimensions as small as few angstroms. The fabrication principle is simple: a monolayer is placed on top of another monolayer or a few-layer crystal and another 2-D crystal is added and so on. The resulting stack represents an artificial material assembled in a chosen sequence with blocks defined with single-atomic-plane precision, **Fig. 19A**.[89] The strong covalent bonds ensure in-plane stability of the 2-D crystals, whereas the relatively weak van der Waals forces are sufficient to keep the stack together. Moreover, recent experiments have demonstrated that multilayer van der Waals heterostructures can be made, as well.[334–339] For example, Ponomarenko *et al.*[334] developed a multilayer van der Waals heterostructure beyond using h-BN, mica and similar substrates. Radha *et al.*[91] also used this method and fabricated angstrom-size slits where graphene layers were separated by 2-D crystals as spacers (**Fig. 19B**). The height of the channel, hence, was determined by the size of the spacer material.

Jung *et al.*[247] used a different method for fabrication of all graphene covered channels with rectangular cross-sections and heights as small as 3.6 nm. They directly transferred CVD-grown monolayer graphene onto thermally annealed and polished glass/silica with prepatterned nanochannel structure, as demonstrated in **Fig. 19C**. The direct transfer technique effectively reduced the appearance of any residues or defects such as tearing or folding on graphene surface which are common in wet transferring.

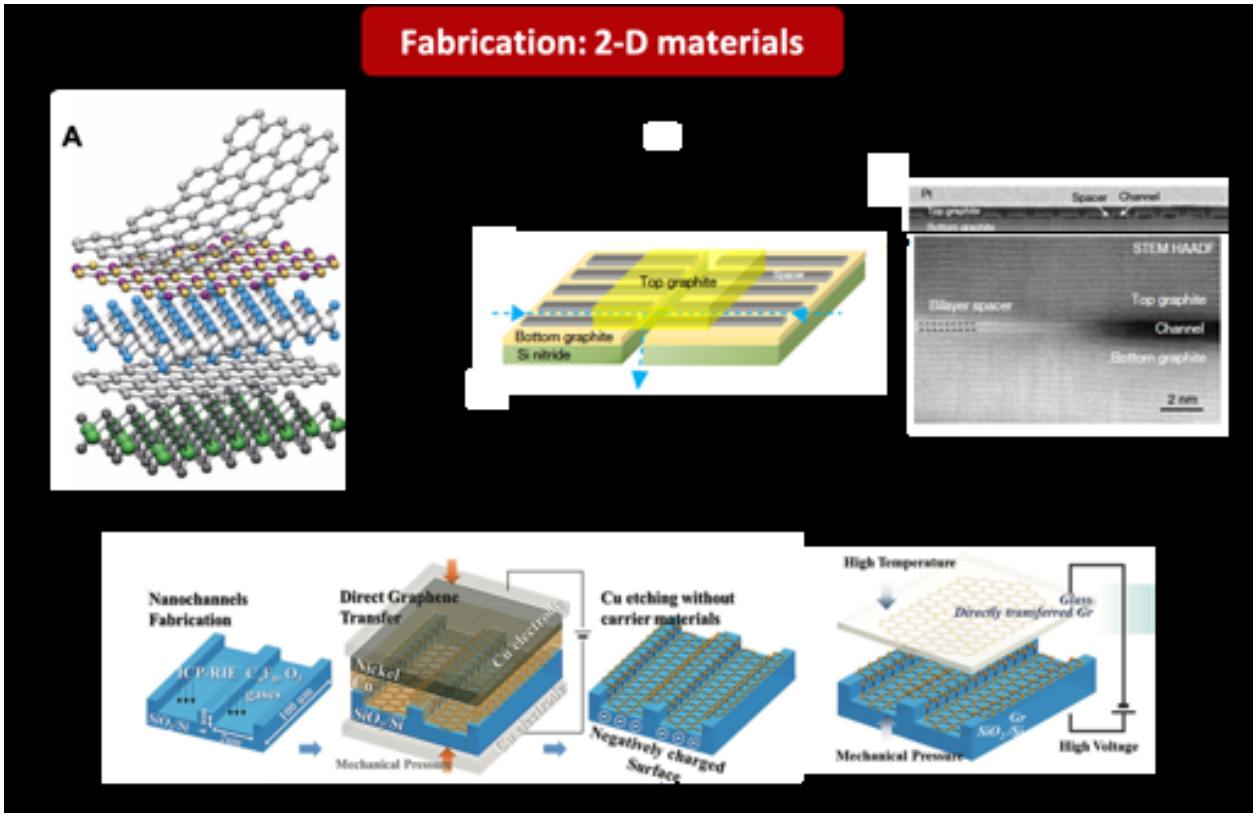


**Figure 19.** 2-D materials: (**A)** Two-dimensional atomic crystal materials, such as graphene, hexagonal boron nitride and molybdenum disulfide, are great candidates to form a nanofluidic devices with atomic size precession. Adapted with permission from ref [89] Copyright 2013 Springer Nature. (**B)** Schematic of nanocapillary device made by van der Waals assembly of graphene monolayers. As the top SEM image shows, the parallel arrays of graphene strips are used as the spacer to create the nanochannels structure. In fact, the height of these spacers determines the final

dimension of the channels which can be obtained down to several angstroms. Adapted with permission from ref [91] Copyright 2016 Springer Nature. **(C)** Graphene nanochannels are developed by direct and dry transfer of CVD grown graphene onto 2-D planar silicon nanochannels fabricated by MEMS techniques. Adapted with permission from ref [247] Copyright 2017 John Wiley and Sons.

## Future outlook

Nano/molecular transport is an interdisciplinary area with contributions from different areas of science such as fluid dynamics, statistical physics, materials science, chemistry, biology and has applications in a variety of fields including energy conversion, separation, drug delivery and nanofabrication. Hence, any scientific progress of this transport concept can inevitably advance these relevant fields. To envision the future directions for this field, it is imperative to consider its different applications. Nano/molecular channel-based devices offer great versatility for different industrial and medical applications, and ideally, can be used as a replacement for biological channels. However, even the most sophisticated synthetic channels developed so far cannot compete with their biological counterparts. In fact, while different synthetic channels have been fabricated that meet (or in some cases surpass) the effectiveness of a biological channel in some specific aspect, but they are often single-faceted and do not provide all functionalities simultaneously. Reconciling the variety of available synthetic nanochannel-based material and incorporating them to develop a nano/molecular fluidic device that offers all the advantages under the same umbrella can result in a giant leap in biotechnology and, hence, should be prioritized.

Selectivity is another property of nano/molecular channels that makes them an excellent choice for applications requiring ion gating and/or ion rectification. Among different technologies introduced to develop nano/molecular fluidic ionic diodes, those with active control measures may function as the building block to create an on-demand, reconfigurable, large-scale integrated

fluidic circuits for digitally programmed manipulation of biomolecules such as polynucleotides and proteins.

Mass/ion transport in single digit nanochannels showcase a variety of intriguing transport phenomena with a wide range of potential applications that underscores its importance for both scientific and industrial communities. So far, promising materials such as carbon and boron nitride nanotubes as 1-D material, graphene and hexagonal boron nitride (h-BN) sheets as 2-D material in addition to zero-dimensional material (made by piercing nanopores in solid-state or 2-D material) have been commonly used for development of nano/molecular channel-based devices. More recently, alternative structures such as MXenes, made of transition metal carbides or nitrides and van der Waals assembly of exfoliated sheets have been developed and had significant impacts on the field. It is imaginable that the extent of material and structures used for nano/molecular fluidics continue to grow in the future. The development of nanoslits with precise angstrom-size heights using van der Waals assembly technique, can make significant progress in the field with especial benefits for applications in membrane science where they can be used for energy harvesting (*e.g.*, electricity generation from osmotic energy) and filtration purposes. In fact, the emergence of 2-D nanoslits made of carbon and h-BN followed by exfoliated $MoS_2$ and graphene oxide, which combine high permeability with excellent sieving performance can completely circumvent the so-called permeability-selectivity trade-off and promise a bright future for artificial membrane technology. The chain-like transport mechanism observed in sub-nanometer CNT porins also has great potential for future applications as it offers extremely high flow rates as well as excellent ionic selectivity. Indeed, while extremely fast water flows in nanoscale CNTs (primarily due to flow slippage) was demonstrated previously, the flow rate improves by an order of magnitude when the channel dimension shrinks further to sub-nanometer zone. This intriguing

phenomenon promises advancements in a wide range of applications such as liquid transport and ionic diodes.

In addition, the recently developed osmotic diodes show great promise for incorporation in water purification strategies based on voltage-induced reverse osmosis or oscillating electric fields. In fact, these devices facilitate the fabrication of true fluidic analogues of nano-electronic components in order to control fluid flow at the nanoscale.

Advancements in fabrication and characterization techniques are also expected to greatly help the progress in nano/molecular fluidics. Direct observations have always played a substantial role in understanding the transport phenomena and advancement of nanofluidics. Transport in sub-10 nm channels has been recently visualized, however, with the progress in fabrication technology and the move toward angstrom-size channel, further technological advancements are required to make direct observation feasible. There is still a gap between functionality of the synthetic channels and their biological counterparts that is expected to come to a close with the considerable progress in biomimetic membranes. The application of nanochannels for energy harvesting can also be enhanced by improving the efficiency of the membranes. The increased flow rates and fast ion transport in CNTs and graphitic nanochannels especially in sub-2 nm conduits still lack a complete explanations. Also, the solid-like crystalized structure of water in hydrophilic nanoconfinements at room temperature and the chain-like liquid transport are intriguing phenomena with enhanced features such as very high conductivity; but require further investigations to be utilized for different applications. The characteristically different transport of water in CNTs and h-BN tubes despite their analogous crystallography and surface roughness is yet another subject that needs further investigation to unfold the role of electrical conductivity of the walls in nanoscopic transport phenomena. Molecular simulation is also another major player

in analysis of transport phenomena in nanoconfined fluids, however, its improvement in several aspects is quite critical. Current simulations typically predict the system dynamics for a very short time. It is strongly desired that simulations model the system for more relevant time scales, *i.e.*, time scales that match those in the experiment. This goal is becoming more achievable as advanced processing techniques and streamlined simulation methods have joined forces to achieve faster processing. In fact, the increasing processing power of computers based on the Moore's law and the development of advanced algorithms and specialized MD computer architecture, make the super-speed MD simulations that are orders of magnitude faster than previous ones, more possible. Such improvements in computing power helps the MD simulations timescale enter the experimental timescale and this overlap further enables MD simulations to be validated or improved by the experiment and vice versa.

In addition, molecular simulations cannot model large defects found in real samples as the typical simulation sizes are below a few hundred nanometers. Bridging the scale gap by using a multiscale modeling technique which combines molecular simulation with the mesoscale constitutive models may allow the study of larger systems; but studying transport properties with these techniques is usually challenging. The best solution is to use MD simulations to provide essential parameters needed for the mesoscale modeling such as interface energy, surface tension, density-dependent viscosity, interfacial thermal conductance, *etc.* In other words, molecular simulations and mesoscale models can be combined sequentially to form a hybrid method.

On the other hand, MD simulations rely on high fidelity force fields to correctly model the dynamics of the molecular system, but existing force fields can be inaccurate or even missing for certain interactions. Such challenges can be addressed by utilizing quantum mechanical based approach *i.e.* density functional theory (DFT) to parameterize more accurate force fields, such as

polarizable force field, reactive force field and *etc.* However, this process is usually not trivial. For example, for the extensively studied liquid, *i.e.*, water, there are more than 10 different models but none of them can accurately capture all the thermodynamic properties. One may need to find the suitable force field for studying a specific property or phenomenon of interest while compromising accuracy on other properties. Despite these limitations, that are mostly to be overcome, the main advantage of molecular simulation is to target a few specific features of potential impact to the property of interest and perform parametric studies so as to help elucidate some physical aspects that are not clear in experiments.

Scale-up is another challenge that need to be addressed. While, promising results have been obtained from laboratory prototypes, methodologies for rapid mass production of nano/molecular fluidic devices are still not available. The very low flow rates in nanochannels due to their small cross-sections, necessitates the use of a large number of devices for real applications. Thus, appropriate assembly, inter-connectivity and proper engagement of all nano/molecular fluidic devices incorporated in the system are important.

**VOCABULARY:**

Nanofluidics - the study of behavior and control of fluids confined to structures with nanometer length scales.

Ion channels - protein-based pores with sub-nanometer dimensions within biological membranes that play a crucial role in biological processes by providing pathways for selected ions to cross the membrane.

Molecular dynamics (MD) - a molecular simulation technique used to predict the behavior of a system based on interactions between its constituents such as molecules or molecular groups.

Slip length - a hypothetical distance from the liquid/solid interface where the liquid velocity vanishes.

Electric double layer (EDL) - a double layer of oppositely charged ions formed on a charged interface when it is exposed to a fluid due to electrostatic interactions.

## AUTHOR INFORMATION


### Corresponding Author

Hadi Ghasemi - *Department of Mechanical Engineering, University of Houston,*
Email: hghasemi@uh.edu
Tengfei Luo, *Department of Aerospace and Mechanical Engineering, University of Notre Dame*
Email: tluod@uh.edu


### Author Contributions

The manuscript was written through contributions of all authors. All authors have given approval to the final version of the manuscript. ‡These authors contributed equally.


### Acknowledgement

The authors gratefully acknowledge funding support from National Science Foundation (Grant NSF- 1804204) and ACS Petroleum Research Fund (Grant No. 59590) with Burtrand Lee as the program manager.


### Conflict of Interests

Hadi Ghasemi is a co-founder of SurfEllent LLC specialized in development of stress-localized durable icephobic surfaces. The authors declare no other conflicting financial interests.

## References


(1) Wheeler, T. D.; Stroock, A. D. The Transpiration of Water at Negative Pressures in a Synthetic Tree. *Nature* **2008**, *455*, 208–212.

(2) Shi, W.; Vieitez, J. R.; Berrier, A. S.; Roseveare, M. W.; Surinach, D. A.; Srijanto, B. R.; Collier, C. P.; Boreyko, J. B. Self-Stabilizing Transpiration in Synthetic Leaves. *ACS Appl. Mater. Interfaces* **2019**, *11* (14), 13768–13776. https://doi.org/10.1021/acsami.9b00041.

(3) Wang, Y.; Lee, J.; Werber, J. R.; Elimelech, M. Capillary-Driven Desalination in a Synthetic Mangrove. *Sci. Adv.* **2020**, *6* (8). https://doi.org/10.1126/sciadv.aax5253.

(4) Li, J. M.; Liu, C.; Xu, Z.; Zhang, K. P.; Ke, X.; Li, C. Y.; Wang, L. D. A Bio-Inspired Micropump Based on Stomatal Transpiration in Plants. *Lab Chip* **2011**, *11* (16), 2785–2789. https://doi.org/10.1039/c1lc20313d.

(5) Jingmin, L.; Chong, L.; Zheng, X.; Kaiping, Z.; Xue, K.; Liding, W. A Microfluidic Pump/Valve Inspired by Xylem Embolism and Transpiration in Plants. *PLoS One* **2012**, *7* (11), e50320. https://doi.org/10.1371/journal.pone.0050320.

(6) Kim, H.; Kim, K.; Lee, S. J. Compact and Thermosensitive Nature-Inspired Micropump. *Sci. Rep.* **2016**, *6* (1), 1–10. https://doi.org/10.1038/srep36085.

(7) Borno, R. T.; Steinmeyer, J. D.; Maharbiz, M. M. Charge-Pumping in a Synthetic Leaf for Harvesting Energy from Evaporation-Driven Flows. *Appl. Phys. Lett.* **2009**, *95* (1), 013705. https://doi.org/10.1063/1.3157144.

(8) Gruber, P.; Rupp, A. I. K. S. Investigation of Leaf Shape and Edge Design for Faster Evaporation in Biomimetic Heat Dissipation Systems. In *Bioinspiration, Biomimetics, and Bioreplication VIII*; Lakhtakia, A., Ed.; SPIE, 2018; Vol. 10593, p 14. https://doi.org/10.1117/12.2302516.

(9) Chen, I.-T.; Pharkya, A.; Stroock, A. D. Analysis of Superheated Loop Heat Pipes Exploiting Nanoporous Wick Membranes. *AIChE J.* **2014**, *60* (2), 762–777. https://doi.org/10.1002/aic.14303.

(10) Sajadi, S. M.; Irajizad, P.; Kashyap, V.; Farokhnia, N.; Ghasemi, H. Surfaces for High Heat Dissipation with No Leidenfrost Limit. *Appl. Phys. Lett.* **2017**, *111* (2), 021605. https://doi.org/10.1063/1.4993775.

(11) Farokhnia, N.; Irajizad, P.; Sajadi, S. M.; Ghasemi, H. Rational Micro/Nanostructuring for Thin-Film Evaporation. *J. Phys. Chem. C* **2016**, *120* (16), 8742–8750. https://doi.org/10.1021/acs.jpcc.6b01362.

(12) Sun, Y.; Chen, S.; Chen, X.; Xu, Y.; Zhang, S.; Ouyang, Q.; Yang, G.; Li, H. A Highly Selective and Recyclable NO-Responsive Nanochannel Based on a Spiroring Opening−Closing Reaction Strategy. *Nat. Commun.* **2019**, *10* (1), 1–8. https://doi.org/10.1038/s41467-019-09163-4.

(13) Nguyen, P. T.; DeMarco, K. R.; Vorobyov, I.; Clancy, C. E.; Yarov-Yarovoy, V. Structural Basis for Antiarrhythmic Drug Interactions with the Human Cardiac Sodium Channel. *Proc. Natl. Acad. Sci. U. S. A.* **2019**, *116* (8), 2945–2954. https://doi.org/10.1073/pnas.1817446116.

(14) Hutson, M. R.; Keyte, A. L.; Hernández-Morales, M.; Gibbs, E.; Kupchinsky, Z. A.; Argyridis, I.; Erwin, K. N.; Pegram, K.; Kneifel, M.; Rosenberg, P. B.; Matak, P.; Xie, L.; Grandl, J.; Davis, E. E.; Katsanis, N.; Liu, C.; Benner, E. J. Temperature-Activated Ion Channels in Neural Crest Cells Confer Maternal Fever-Associated Birth Defects. *Sci. Signal.* **2017**, *10* (500), 1–17. https://doi.org/10.1126/scisignal.aal4055.

(15) Saotome, K.; Murthy, S. E.; Kefauver, J. M.; Whitwam, T.; Patapoutian, A.; Ward, A. B. Structure of the Mechanically Activated Ion Channel Piezo1. *Nature* **2018**, *554* (7693), 481–486. https://doi.org/10.1038/nature25453.

(16) Jensen, M.; Jogini, V.; Borhani, D. W.; Leffler, A. E.; Dror, R. O.; Shaw, D. E. Mechanism of Voltage Gating in Potassium Channels. *Science (80-. ).* **2012**, *336* (6078), 229–233. https://doi.org/10.1126/science.1216533.

(17) Yellen, G. The Voltage-Gated K+ Channels and Their Relatives. *Nature* **2002**, *419* (September), 35–42.

(18) Burns, J. R.; Seifert, A.; Fertig, N.; Howorka, S. A Biomimetic DNA-Based Channel for the Ligand-Controlled Transport of Charged Molecular Cargo across a Biological Membrane. *Nat. Nanotechnol.* **2016**, *11* (2), 152–156. https://doi.org/10.1038/nnano.2015.279.

(19) Longden, T. A.; Dabertrand, F.; Koide, M.; Gonzales, A. L.; Tykocki, N. R.; Brayden, J. E.; Hill-Eubanks, D.; Nelson, M. T. Capillary K+-Sensing Initiates Retrograde Hyperpolarization to Increase Local Cerebral Blood Flow. *Nat. Neurosci.* **2017**, *20* (5), 717–726. https://doi.org/10.1038/nn.4533.

(20) Zhang, Z.; Wen, L.; Jiang, L. Bioinspired Smart Asymmetric Nanochannel Membranes. *Chem. Soc. Rev.* **2018**, *47* (2), 322–356. https://doi.org/10.1039/c7cs00688h.

(21) Bocquet, L.; Tabeling, P. Physics and Technological Aspects of Nanofluidics. *Lab Chip* **2014**, *14* (17), 3143–3158. https://doi.org/10.1039/c4lc00325j.

(22) Bao, B.; Riordon, J.; Mostowfi, F.; Sinton, D. Microfluidic and Nanofluidic Phase Behaviour Characterization for Industrial CO2, Oil and Gas. *Lab Chip* **2017**, *17* (16), 2740–2759. https://doi.org/10.1039/c7lc00301c.

(23) Cheng, Y.; Jiao, X.; Zhao, L.; Liu, Y.; Wang, F.; Wen, Y.; Zhang, X. Wetting Transition in Nanochannels for Biomimetic Free-Blocking on-Demand Drug Transport. *J. Mater. Chem. B* **2018**, *6* (39), 6269–6277. https://doi.org/10.1039/C8TB01838C.

(24) Siria, A.; Bocquet, M. L.; Bocquet, L. New Avenues for the Large-Scale Harvesting of Blue Energy. *Nat. Rev. Chem.* **2017**, *1* (11), 1–10. https://doi.org/10.1038/s41570-017-0091.

(25) Marbach, S.; Bocquet, L. Osmosis, from Molecular Insights to Large-Scale Applications. *Chemical Society Reviews*. Royal Society of Chemistry June 7, 2019, pp 3102–3144. https://doi.org/10.1039/c8cs00420j.

(26) Karnik, R.; Fan, R.; Yue, M.; Li, D.; Yang, P.; Majumdar, A. Electrostatic Control of Ions and Molecules in Nanofluidic Transistors. *Nano Lett.* **2005**, *5* (5), 943–948. https://doi.org/10.1021/nl050493b.

(27) Karnik, R.; Duan, C.; Castelino, K.; Daiguji, H.; Majumdar, A. Rectification of Ionic Current in a Nanofluidic Diode. *Nano Lett.* **2007**, *7* (3), 547–551. https://doi.org/10.1021/nl062806o.

(28) Bocquet, L.; Charlaix, E. Nanofluidics, from Bulk to Interfaces. *Chem. Soc. Rev.* **2010**, *39* (3), 1073–1095. https://doi.org/10.1039/b909366b.

(29) Sparreboom, W.; Van Den Berg, A.; Eijkel, J. C. T. Transport in Nanofluidic Systems: A Review of Theory and Applications. *New J. Phys.* **2010**, *12*. https://doi.org/10.1088/1367-2630/12/1/015004.

(30) Eijkel, J. C. T.; van den Berg, A. Nanofluidics: What Is It and What Can We Expect from It? *Microfluid. Nanofluidics* **2005**, *1* (3), 249–267. https://doi.org/10.1007/s10404-004-0012-9.

(31) Zhu, Z.; Wang, D.; Tian, Y.; Jiang, L. Ion/Molecule Transportation in Nanopores and Nanochannels: From Critical Principles to Diverse Functions. *Journal of the American Chemical Society*. 2019, pp 8658–8669. https://doi.org/10.1021/jacs.9b00086.

(32) Yip, N. Y.; Brogioli, D.; Hamelers, H. V. M.; Nijmeijer, K. Salinity Gradients for Sustainable Energy: Primer, Progress, and Prospects. *Environ. Sci. Technol.* **2016**, *50* (22), 12072–12094. https://doi.org/10.1021/acs.est.6b03448.

(33) Sharma, M.; Chakraborty, A.; Kuttippurath, J.; Kumar Yadav, A. Potential Power Production from Salinity Gradient at the Hooghly Estuary System. **2018**. https://doi.org/10.4172/2576-1463.1000210.

(34) Siria, A.; Poncharal, P.; Biance, A. L.; Fulcrand, R.; Blase, X.; Purcell, S. T.; Bocquet, L. Giant Osmotic Energy Conversion Measured in a Single Transmembrane Boron Nitride Nanotube. *Nature* **2013**, *494* (7438), 455–458. https://doi.org/10.1038/nature11876.

(35) Feng, J.; Graf, M.; Liu, K.; Ovchinnikov, D.; Dumcenco, D.; Heiranian, M.; Nandigana, V.; Aluru, N. R.; Kis, A.; Radenovic, A. Single-Layer MoS2 Nanopores as Nanopower Generators. *Nature* **2016**, *536* (7615), 197–200. https://doi.org/10.1038/nature18593.

(36) Logan, B. E.; Elimelech, M. Membrane-Based Processes for Sustainable Power Generation Using Water. *Nature* **2012**, *488* (7411), 313–319. https://doi.org/10.1038/nature11477.

(37) Zhang, Z.; Sui, X.; Li, P.; Xie, G.; Kong, X. Y.; Xiao, K.; Gao, L.; Wen, L.; Jiang, L. Ultrathin and Ion-Selective Janus Membranes for High-Performance Osmotic Energy Conversion. *J. Am. Chem. Soc.* **2017**, *139* (26), 8905–8914. https://doi.org/10.1021/jacs.7b02794.

(38) Chen, G.; Sachar, H. S.; Das, S. Efficient Electrochemomechanical Energy Conversion in Nanochannels Grafted with End-Charged Polyelectrolyte Brushes at Medium and High Salt Concentration. *Soft Matter* **2018**, *14* (25), 5246–5255. https://doi.org/10.1039/c8sm00768c.

(39) Van Der Heyden, F. H. J.; Bonthuis, D. J.; Stein, D.; Meyer, C.; Dekker, C. Power Generation by Pressure-Driven Transport of Ions in Nanofluidic Channels. *Nano Lett.* **2007**, *7* (4), 1022–1025. https://doi.org/10.1021/nl070194h.

(40) Daiguji, H.; Yang, P.; Szeri, A. J.; Majumdar, A. Electrochemomechanical Energy Conversion in Nanofluidic Channels. *Nano Lett.* **2004**, *4* (12), 2315–2321. https://doi.org/10.1021/nl0489945.

(41) Steinberg-Yfrach, G.; Liddell, P. A.; Hung, S. C.; Moore, A. L.; Gust, D.; Moore, T. A. Conversion of Light Energy to Proton Potential in Liposomes by Artificial Photosynthetic Reaction Centres. *Nature* **1997**, *385* (6613), 239–241. https://doi.org/10.1038/385239a0.

(42) Gust, D.; Moore, T. A.; Moore, A. L. Mimicking Photosynthetic Solar Energy Transduction. *Acc. Chem. Res.* **2001**, *34* (1), 40–48. https://doi.org/10.1021/ar9801301.

(43) Steinberg-Yfrach, G.; Rigaud, J. L.; Durantini, E. N.; Moore, A. L.; Gust, D.; Moore, T. A. Light-Driven Production of ATP Catalysed by F0F1-ATP Synthase in an Artificial Photosynthetic Membrane. *Nature* **1998**, *392* (6675), 479–482. https://doi.org/10.1038/33116.

(44) White, W.; Sanborn, C. D.; Fabian, D. M.; Ardo, S. Conversion of Visible Light into Ionic Power Using Photoacid-Dye-Sensitized Bipolar Ion-Exchange Membranes. *Joule* **2018**, *2* (1), 94–109. https://doi.org/10.1016/j.joule.2017.10.015.

(45) Xie, X.; Crespo, G. A.; Mistlberger, G.; Bakker, E. Photocurrent Generation Based on a Light-Driven Proton Pump in an Artificial Liquid Membrane. *Nat. Chem.* **2014**, *6* (3), 202–207. https://doi.org/10.1038/nchem.1858.

(46) Tian, Y.; Jiang, L. Biomimetic Photoelectric Conversion Systems Based on Artificial Membranes. *Sci. China Chem.* **2011**, *54* (4), 603–610. https://doi.org/10.1007/s11426-011-4229-7.

(47) Xiao, K.; Chen, L.; Chen, R.; Heil, T.; Lemus, S. D. C.; Fan, F.; Wen, L.; Jiang, L.; Antonietti, M. Artificial Light-Driven Ion Pump for Photoelectric Energy Conversion. *Nat. Commun.* **2019**, *10* (1), 1–7. https://doi.org/10.1038/s41467-018-08029-5.

(48) Straub, A. P.; Yip, N. Y.; Lin, S.; Lee, J.; Elimelech, M. Harvesting Low-Grade Heat Energy Using Thermo-Osmotic Vapour Transport through Nanoporous Membranes. *Nat. Energy* **2016**, *1* (7), 1–6. https://doi.org/10.1038/nenergy.2016.90.

(49) Chen, W.; Fan, Z.; Pan, X.; Bao, X. Effect of Confinement in Carbon Nanotubes on the Activity of Fischer-Tropsch Iron Catalyst. *J. Am. Chem. Soc.* **2008**, *130* (29), 9414–9419. https://doi.org/10.1021/ja8008192.

(50) Zhang, J.; Yu, Z.; Gao, Z.; Ge, H.; Zhao, S.; Chen, C.; Chen, S.; Tong, X.; Wang, M.; Zheng, Z.; Qin, Y. Porous TiO2Nanotubes with Spatially Separated Platinum and CoOxCocatalysts Produced by Atomic Layer Deposition for Photocatalytic Hydrogen Production. *Angew. Chemie - Int. Ed.* **2017**, *56* (3), 816–820. https://doi.org/10.1002/anie.201611137.

(51) Zhang, J.; Müller, J. O.; Zheng, W.; Wang, D.; Su, D.; Schlögl, R. Individual Fe-Co Alloy Nanoparticles on Carbon Nanotubes: Structural and Catalytic Properties. *Nano Lett.* **2008**, *8* (9), 2738–2743. https://doi.org/10.1021/nl8011984.

(52) Zhang, S.; Zhang, B.; Liang, H.; Liu, Y.; Qiao, Y.; Qin, Y. Encapsulation of Homogeneous Catalysts in Mesoporous Materials Using Diffusion-Limited Atomic Layer Deposition. *Angew. Chemie - Int. Ed.* **2018**, *57* (4), 1091–1095. https://doi.org/10.1002/anie.201712010.

(53) Levin, S.; Fritzsche, J.; Nilsson, S.; Runemark, A.; Dhokale, B.; Ström, H.; Sundén, H.; Langhammer, C.; Westerlund, F. A Nanofluidic Device for Parallel Single Nanoparticle Catalysis in Solution. *Nat. Commun.* **2019**, *10* (1). https://doi.org/10.1038/s41467-019-12458-1.

(54) Karan, S.; Samitsu, S.; Peng, X.; Kurashima, K.; Ichinose, I. Ultrafast Viscous Permeation of Organic Solvents through Diamond-Like Carbon Nanosheets. *Science (80-. ).* **2012**, *335* (6067), 444–447. https://doi.org/10.1126/science.1212101.

(55) Liu, J.; Wang, N.; Yu, L. J.; Karton, A.; Li, W.; Zhang, W.; Guo, F.; Hou, L.; Cheng, Q.; Jiang, L.; Weitz, D. A.; Zhao, Y. Bioinspired Graphene Membrane with Temperature Tunable Channels for Water Gating and Molecular Separation. *Nat. Commun.* **2017**, *8* (1), 1–8. https://doi.org/10.1038/s41467-017-02198-5.

(56) Surwade, S. P.; Smirnov, S. N.; Vlassiouk, I. V.; Unocic, R. R.; Veith, G. M.; Dai, S.; Mahurin, S. M. Water Desalination Using Nanoporous Single-Layer Graphene. *Nat. Nanotechnol.* **2015**, *10*

(5), 459–464. https://doi.org/10.1038/nnano.2015.37.

(57) Zhang, H.; Hou, J.; Hu, Y.; Wang, P.; Ou, R.; Jiang, L.; Zhe Liu, J.; Freeman, B. D.; Hill, A. J.; Wang, H. Ultrafast Selective Transport of Alkali Metal Ions in Metal Organic Frameworks with Subnanometer Pores. *Sci. Adv.* **2018**, *4* (2). https://doi.org/10.1126/sciadv.aaq0066.

(58) Shen, Y. X.; Song, W. C.; Ryan Barden, D.; Ren, T.; Lang, C.; Feroz, H.; Henderson, C. B.; Saboe, P. O.; Tsai, D.; Yan, H.; Butler, P. J.; Bazan, G. C.; Phillip, W. A.; Hickey, R. J.; Cremer, P. S.; Vashisth, H.; Kumar, M. Achieving High Permeability and Enhanced Selectivity for Angstrom-Scale Separations Using Artificial Water Channel Membranes. *Nat. Commun.* **2018**, *9* (1). https://doi.org/10.1038/s41467-018-04604-y.

(59) Yang, Y.; Yang, X.; Liang, L.; Gao, Y.; Cheng, H.; Li, X.; Zou, M.; Ma, R.; Yuan, Q.; Duan, X. Large-Area Graphene-Nanomesh/Carbon-Nanotube Hybrid Membranes for Ionic and Molecular Nanofiltration. *Science (80-. ).* **2019**, *364* (6445), 1057–1062. https://doi.org/10.1126/science.aau5321.

(60) Li, H.; Qiu, C.; Ren, S.; Dong, Q.; Zhang, S.; Zhou, F.; Liang, X.; Wang, J.; Li, S.; Yu, M. Na+-Gated Water-Conducting Nanochannels for Boosting CO2 Conversion to Liquid Fuels. *Science (80-. ).* **2020**, *367* (6478), 667–671. https://doi.org/10.1126/science.aaz6053.

(61) Esfandiar, A.; Radha, B.; Wang, F. C.; Yang, Q.; Hu, S.; Garaj, S.; Nair, R. R.; Geim, A. K.; Gopinadhan, K. Size Effect in Ion Transport through Angstrom-Scale Slits. *Science (80-. ).* **2017**, *358* (6362), 511–513. https://doi.org/10.1126/science.aan5275.

(62) Mouterde, T.; Keerthi, A.; Poggioli, A. R.; Dar, S. A.; Siria, A.; Geim, A. K.; Bocquet, L.; Radha, B. Molecular Streaming and Its Voltage Control in Ångström-Scale Channels. *Nature* **2019**, *567* (7746), 87–90. https://doi.org/10.1038/s41586-019-0961-5.

(63) Gopinadhan, K.; Hu, S.; Esfandiar, A.; Lozada-Hidalgo, M.; Wang, F. C.; Yang, Q.; Tyurnina, A. V.; Keerthi, A.; Radha, B.; Geim, A. K. Complete Steric Exclusion of Ions and Proton Transport through Confined Monolayer Water. *Science (80-. ).* **2019**, *363* (6423), 145–148. https://doi.org/10.1126/science.aau6771.

(64) Lee, J.; Laoui, T.; Karnik, R. Nanofluidic Transport Governed by the Liquid/Vapour Interface. *Nat. Nanotechnol.* **2014**, *9* (4), 317–323. https://doi.org/10.1038/nnano.2014.28.

(65) Bocquet, L. Nanofluidics: Bubbles as Osmotic Membranes. *Nat. Nanotechnol.* **2014**, *9* (4), 249–251. https://doi.org/10.1038/nnano.2014.61.

(66) Mi, L.; Sui, J.; Wu, Y.; Liang, G.; Zhang, Y.; Pu, Y.; Tian, Y.; Liu, S.; Jiang, L. Bioinspired *in Vitro* Lung Airway Model for Inflammatory Analysis *via* Hydrophobic Nanochannel Membrane with Joint Three-Phase Interface. *Anal. Chem.* **2019**, *91* (24), 15804–15810. https://doi.org/10.1021/acs.analchem.9b04114.

(67) Sinha, P. M.; Valco, G.; Sharma, S.; Liu, X.; Ferrari, M. Nanoengineered Device for Drug Delivery Application. *Nanotechnology* **2004**, *15* (10). https://doi.org/10.1088/0957-4484/15/10/015.

(68) Duan, R.; Xia, F.; Jiang, L. Constructing Tunable Nanopores and Their Application in Drug Delivery. *ACS Nano*. 2013, pp 8344–8349. https://doi.org/10.1021/nn405092w.

(69) Ferrati, S.; Fine, D.; You, J.; De Rosa, E.; Hudson, L.; Zabre, E.; Hosali, S.; Zhang, L.; Hickman, C.; Sunder Bansal, S.; Cordero-Reyes, A. M.; Geninatti, T.; Sih, J.; Goodall, R.; Palapattu, G.; Kloc, M.; Ghobrial, R. M.; Ferrari, M.; Grattoni, A. Leveraging Nanochannels for Universal, Zero-Order Drug Delivery *in Vivo*. *J. Control. Release* **2013**, *172* (3), 1011–1019. https://doi.org/10.1016/j.jconrel.2013.09.028.

(70) Di Trani, N.; Silvestri, A.; Sizovs, A.; Wang, Y.; Erm, D. R.; Demarchi, D.; Liu, X.; Grattoni, A. Electrostatically Gated Nanofluidic Membrane for Ultra-Low Power Controlled Drug Delivery. *Lab Chip* **2020**, *20* (9), 1562–1576. https://doi.org/10.1039/d0lc00121j.

(71) Ballerini, A.; S. Filgueira, C.; Nicolov, E.; Jain, P.; Bruno, G.; L. Hood, R.; Scaglione, F.; Grattoni, A. Sustained Delivery of Tamoxifen from a Nanofluidic Delivery Platform. *Drug Deliv. Lett.* **2017**, *6* (2), 127–133. https://doi.org/10.2174/2210303106666161129163850.

(72) Di Trani, N.; Jain, P.; Chua, C. Y. X.; Ho, J. S.; Bruno, G.; Susnjar, A.; Pons-Faudoa, F. P.; Sizovs, A.; Hood, R. L.; Smith, Z. W.; Ballerini, A.; Filgueira, C. S.; Grattoni, A. Nanofluidic Microsystem for Sustained Intraocular Delivery of Therapeutics. *Nanomedicine Nanotechnology, Biol. Med.* **2019**, *16* (November), 1–9. https://doi.org/10.1016/j.nano.2018.11.002.

(73) Ding, J.; Li, X.; Zhou, L.; Yang, R.; Yan, F.; Su, B. Electrodeposition of Nickel Nanostructures Using Silica Nanochannels as Confinement for Low-Fouling Enzyme-Free Glucose Detection. *J. Mater. Chem. B* **2020**, *8* (16), 3616–3622. https://doi.org/10.1039/c9tb02472g.

(74) García-Gutiérrez, M. C.; Linares, A.; Hernández, J. J.; Rueda, D. R.; Ezquerra, T. A.; Poza, P.; Davies, R. J. Confinement-Induced One-Dimensional Ferroelectric Polymer Arrays. *Nano Lett.* **2010**, *10* (4), 1472–1476. https://doi.org/10.1021/nl100429u.

(75) Cauda, V.; Stassi, S.; Bejtka, K.; Canavese, G. Nanoconfinement: An Effective Way to Enhance PVDF Piezoelectric Properties. *ACS Appl. Mater. Interfaces* **2013**, *5* (13), 6430–6437. https://doi.org/10.1021/am4016878.

(76) Liu, W.; Lin, D.; Pei, A.; Cui, Y. Stabilizing Lithium Metal Anodes by Uniform Li-Ion Flux Distribution in Nanochannel Confinement. *J. Am. Chem. Soc.* **2016**, *138* (47), 15443–15450. https://doi.org/10.1021/jacs.6b08730.

(77) Alibakhshi, M. A.; Xie, Q.; Li, Y.; Duan, C. Accurate Measurement of Liquid Transport through Nanoscale Conduits. *Sci. Rep.* **2016**, *6* (March), 1–8. https://doi.org/10.1038/srep24936.

(78) Li, Y.; Chen, H.; Xiao, S.; Alibakhshi, M. A.; Lo, C. W.; Lu, M. C.; Duan, C. Ultrafast Diameter-Dependent Water Evaporation from Nanopores. *ACS Nano* **2019**, *13* (3), 3363–3372. https://doi.org/10.1021/acsnano.8b09258.

(79) Li, Y.; Alibakhshi, M. A.; Zhao, Y.; Duan, C. Exploring Ultimate Water Capillary Evaporation in Nanoscale Conduits. *Nano Lett.* **2017**, *17* (8), 4813–4819. https://doi.org/10.1021/acs.nanolett.7b01620.

(80) Xie, Q.; Xiao, S.; Duan, C. Geometry-Dependent Drying in Dead-End Nanochannels. *Langmuir* **2017**, *33* (34), 8395–8403. https://doi.org/10.1021/acs.langmuir.7b02027.

(81) Zhong, J.; Riordon, J.; Zandavi, S. H.; Xu, Y.; Persad, A. H.; Mostowfi, F.; Sinton, D. Capillary Condensation in 8 Nm Deep Channels. *J. Phys. Chem. Lett.* **2018**, *9* (3), 497–503. https://doi.org/10.1021/acs.jpclett.7b03003.

(82) Zhong, J.; Zandavi, S. H.; Li, H.; Bao, B.; Persad, A. H.; Mostowfi, F.; Sinton, D. Condensation in One-Dimensional Dead-End Nanochannels. *ACS Nano* **2017**, *11* (1), 304–313. https://doi.org/10.1021/acsnano.6b05666.

(83) Li, H.; Zhong, J.; Pang, Y.; Zandavi, S. H.; Persad, A. H.; Xu, Y.; Mostowfi, F.; Sinton, D. Direct Visualization of Fluid Dynamics in Sub-10 Nm Nanochannels. *Nanoscale* **2017**, *9* (27), 9556–9561. https://doi.org/10.1039/c7nr02176c.

(84) Nazari, M.; Nazifi, S.; Huang, Z.; Tong, T.; Ouro-Koura, H.; Bao, J.; Das, K.; Ghasemi, H. Surface Tension Nanogates for Controlled Ion Transport. *ACS Appl. Nano Mater.* **2020**. https://doi.org/10.1021/acsanm.0c01304.

(85) Zhong, J.; Talebi, S.; Xu, Y.; Pang, Y.; Mostowfi, F.; Sinton, D. Fluorescence in Sub-10 Nm Channels with an Optical Enhancement Layer. *Lab Chip* **2018**, *18* (4), 568–573. https://doi.org/10.1039/c7lc01193h.

(86) Pía Rossi, M.; Ye, H.; Gogotsi, Y.; Babu, S.; Ndungu, P.; Bradley, J. C. Environmental Scanning Electron Microscopy Study of Water in Carbon Nanopipes. *Nano Lett.* **2004**, *4* (5), 989–993. https://doi.org/10.1021/nl049688u.

(87) Tomo, Y.; Askounis, A.; Ikuta, T.; Takata, Y.; Sefiane, K.; Takahashi, K. Superstable Ultrathin Water Film Confined in a Hydrophilized Carbon Nanotube. *Nano Lett.* **2018**, *18* (3), 1869–1874. https://doi.org/10.1021/acs.nanolett.7b05169.

(88) Fumagalli, L.; Esfandiar, A.; Fabregas, R.; Hu, S.; Ares, P.; Janardanan, A.; Yang, Q.; Radha, B.; Taniguchi, T.; Watanabe, K.; Gomila, G.; Novoselov, K. S.; Geim, A. K. Anomalously Low Dielectric Constant of Confined Water. *Science (80-. ).* **2018**, *360* (6395), 1339–1342. https://doi.org/10.1126/science.aat4191.

(89) Geim, A. K.; Grigorieva, I. V. van der Waals Heterostructures. *Nature* **2013**, *499* (7459), 419–425. https://doi.org/10.1038/nature12385.

(90) Yao, L.; Filice, F. P.; Yang, Q.; Ding, Z.; Su, B. Quantitative Assessment of Molecular Transport through Sub-3 Nm Silica Nanochannels by Scanning Electrochemical Microscopy. *Anal. Chem.* **2019**, *91* (2), 1548–1556. https://doi.org/10.1021/acs.analchem.8b04795.

(91) Radha, B.; Esfandiar, A.; Wang, F. C.; Rooney, A. P.; Gopinadhan, K.; Keerthi, A.; Mishchenko, A.; Janardanan, A.; Blake, P.; Fumagalli, L.; Lozada-Hidalgo, M.; Garaj, S.; Haigh, S. J.; Grigorieva, I. V.; Wu, H. A.; Geim, A. K. Molecular Transport through Capillaries Made with Atomic-Scale Precision. *Nature* **2016**, *538* (7624), 222–225. https://doi.org/10.1038/nature19363.

(92) Max, L. G.; Song, Z. X. Nanoporous Materials-An Overview. In *Nanoporous Materials: Science And Engineering*; World Scientific: London, 2004; Vol. 4, pp 5–12.

(93) Baker, R. W. Reverse Osmosis. In *Membrane Technology and Applications*; John Wiley & Sons: Chichester, 2012; Vol. 1, pp 237–246.

(94) Baker, R. W. Gas Separation. In *Membrane Technology and Applications*; John Wiley & Sons: Chichester, 2012; Vol. 1, pp 349–373.

(95) Keerthi, A.; Geim, A. K.; Janardanan, A.; Rooney, A. P.; Esfandiar, A.; Hu, S.; Dar, S. A.; Grigorieva, I. V.; Haigh, S. J.; Wang, F. C.; Radha, B. Ballistic Molecular Transport through Two-Dimensional Channels. *Nature* **2018**, *558* (7710), 420–423. https://doi.org/10.1038/s41586-018-0203-2.

(96) Inkson, B. J. Scanning Electron Microscopy (SEM) and Transmission Electron Microscopy (TEM) for Materials Characterization. In *Materials Characterization Using Nondestructive Evaluation (NDE) Methods*; Elsevier Inc., 2016; pp 17–43. https://doi.org/10.1016/B978-0-08-100040-3.00002-X.

(97) Huang, D.; Zhang, T.; Xiong, G.; Xu, L.; Qu, Z.; Lee, E.; Luo, T. Tuning Water Slip Behavior in Nanochannels Using Self-Assembled Monolayers. *ACS Appl. Mater. Interfaces* **2019**, *11* (35), 32481–32488. https://doi.org/10.1021/acsami.9b09509.

(98) Striolo, A.; Chialvo, A. A.; Gubbins, K. E.; Cummings, P. T. Water in Carbon Nanotubes: Adsorption Isotherms and Thermodynamic Properties from Molecular Simulation. *J. Chem. Phys.* **2005**, *122* (23). https://doi.org/10.1063/1.1924697.

(99) Wei, X.; Luo, T. Effects of Electrostatic Interaction and Chirality on the Friction Coefficient of Water Flow Inside Single-Walled Carbon Nanotubes and Boron Nitride Nanotubes. *J. Phys.*

*Chem. C* **2018**, *122* (9), 5131–5140. https://doi.org/10.1021/acs.jpcc.7b11657.

(100) Plimpton, S. Fast Parallel Algorithms for Short-Range Molecular Dynamics. *J. Comput. Phys.* **1995**, *117* (1), 1–19. https://doi.org/10.1006/jcph.1995.1039.

(101) van der Spoel, D.; Lindahl, E.; Hess, B.; Groenhof, G.; Mark, A. E.; Berendsen, H. J. C. GROMACS: Fast, Flexible, and Free. *Journal of Computational Chemistry*. John Wiley & Sons, Ltd December 1, 2005, pp 1701–1718. https://doi.org/10.1002/jcc.20291.

(102) Case, D. A.; Darden, T.; Cheatham III, T. E.; Carlos Simmerling; Wang, J.; Duke, R. E.; Crowley, M.; Walker, R.; Zhang, W.; Merz, K.; Wang, B.; Hayik, S.; Roitberg, A.; Seabra, G.; Wong, S. K.; Paesani, F.; Brozell, S.; Steinbrecher, T.; Gohlke, H.; Yang, L.; Tan, C.; Mongan, J.; Hornak, V.; Cui, G.; Mathews, D. H.; Seetin, M. G.; Sagui, C.; Babin, V.; Kollman, P. A. AMBER. University of California: San Fransisco 2008.

(103) Dinh, Q. Van; Vo, T. Q.; Kim, B. H. Viscous Heating and Temperature Profiles of Liquid Water Flows in Copper Nanochannel. *J. Mech. Sci. Technol.* **2019**, *33* (7), 3257–3263. https://doi.org/10.1007/s12206-019-0621-6.

(104) YIN, C. Y.; Mohanad, E. H. Simulation of Liquid Argon Flow along a Nanochannel: Effect of Applied Force. *Chinese J. Chem. Eng.* **2009**, *17* (5), 734–738. https://doi.org/10.1016/S1004-9541(08)60269-4.

(105) Kallman, J. S.; Hoover, W. G.; Hoover, C. G.; De Groot, A. J.; Lee, S. M.; Wooten, F. Molecular Dynamics of Silicon Indentation. *Phys. Rev. B* **1993**, *47* (13), 7705–7709. https://doi.org/10.1103/PhysRevB.47.7705.

(106) Huang, D.; Ma, R.; Zhang, T.; Luo, T. Origin of Hydrophilic Surface Functionalization-Induced Thermal Conductance Enhancement across Solid-Water Interfaces. *ACS Appl. Mater. Interfaces* **2018**, *10* (33). https://doi.org/10.1021/acsami.8b03709.

(107) Maginn, E. J.; Messerly, R. A.; Carlson, D. J.; Roe, D. R.; Elliott, J. R. Best Practices for Computing Transport Properties 1. Self-Diffusivity and Viscosity from Equilibrium Molecular Dynamics [Article v1.0]. *Living J. Comput. Mol. Sci.* **2019**, *1* (1), 1–20. https://doi.org/10.33011/livecoms.1.1.6324.

(108) Schelling, P. K.; Phillpot, S. R.; Keblinski, P. Comparison of Atomic-Level Simulation Methods for Computing Thermal Conductivity. *Phys. Rev. B - Condens. Matter Mater. Phys.* **2002**, *65* (14), 1–12. https://doi.org/10.1103/PhysRevB.65.144306.

(109) Luo, T.; Lloyd, J. R. Enhancement of Thermal Energy Transport across Graphene/Graphite and Polymer Interfaces: A Molecular Dynamics Study. *Adv. Funct. Mater.* **2012**, *22* (12), 2495–2502. https://doi.org/10.1002/adfm.201103048.

(110) Cao, B. Y. Nonequilibrium Molecular Dynamics Calculation of the Thermal Conductivity Based on an Improved Relaxation Scheme. *J. Chem. Phys.* **2008**, *129* (7), 1–8. https://doi.org/10.1063/1.2969762.

(111) Hansen, J.-P.; McDonald, I. R. Static Properties of Liquids: Thermodynamics and Structure. In *Theory of Simple Liquids: with Applications to Soft Matter*; Elsevier: Oxford, 2013; Vol. 1, pp 61–72.

(112) Jamali, S. H.; Wolff, L.; Becker, T. M.; Bardow, A.; Vlugt, T. J. H.; Moultos, O. A. Finite-Size Effects of Binary Mutual Diffusion Coefficients from Molecular Dynamics. *J. Chem. Theory Comput.* **2018**, *14* (5), 2667–2677. https://doi.org/10.1021/acs.jctc.8b00170.

(113) Nazari, M.; Davoodabadi, A.; Huang, D.; Luo, T.; Ghasemi, H. On Interfacial Viscosity in Nanochannels. *Nanoscale* **2020**. https://doi.org/10.1039/D0NR02294B.

(114) Zhang, T.; Luo, T. Giant Thermal Rectification from Polyethylene Nanofiber Thermal Diodes. *Small* **2015**, *11* (36), 4657–4665. https://doi.org/10.1002/smll.201501127.

(115) Wei, X.; Ma, R.; Luo, T. Thermal Conductivity of Polyelectrolytes with Different Counterions. *J. Phys. Chem. C* **2020**, *124* (8), 4483–4488. https://doi.org/10.1021/acs.jpcc.9b11689.

(116) Wei, X.; Zhang, T.; Luo, T. Thermal Energy Transport across Hard-Soft Interfaces. *ACS Energy Lett.* **2017**, *2* (10), 2283–2292. https://doi.org/10.1021/acsenergylett.7b00570.

(117) Wei, X.; Zhang, T.; Luo, T. Molecular Fin Effect from Heterogeneous Self-Assembled Monolayer Enhances Thermal Conductance across Hard-Soft Interfaces. *ACS Appl. Mater. Interfaces* **2017**, *9* (39), 33740–33748. https://doi.org/10.1021/acsami.7b07169.

(118) Zhang, T.; Gans-Forrest, A. R.; Lee, E.; Zhang, X.; Qu, C.; Pang, Y.; Sun, F.; Luo, T. Role of Hydrogen Bonds in Thermal Transport across Hard/Soft Material Interfaces. https://doi.org/10.1021/acsami.6b12073.

(119) Sun, F.; Zhang, T.; Jobbins, M. M.; Guo, Z.; Zhang, X.; Zheng, Z.; Tang, D.; Ptasinska, S.; Luo, T. Molecular Bridge Enables Anomalous Enhancement in Thermal Transport across Hard-Soft Material Interfaces. *Adv. Mater.* **2014**, *26* (35), 6093–6099. https://doi.org/10.1002/adma.201400954.

(120) Ryan, D.; Parviz, B. A.; Linder, V.; Semetey, V.; Sia, S. K.; Su, J.; Mrksich, M.; Whitesides, G. M. Patterning Multiple Aligned Self-Assembled Monolayers Using Light. *Langmuir* **2004**, *20* (21), 9080–9088. https://doi.org/10.1021/la048443u.

(121) Mrksich, M.; Chen, C. S.; Xia, Y.; Dike, L. E.; Ingber, D. E.; Whitesides, G. M. Controlling Cell Attachment on Contoured Surfaces with Self-Assembled Monolayers of Alkanethiolates on Gold. *Proc. Natl. Acad. Sci. U. S. A.* **1996**, *93* (20), 10775–10778. https://doi.org/10.1073/pnas.93.20.10775.

(122) Lane, J. M. D.; Chandross, M.; Stevens, M. J.; Grest, G. S. Water in Nanoconfinement between Hydrophilic Self-Assembled Monolayers. *Langmuir* **2008**, *24* (10), 5209.

(123) Hu, M.; Goicochea, J. V; Michel, B.; Poulikakos, D. Water Nanoconfinement Induced Thermal Enhancement at Hydrophilic Quartz Interfaces. *Nano Lett.* **2010**, *10* (1), 279–285. https://doi.org/10.1021/nl9034658.

(124) Zhang, C.; Lu, P.; Chen, Y. Molecular Dynamics Simulation of Electroosmotic Flow in Rough Nanochannels. *Int. Commun. Heat Mass Transf.* **2014**, *59*, 101–105. https://doi.org/10.1016/j.icheatmasstransfer.2014.10.024.

(125) Tas, N. R.; Haneveld, J.; Jansen, H. V.; Elwenspoek, M.; Van Den Berg, A. Capillary Filling Speed of Water in Nanochannels. *Appl. Phys. Lett.* **2004**, *85* (15), 3274–3276. https://doi.org/10.1063/1.1804602.

(126) Haneveld, J.; Tas, N. R.; Brunets, N.; Jansen, H. V.; Elwenspoek, M. Capillary Filling of Sub- 10 Nm Nanochannels. *J. Appl. Phys.* **2008**, *104* (1). https://doi.org/10.1063/1.2952053.

(127) Mortensen, N. A.; Kristensen, A. Electroviscous Effects in Capillary Filling of Nanochannels. *Appl. Phys. Lett.* **2008**, *92* (6). https://doi.org/10.1063/1.2857470.

(128) Thamdrup, L. H.; Persson, F.; Bruus, H.; Kristensen, A.; Flyvbjerg, H. Experimental Investigation of Bubble Formation during Capillary Filling of Si O2 Nanoslits. *Appl. Phys. Lett.* **2007**, *91* (16). https://doi.org/10.1063/1.2801397.

(129) Chauvet, F.; Geoffroy, S.; Hamoumi, A.; Prat, M.; Joseph, P. Roles of Gas in Capillary Filling of Nanoslits. *Soft Matter* **2012**, *8* (41), 10738–10749. https://doi.org/10.1039/c2sm25982f.

(130) Cao, B. Y.; Chen, M.; Guo, Z. Y. Liquid Flow in Surface-Nanostructured Channels Studied by Molecular Dynamics Simulation. *Phys. Rev. E - Stat. Nonlinear, Soft Matter Phys.* **2006**, *74* (6), 1–7. https://doi.org/10.1103/PhysRevE.74.066311.

(131) Ma, Y.; Xue, S.; Hsu, S. C.; Yeh, L. H.; Qian, S.; Tan, H. Programmable Ionic Conductance in a PH-Regulated Gated Nanochannel. *Phys. Chem. Chem. Phys.* **2014**, *16* (37), 20138–20146. https://doi.org/10.1039/c4cp02349h.

(132) Feng, D.; Li, X.; Wang, X.; Li, J.; Zhang, X. Capillary Filling under Nanoconfinement: The Relationship between Effective Viscosity and Water-Wall Interactions. *Int. J. Heat Mass Transf.* **2018**, *118*, 900–910. https://doi.org/10.1016/j.ijheatmasstransfer.2017.11.049.

(133) Zhu, Y.; Granick, S. Viscosity of Interfacial Water. *Phys. Rev. Lett.* **2001**, *87*, 096104. https://doi.org/10.1103/PhysRevLett.87.096104.

(134) Franzese, G.; Hernando-Martinez, A.; Kumar, P.; Mazza, M. G.; Stokely, K.; Strekalova, E. G.; de los Santos, F.; Stanley, H. E. Phase Transitions and Dynamics of Bulk and Interfacial Water. *J. Phys. Condens. Matter* **2010**, *22*, 284103.

(135) Milischuk, A. A.; Ladanyi, B. M.; Ladanyia, B. M. Structure and Dynamics of Water Confined in Silica Nanopores. *J. Chem. Phys.* **2011**, *135* (17), 174709. https://doi.org/10.1063/1.3657408.

(136) Oh, J. M.; Faez, T.; De Beer, S.; Mugele, F. Capillarity-Driven Dynamics of Water-Alcohol Mixtures in Nanofluidic Channels. *Microfluid. Nanofluidics* **2010**, *9* (1), 123–129. https://doi.org/10.1007/s10404-009-0517-3.

(137) Sousa, J. J.; Afonso, A. M.; Pinho, F. T.; Alves, M. A. Effect of the Skimming Layer on Electro-Osmotic-Poiseuille Flows of Viscoelastic Fluids. *Microfluid. Nanofluidics* **2011**, *10* (1), 107–122. https://doi.org/10.1007/s10404-010-0651-y.

(138) Lee, J. W.; Nilson, R. H.; Templeton, J. A.; Griffiths, S. K.; Kung, A.; Wong, B. M. Comparison of Molecular Dynamics with Classical Density Functional and Poisson-Boltzmann Theories of the Electric Double Layer in Nanochannels. *J. Chem. Theory Comput.* **2012**, *8* (6), 2012–2022. https://doi.org/10.1021/ct3001156.

(139) Thompson, P. A.; Robbins, M. O. Shear Flow near Solids: Epitaxial Order and Flow Boundary Conditions. *Phys. Rev. A At., Mol., Opt. Phys.* **1990**, *41* (12), 6830.

(140) Thompson, P. A.; Troian, S. M. A General Boundary Condition for Liquid Flow at Solid Surfaces. *Nature* **1997**, *389* (6649), 360.

(141) Thomas, M.; Corry, B.; Hilder, T. A. What Have We Learnt about the Mechanisms of Rapid Water Transport, Ion Rejection and Selectivity in Nanopores from Molecular Simulation? *Small* **2014**, *10*, 1453.

(142) Wagemann, E.; Oyarzua, E.; Walther, J. H.; Zambrano, H. A. Slip Divergence of Water Flow in Graphene Nanochannels: The Role of Chirality. *Phys. Chem. Chem. Phys.* **2017**, *19* (13), 8646.

(143) Zhu, Y.; Granick, S. Rate-Dependent Slip of Newtonian Liquid at Smooth Surfaces. *Phys. Rev. Lett.* **2001**, *87* (9), 96105.

(144) Priezjev, N. V. Shear Rate Threshold for the Boundary Slip in Dense Polymer Films. *Phys. Rev. E* **2009**, *80* (3), 31608.

(145) Priezjev, N. V. Relationship between Induced Fluid Structure and Boundary Slip in Nanoscale Polymer Films. *Phys. Rev. E* **2010**, *82* (5), 51603.

(146) Priezjev, N. V; Troian, S. M. Molecular Origin and Dynamic Behavior of Slip in Sheared Polymer Films. *Phys. Rev. Lett.* **2004**, *92* (1), 18302.

(147) Ewen, J. P.; Gattinoni, C.; Zhang, J.; Heyes, D. M.; Spikes, H. A.; Dini, D. On the Effect of Confined Fluid Molecular Structure on Nonequilibrium Phase Behaviour and Friction. *Phys. Chem. Chem. Phys.* **2017**, *19* (27), 17883.

(148) Corry, B. Designing Carbon Nanotube Membranes for Efficient Water Desalination. *J. Phys. Chem. B* **2008**, *112* (5), 1427–1434. https://doi.org/10.1021/jp709845u.

(149) Hummer, G.; Rasaiah, J. C.; Noworyta, J. P. Water Conduction through the Hydrophobic Channel of a Carbon Nanotube. *Nature* **2001**, *414* (6860), 188–190. https://doi.org/10.1038/35102535.

(150) Joseph, S.; Aluru, N. R. Why Are Carbon Nanotubes Fast Transporters of Water? *Nano Lett.* **2008**, *8* (2), 452–458. https://doi.org/10.1021/nl072385q.

(151) Majumder, M.; Chopra, N.; Andrews, R.; Hinds, B. J. Enhanced Flow in Carbon Nanotubes. *Nature* **2005**, *438* (7064), 44–44. https://doi.org/10.1038/43844a.

(152) Holt, J. K.; Park, H. G.; Wang, Y.; Stadermann, M.; Artyukhin, A. B.; Grigoropoulos, C. P.; Noy, A.; Bakajin, O. Fast Mass Transport through Sub-2-Nanometer Carbon Nanotubes. *Science (80-. ).* **2006**, *312* (5776), 1034–1037. https://doi.org/10.1126/science.1126298.

(153) Secchi, E.; Marbach, S.; Niguès, A.; Stein, D.; Siria, A.; Bocquet, L. Massive Radius-Dependent Flow Slippage in Carbon Nanotubes. *Nature* **2016**, *537* (7619), 210–213. https://doi.org/10.1038/nature19315.

(154) Falk, K.; Sedlmeier, F.; Joly, L.; Netz, R. R.; Bocquet, L. Molecular Origin of Fast Water Transport in Carbon Nanotube Membranes: Superlubricity *versus* Curvature Dependent Friction. *Nano Lett.* **2010**, *10* (10), 4067–4073. https://doi.org/10.1021/nl1021046.

(155) Babu, J. S.; Sathian, S. P. Combining Molecular Dynamics Simulation and Transition State Theory to Evaluate Solid-Liquid Interfacial Friction in Carbon Nanotube Membranes. *Phys. Rev. E* **2012**, *85* (5), 1–8. https://doi.org/10.1103/physreve.85.051205.

(156) Ma, M.; Grey, F.; Shen, L.; Urbakh, M.; Wu, S.; Liu, J. Z.; Liu, Y.; Zheng, Q. Water Transport Inside Carbon Nanotubes Mediated by Phonon-Induced Oscillating Friction. *J. Chem. Phys.* **2015**, *10*, 692.

(157) Suk, M. E.; Aluru, N. R. Modeling Water Flow Through Carbon Nanotube Membranes with Entrance/Exit Effects. *Nanoscale Microscale Thermophys. Eng.* **2017**, *21* (4), 247–262. https://doi.org/10.1080/15567265.2017.1355949.

(158) Walther, J. H.; Ritos, K.; Cruz-Chu, E. R.; Megaridis, C. M.; Koumoutsakos, P. Barriers to Superfast Water Transport in Carbon Nanotube Membranes. *Nano Lett.* **2013**, *13*, 1910.

(159) Ortiz-Young, D.; Chiu, H. C.; Kim, S.; Voïtchovsky, K.; Riedo, E. The Interplay between Apparent Viscosity and Wettability in Nanoconfined Water. *Nat. Commun.* **2013**, *4*. https://doi.org/10.1038/ncomms3482.

(160) Joseph, P.; Cottin-Bizonne, C.; Benoît, J. M.; Ybert, C.; Journet, C.; Tabeling, P.; Bocquet, L. Slippage of Water Past Superhydrophobic Carbon Nanotube Forests in Microchannels. *Phys. Rev. Lett.* **2006**, *97* (15), 1–4. https://doi.org/10.1103/PhysRevLett.97.156104.

(161) Thomas, J. A.; McGaughey, A. J. H. Reassessing Fast Water Transport through Carbon Nanotubes. *Nano Lett.* **2008**, *8* (9), 2788–2793. https://doi.org/10.1021/nl8013617.

(162) Ma, M. D.; Shen, L.; Sheridan, J.; Liu, J. Z.; Chen, C.; Zheng, Q. Friction of Water Slipping in Carbon Nanotubes. *Phys. Rev. E - Stat. Nonlinear, Soft Matter Phys.* **2011**, *83* (3), 1–7. https://doi.org/10.1103/PhysRevE.83.036316.

(163) Borg, M. K.; Reese, J. M. Multiscale Simulation of Enhanced Water Flow in Nanotubes. *MRS*

*Bull.* **2017**, *42*, 294.

(164) Uddin, N. M.; Capaldi, F. M.; Farouk, B. Molecular Dynamics Simulations of Carbon Nanotube Dispersions in Water: Effects of Nanotube Length, Diameter, Chirality and Surfactant Structures. *Comput. Mater. Sci.* **2012**, *53* (1), 133–144. https://doi.org/10.1016/j.commatsci.2011.07.041.

(165) Werder, T.; Walther, J. H.; Jaffe, R. L.; Halicioglu, T.; Noca, F.; Koumoutsakos, P. Molecular Dynamics Simulation of Contact Angles of Water Droplets in Carbon Nanotubes. *Nano Lett.* **2001**, *1* (12), 697–702. https://doi.org/10.1021/nl015640u.

(166) Wan, R.; Li, J.; Lu, H.; Fang, H. Controllable Water Channel Gating of Nanometer Dimensions. *J. Am. Chem. Soc.* **2005**, *127* (19), 7166–7170. https://doi.org/10.1021/ja050044d.

(167) Zou, J.; Ji, B.; Feng, X. Q.; Gao, H. Self-Assembly of Single-Walled Carbon Nanotubes into Multi Walled Carbon Nanotubes in Water: Molecular Dynamics Simulations. *Nano Lett.* **2006**, *6* (3), 430–434. https://doi.org/10.1021/nl052289u.

(168) Vijayaraghavan, V.; Wong, C. H. Torsional Characteristics of SingleWalled Carbon Nanotube with Water Interactions by Using Molecular Dynamics Simulation. *Nano-Micro Lett.* **2014**, *6* (3), 268–279. https://doi.org/10.1007/BF03353791.

(169) Ganjiani, S. H.; Hossein Nezhad, A. Molecular Dynamics Simulation of a Nanofluidic Energy Absorption System: Effects of the Chiral Vector of Carbon Nanotubes. *Phys. Chem. Chem. Phys.* **2018**, *20* (7), 5140–5148. https://doi.org/10.1039/c7cp07395j.

(170) Zambrano, H. A.; Walther, J. H.; Koumoutsakos, P.; Sbalzarini, I. F. Thermophoretic Motion of Water Nanodroplets Confined inside Carbon Nanotubes. *Nano Lett.* **2009**, *9* (1), 66–71. https://doi.org/10.1021/nl802429s.

(171) Feng, J. W.; Ding, H. M.; Ren, C. L.; Ma, Y. Q. Pumping of Water by Rotating Chiral Carbon Nanotube. *Nanoscale* **2014**, *6* (22), 13606–13612. https://doi.org/10.1039/c4nr03407d.

(172) Sam, A.; Vishnu Prasad, K.; Sathian, S. P. Water Flow in Carbon Nanotubes: The Role of Tube Chirality. *Phys. Chem. Chem. Phys.* **2019**, *21* (12), 6566–6573. https://doi.org/10.1039/c9cp00429g.

(173) Liu, B.; Li, X.; Li, B.; Xu, B.; Zhao, Y. Carbon Nanotube Based Artificial Water Channel Protein: Membrane Perturbation and Water Transportation. *Nano Lett.* **2009**, *9* (4), 1386–1394. https://doi.org/10.1021/nl8030339.

(174) Zuo, G.; Shen, R.; Ma, S.; Guo, W. Transport Properties of Single-File Water Molecules inside a Carbon Nanotube Biomimicking Water Channel. *ACS Nano* **2010**, *4* (1), 205–210. https://doi.org/10.1021/nn901334w.

(175) Lee, K. P.; Leese, H.; Mattia, D. Water Flow Enhancement in Hydrophilic Nanochannels. *Nanoscale* **2012**, *4* (8), 2621–2627. https://doi.org/10.1039/c2nr30098b.

(176) Murad, S.; Luo, L.; Chu, L. Y. Anomalous Flow Behavior in Nanochannels: A Molecular Dynamics Study. *Chem. Phys. Lett.* **2010**, *492* (4–6), 285–289. https://doi.org/10.1016/j.cplett.2010.04.070.

(177) Dai, H.; Xu, Z.; Yang, X. Water Permeation and Ion Rejection in Layer-by-Layer Stacked Graphene Oxide Nanochannels: A Molecular Dynamics Simulation. *J. Phys. Chem. C* **2016**, *120* (39), 22585–22596. https://doi.org/10.1021/acs.jpcc.6b05337.

(178) Yang, Y.; Dementyev, P.; Biere, N.; Emmrich, D.; Stohmann, P.; Korzetz, R.; Zhang, X.; Beyer, A.; Koch, S.; Anselmetti, D.; Gölzhäuser, A. Rapid Water Permeation through Carbon Nanomembranes with Sub-Nanometer Channels. *ACS Nano* **2018**, *12* (5), 4695–4701. https://doi.org/10.1021/acsnano.8b01266.

(179) Liu, Y.; Wang, Q.; Lu, L. Transport Properties and Distribution of Water Molecules Confined in Hydrophobic Nanopores and Nanoslits. *Langmuir* **2004**, *20* (16), 6921–6926. https://doi.org/10.1021/la036325l.

(180) Zaragoza, A.; Gonzalez, M. A.; Joly, L.; López-Montero, I.; Canales, M. A.; Benavides, A. L.; Valeriani, C. Molecular Dynamics Study of Nanoconfined TIP4P/2005 Water: How Confinement and Temperature Affect Diffusion and Viscosity. *Phys. Chem. Chem. Phys.* **2019**, *21* (25), 13653–13667. https://doi.org/10.1039/c9cp02485a.

(181) Kim, D.; Darve, E. Molecular Dynamics Simulation of Electro-Osmotic Flows in Rough Wall Nanochannels. https://doi.org/10.1103/PhysRevE.73.051203.

(182) Kannam, S. K.; Daivis, P. J.; Todd, B. D. Modeling Slip and Flow Enhancement of Water in Carbon Nanotubes. *MRS Bull.* **2017**, *42*, 283.

(183) Guo, W.; Cheng, C.; Wu, Y.; Jiang, Y.; Gao, J.; Li, D.; Jiang, L. Bio-Inspired Two-Dimensional Nanofluidic Generators Based on a Layered Graphene Hydrogel Membrane. *Adv. Mater.* **2013**, *25* (42), 6064–6068. https://doi.org/10.1002/adma.201302441.

(184) Kamitani, A.; Morishita, S.; Kotaki, H.; Arscott, S. Microfabricated Microfluidic Fuel Cells. *Sensors Actuators, B Chem.* **2011**, *154* (2), 174–180. https://doi.org/10.1016/j.snb.2009.11.014.

(185) Storm, M. M.; Johnsen, R. E.; Younesi, R.; Norby, P. Capillary Based Li-Air Batteries for *in Situ* Synchrotron X-Ray Powder Diffraction Studies. *J. Mater. Chem. A* **2015**, *3* (6), 3113–3119. https://doi.org/10.1039/c4ta04291c.

(186) Davoodabadi, A.; Li, J.; Liang, Y.; Wood, D. L.; Singler, T. J.; Jin, C. Analysis of Electrolyte Imbibition through Lithium-Ion Battery Electrodes. *J. Power Sources* **2019**, *424*, 193–203. https://doi.org/10.1016/j.jpowsour.2019.03.115.

(187) Gostick, J. T.; Ioannidis, M. A.; Fowler, M. W.; Pritzker, M. D. Wettability and Capillary Behavior of Fibrous Gas Diffusion Media for Polymer Electrolyte Membrane Fuel Cells. *J. Power Sources* **2009**, *194* (1), 433–444. https://doi.org/10.1016/j.jpowsour.2009.04.052.

(188) Liu, S.; Pu, Q.; Gao, L.; Korzeniewski, C.; Matzke, C. From Nanochannel-Induced Proton Conduction Enhancement to a Nanochannel-Based Fuel Cell. *Nano Lett.* **2005**, *5* (7), 1389–1393. https://doi.org/10.1021/nl050712t.

(189) Kim, S. J.; Ko, S. H.; Kang, K. H.; Han, J. Direct Seawater Desalination by Ion Concentration Polarization. *Nat. Nanotechnol.* **2010**, *5* (4), 297–301. https://doi.org/10.1038/nnano.2010.34.

(190) Liu, Y.; Lou, J.; Ni, M.; Song, C.; Wu, J.; Dasgupta, N. P.; Tao, P.; Shang, W.; Deng, T. Bioinspired Bifunctional Membrane for Efficient Clean Water Generation. *ACS Appl. Mater. Interfaces* **2016**, *8* (1), 772–779. https://doi.org/10.1021/acsami.5b09996.

(191) Werber, J. R.; Elimelech, M. Permselectivity Limits of Biomimetic Desalination Membranes. *Sci. Adv.* **2018**, *4* (6). https://doi.org/10.1126/sciadv.aar8266.

(192) Cho, H. J.; Preston, D. J.; Zhu, Y.; Wang, E. N. Nanoengineered Materials for Liquid-Vapour Phase-Change Heat Transfer. *Nat. Rev. Mater.* **2016**, *2* (2), 1–17. https://doi.org/10.1038/natrevmats.2016.92.

(193) Nazari, M.; Masoudi, A.; Jafari, P.; Irajizad, P.; Kashyap, V.; Ghasemi, H. Ultrahigh Evaporative Heat Fluxes in Nanoconfined Geometries. *Langmuir* **2019**, *35* (1), 78–85. https://doi.org/10.1021/acs.langmuir.8b03463.

(194) Li, J.; Fu, W.; Zhang, B.; Zhu, G.; Miljkovic, N. Ultrascalable Three-Tier Hierarchical Nanoengineered Surfaces for Optimized Boiling. *ACS Nano* **2019**, *13* (12), 14080–14093. https://doi.org/10.1021/acsnano.9b06501.

(195) Farokhnia, N.; Sajadi, S. M.; Irajizad, P.; Ghasemi, H. Decoupled Hierarchical Structures for Suppression of Leidenfrost Phenomenon. *Langmuir* **2017**, *33* (10), 2541–2550. https://doi.org/10.1021/acs.langmuir.7b00163.

(196) Xue, Y.; Markmann, J.; Duan, H.; Weissmüller, J.; Huber, P. Switchable Imbibition in Nanoporous Gold. *Nat. Commun.* **2014**, *5*. https://doi.org/10.1038/ncomms5237.

(197) de Gennes, P. G.; Brochard-Wyart, F.; Quere, D. Wetting and Long-Range Forces. In *Capillarity and Wetting Phenomena: Drops, Bubbles, Pearls, Waves*; Springer: New York, 2013; Vol. 1, pp 87–103.

(198) Nomura, K.; Kaneko, T.; Bai, J.; Francisco, J. S.; Yasuoka, K.; Zeng, X. C. Evidence of Low-Density and High-Density Liquid Phases and Isochore End Point for Water Confined to Carbon Nanotube. *Proc. Natl. Acad. Sci. U. S. A.* **2017**, *114* (16), 4066–4071. https://doi.org/10.1073/pnas.1701609114.

(199) Tretheway, D. C.; Meinhart, C. D. Apparent Fluid Slip at Hydrophobic Microchannel Walls. *Phys. Fluids* **2002**, *14* (3). https://doi.org/10.1063/1.1432696.

(200) Voronov, R. S.; Papavassiliou, D. V.; Lee, L. L. Boundary Slip and Wetting Properties of Interfaces: Correlation of the Contact Angle with the Slip Length. *J. Chem. Phys.* **2006**, *124* (20), 204701. https://doi.org/10.1063/1.2194019.

(201) Tsai, P.; Peters, A. M.; Pirat, C.; Wessling, M.; Lammertink, R. G. H.; Lohse, D. Quantifying Effective Slip Length over Micropatterned Hydrophobic Surfaces. *Phys. Fluids* **2009**, *21* (11), 1–8. https://doi.org/10.1063/1.3266505.

(202) Israelachvili, J.; Wennerstrom, H. Role of Hydration and Water Structure in Biological and Colloidal Interactions. *Nature* **1996**, *379*, 219–225.

(203) Kelly, S.; Torres-Verdín, C.; Balhoff, M. T. Anomalous Liquid Imbibition at the Nanoscale: The Critical Role of Interfacial Deformations. *Nanoscale* **2016**, *8* (5), 2751–2767. https://doi.org/10.1039/c5nr04462f.

(204) Deroche, I.; Daou, T. J.; Picard, C.; Coasne, B. Reminiscent Capillarity in Subnanopores. *Nat. Commun.* **2019**, *10* (1), 1–10. https://doi.org/10.1038/s41467-019-12418-9.

(205) Perez Sirkin, Y. A.; Tagliazucchi, M.; Szleifer, I. Transport in Nanopores and Nanochannels: Some Fundamental Challenges and Nature-Inspired Solutions. *Mater. Today Adv.* **2020**, *5*, 100047. https://doi.org/10.1016/j.mtadv.2019.100047.

(206) Jiao, S.; Xu, Z. Non-Continuum Intercalated Water Diffusion Explains Fast Permeation through Graphene Oxide Membranes. *ACS Nano* **2017**, *11* (11), 11152–11161. https://doi.org/10.1021/acsnano.7b05419.

(207) Wu, K.; Chen, Z.; Li, J.; Li, X.; Xu, J.; Dong, X. Wettability Effect on Nanoconfined Water Flow. *Proc. Natl. Acad. Sci. U. S. A.* **2017**, *114* (13), 3358–3363. https://doi.org/10.1073/pnas.1612608114.

(208) Heinbuch, U.; Fischer, J. Liquid Flow in Pores: Slip, No-Slip, or Multilayer Sticking. *Phys. Rev. A* **1989**, *40* (2), 1144–1146. https://doi.org/10.1103/PhysRevA.40.1144.

(209) Thompson, P. A.; Robbins, M. O. Origin of Stick-Slip Motion in Boundary Lubrication. *Science (80-. ).* **1990**, *250* (4982), 792–794. https://doi.org/10.1126/science.250.4982.792.

(210) Raviv, U.; Laurat, P.; Klein, J. Fluidity of Water Confined to Subnanometre Films. *Nature* **2001**, *413* (6851), 51–54. https://doi.org/10.1038/35092523.

(211) Feibelman, P. J. Viscosity of Ultrathin Water Films Confined between Aluminol Surfaces of

Kaolinite: *ab Initio* Simulations. *J. Phys. Chem. C* **2013**, *117* (12), 6088–6095. https://doi.org/10.1021/jp312152h.

(212) Govind Rajan, A.; Strano, M. S.; Blankschtein, D. Liquids with Lower Wettability Can Exhibit Higher Friction on Hexagonal Boron Nitride: The Intriguing Role of Solid-Liquid Electrostatic Interactions. *Nano Lett.* **2019**, *19* (3), 1539–1551. https://doi.org/10.1021/acs.nanolett.8b04335.

(213) Huang, D. M.; Sendner, C.; Horinek, D.; Netz, R. R.; Bocquet, L. Water Slippage *versus* Contact Angle: A Quasiuniversal Relationship. *Phys. Rev. Lett.* **2008**, *101* (22), 226101. https://doi.org/10.1103/PhysRevLett.101.226101.

(214) Majumder, M.; Chopra, N.; Hinds, B. J. Mass Transport through Carbon Nanotube Membranes in Three Different Regimes: Ionic Diffusion and Gas and Liquid Flow. *ACS Nano* **2011**, *5* (5), 3867–3877. https://doi.org/10.1021/nn200222g.

(215) Suk, M. E.; Raghunathan, A. V.; Aluru, N. R. Fast Reverse Osmosis Using Boron Nitride and Carbon Nanotubes. *Appl. Phys. Lett.* **2008**, *92* (13), 133120. https://doi.org/10.1063/1.2907333.

(216) Hilder, T. A.; Gordon, D.; Chung, S. H. Salt Rejection and Water Transport through Boron Nitride Nanotubes. *Small* **2009**, *5* (19), 2183–2190. https://doi.org/10.1002/smll.200900349.

(217) Tocci, G.; Joly, L.; Michaelides, A. Friction of Water on Graphene and Hexagonal Boron Nitride from *ab Initio* Methods: Very Different Slippage despite Very Similar Interface Structures. *Nano Lett.* **2014**, *14* (12), 6872–6877. https://doi.org/10.1021/nl502837d.

(218) Xie, Q.; Alibakhshi, M. A.; Jiao, S.; Xu, Z.; Hempel, M.; Kong, J.; Park, H. G.; Duan, C. Fast Water Transport in Graphene Nanofluidic Channels. *Nat. Nanotechnol.* **2018**, *13* (3), 238–245. https://doi.org/10.1038/s41565-017-0031-9.

(219) Agre, P.; King, L. S.; Yasui, M.; Guggino, W. B.; Ottersen, O. P.; Fujiyoshi, Y.; Engel, A.; Nielsen, S. Aquaporin Water Channels - from Atomic Structure to Clinical Medicine. *J. Physiol.* **2002**, *542* (1), 3–16. https://doi.org/10.1113/jphysiol.2002.020818.

(220) Tang, C. Y.; Zhao, Y.; Wang, R.; Hélix-Nielsen, C.; Fane, a. G. Desalination by Biomimetic Aquaporin Membranes: Review of Status and Prospects. *Desalination* **2013**, *308*, 34–40. https://doi.org/10.1016/j.desal.2012.07.007.

(221) Marbach, S.; Dean, D. S.; Bocquet, L. Transport and Dispersion across Wiggling Nanopores. *Nat. Phys.* **2018**, *14* (11), 1108–1113. https://doi.org/10.1038/s41567-018-0239-0.

(222) Shen, Y. X.; Si, W.; Erbakan, M.; Decker, K.; De Zorzi, R.; Saboe, P. O.; Kang, Y. J.; Majd, S.; Butler, P. J.; Walz, T.; Aksimentiev, A.; Hou, J. L.; Kumar, M.; Weitz, D. A. Highly Permeable Artificial Water Channels That Can Self-Assemble into Two-Dimensional Arrays. *Proc. Natl. Acad. Sci. U. S. A.* **2015**, *112* (32), 9810–9815. https://doi.org/10.1073/pnas.1508575112.

(223) Park, H. G.; Jung, Y. Carbon Nanofluidics of Rapid Water Transport for Energy Applications. *Chem. Soc. Rev.* **2014**, *43* (2), 565–576. https://doi.org/10.1039/c3cs60253b.

(224) Tunuguntla, R. H.; Henley, R. Y.; Yao, Y. C.; Pham, T. A.; Wanunu, M.; Noy, A. Enhanced Water Permeability and Tunable Ion Selectivity in Subnanometer Carbon Nanotube Porins. *Science (80-. ).* **2017**, *357* (6353), 792–796. https://doi.org/10.1126/science.aan2438.

(225) Fan, R.; Huh, S.; Yan, R.; Arnold, J.; Yang, P. Gated Proton Transport in Aligned Mesoporous Silica Films. *Nat. Mater.* **2008**, *7* (4), 303–307. https://doi.org/10.1038/nmat2127.

(226) Duan, C.; Majumdar, A. Anomalous Ion Transport in 2-Nm Hydrophilic Nanochannels. *Nat. Nanotechnol.* **2010**, *5* (12), 848–852. https://doi.org/10.1038/nnano.2010.233.

(227) Wu, K.; Chen, Z.; Xu, J.; Hu, Y.; Li, J.; Dong, X.; Liu, Y.; Chen, M. A Universal Model of Water

Flow through Nanopores in Unconventional Reservoirs: Relationships between Slip, Wettability and Viscosity. In *Proceedings - SPE Annual Technical Conference and Exhibition*; Society of Petroleum Engineers (SPE), 2016; Vol. 2016-January. https://doi.org/10.2118/181543-ms.

(228) Phan, V. N.; Nguyen, N. T.; Yang, C.; Joseph, P.; Djeghlaf, L.; Bourrier, D.; Gue, A. M. Capillary Filling in Closed End Nanochannels. *Langmuir* **2010**, *26* (16), 13251–13255. https://doi.org/10.1021/la1010902.

(229) Shaat, M.; Zheng, Y. Fluidity and Phase Transitions of Water in Hydrophobic and Hydrophilic Nanotubes. *Sci. Rep.* **2019**, *9* (1), 1–12. https://doi.org/10.1038/s41598-019-42101-4.

(230) Kelly, S.; Balhoff, M. T.; Torres-Verdín, C. Quantification of Bulk Solution Limits for Liquid and Interfacial Transport in Nanoconfinements. *Langmuir* **2015**, *31* (7), 2167–2179. https://doi.org/10.1021/la504742w.

(231) Chen, X.; Cao, G.; Han, A.; Punyamurtula, V. K.; Liu, L.; Culligan, P. J.; Kim, T.; Qiao, Y. Nanoscale Fluid Transport: Size and Rate Effects. *Nano Lett.* **2008**, *8* (9), 2988–2992. https://doi.org/10.1021/nl802046b.

(232) Liu, Y.; Wang, Q.; Wu, T.; Zhang, L. Fluid Structure and Transport Properties of Water inside Carbon Nanotubes. *J. Chem. Phys.* **2005**, *123* (23), 234701. https://doi.org/10.1063/1.2131070.

(233) Qin, Z.; Buehler, M. J. Nonlinear Viscous Water at Nanoporous Two-Dimensional Interfaces Resists High-Speed Flow through Cooperativity. *Nano Lett.* **2015**, *15* (6), 3939–3944. https://doi.org/10.1021/acs.nanolett.5b00809.

(234) Wei, N.; Peng, X.; Xu, Z. Breakdown of Fast Water Transport in Graphene Oxides. *Phys. Rev. E - Stat. Nonlinear, Soft Matter Phys.* **2014**, *89* (1), 012113. https://doi.org/10.1103/PhysRevE.89.012113.

(235) Haria, N. R.; Grest, G. S.; Lorenz, C. D. Viscosity of Nanoconfined Water between Hydroxyl Basal Surfaces of Kaolinite: Classical Simulation Results. *J. Phys. Chem. C* **2013**, *117* (12), 6096–6104. https://doi.org/10.1021/jp312181u.

(236) Babu, J. S.; Sathian, S. P. The Role of Activation Energy and Reduced Viscosity on the Enhancement of Water Flow through Carbon Nanotubes. *J. Chem. Phys.* **2011**, *134* (19), 194509. https://doi.org/10.1063/1.3592532.

(237) Stavarache, I.; Lepadatu, A. M.; Teodorescu, V. S.; Ciurea, M. L.; Iancu, V.; Dragoman, M.; Konstantinidis, G.; Buiculescu, R. Electrical Behavior of Multi-Walled Carbon Nanotube Network Embedded in Amorphous Silicon Nitride. *Nanoscale Res. Lett.* **2011**, *6* (1). https://doi.org/10.1186/1556-276X-6-87.

(238) Zhang, H.; Ye, H.; Zheng, Y.; Zhang, Z. Prediction of the Viscosity of Water Confined in Carbon Nanotubes. *Microfluid. Nanofluidics* **2011**, *10* (2), 403–414. https://doi.org/10.1007/s10404-010-0678-0.

(239) Petravic, J.; Harrowell, P. Spatial Dependence of Viscosity and Thermal Conductivity through a Planar Interface. *J. Phys. Chem. B* **2009**, *113* (7), 2059–2065. https://doi.org/10.1021/jp807254b.

(240) Wu, K.; Chen, Z.; Li, J.; Xu, J.; Wang, K.; Wang, S.; Dong, X.; Zhu, Z.; Peng, Y.; Jia, X.; Li, X. Manipulating the Flow of Nanoconfined Water by Temperature Stimulation. *Angew. Chemie - Int. Ed.* **2018**, *57* (28), 8432–8437. https://doi.org/10.1002/anie.201712915.

(241) Geng, X.; Yu, M.; Zhang, W.; Liu, Q.; Yu, X.; Lu, Y. Slip Length and Structure of Liquid Water Flowing Past Atomistic Smooth Charged Walls. *Sci. Rep.* **2019**, *9* (1), 1–8. https://doi.org/10.1038/s41598-019-55491-2.

(242) Scorrano, G.; Bruno, G.; Di Trani, N.; Ferrari, M.; Pimpinelli, A.; Grattoni, A. Gas Flow at the

Ultra-Nanoscale: Universal Predictive Model and Validation in Nanochannels of Ångstrom-Level Resolution. *ACS Appl. Mater. Interfaces* **2018**, *10* (38), 32233–32238. https://doi.org/10.1021/acsami.8b11455.

(243) Cheng, C.; Jiang, G.; Simon, G. P.; Liu, J. Z.; Li, D. Low-Voltage Electrostatic Modulation of Ion Diffusion through Layered Graphene-Based Nanoporous Membranes. *Nat. Nanotechnol.* **2018**, *13* (8), 685–690. https://doi.org/10.1038/s41565-018-0181-4.

(244) Hwang, J.; Daiguji, H. Ion Transport in Sub-10 Nm Nanofluidic Channels: Synthesis, Measurement, and Modeling. *Isr. J. Chem.* **2014**, *54* (11–12), 1509–1518. https://doi.org/10.1002/ijch.201400088.

(245) Vermesh, U.; Choi, J. W.; Vermesh, O.; Fan, R.; Nagarah, J.; Heath, J. R. Fast Nonlinear Ion Transport *via* Field-Induced Hydrodynamic Slip in Sub-20-Nm Hydrophilic Nanofluidic Transistors. *Nano Lett.* **2009**, *9* (4), 1315–1319. https://doi.org/10.1021/nl802931r.

(246) Xie, Q.; Xin, F.; Park, H. G.; Duan, C. Ion Transport in Graphene Nanofluidic Channels. *Nanoscale* **2016**, *8* (47), 19527–19535. https://doi.org/10.1039/C6NR06977K.

(247) Jung, W.; Kim, J.; Kim, S.; Park, H. G.; Jung, Y.; Han, C. S. A Novel Fabrication of 3.6 Nm High Graphene Nanochannels for Ultrafast Ion Transport. *Adv. Mater.* **2017**, *29* (17). https://doi.org/10.1002/adma.201605854.

(248) Agmon, N. The Grotthuss Mechanism. *Chem. Phys. Lett.* **1995**, *244* (5–6), 456–462. https://doi.org/10.1016/0009-2614(95)00905-J.

(249) Bruno, G.; Di Trani, N.; Hood, R. L.; Zabre, E.; Filgueira, C. S.; Canavese, G.; Jain, P.; Smith, Z.; Demarchi, D.; Hosali, S.; Pimpinelli, A.; Ferrari, M.; Grattoni, A. Unexpected Behaviors in Molecular Transport through Size-Controlled Nanochannels down to the Ultra-Nanoscale. *Nat. Commun.* **2018**, *9* (1), 1–10. https://doi.org/10.1038/s41467-018-04133-8.

(250) Wen, L.; Hou, X.; Tian, Y.; Nie, F. Q.; Song, Y.; Zhai, J.; Jiang, L. Bioinspired Smart Gating of Nanochannels toward Photoelectric-Conversion Systems. *Adv. Mater.* **2010**, *22* (9), 1021–1024. https://doi.org/10.1002/adma.200903161.

(251) Sun, Y.; Zhang, F.; Quan, J.; Zhu, F.; Hong, W.; Ma, J.; Pang, H.; Sun, Y.; Tian, D.; Li, H. A Biomimetic Chiral-Driven Ionic Gate Constructed by Pillar[6]Arene-Based Host-Guest Systems. *Nat. Commun.* **2018**, *9* (1), 1–7. https://doi.org/10.1038/s41467-018-05103-w.

(252) Guan, W.; Li, S. X.; Reed, M. A. Voltage Gated Ion and Molecule Transport in Engineered Nanochannels: Theory, Fabrication and Applications. *Nanotechnology* **2014**, *25* (12). https://doi.org/10.1088/0957-4484/25/12/122001.

(253) Sun, L.; Zhou, L.; Yan, F.; Su, B. Ionic Strength Gated Redox Current Rectification by Ferrocene Grafted in Silica Nanochannels. *Langmuir* **2019**, *35* (45), 14486–14491. https://doi.org/10.1021/acs.langmuir.9b02734.

(254) Sheng, Z.; Wang, H.; Tang, Y.; Wang, M.; Huang, L.; Min, L.; Meng, H.; Chen, S.; Jiang, L.; Hou, X. Liquid Gating Elastomeric Porous System with Dynamically Controllable Gas/Liquid Transport. *Sci. Adv.* **2018**, *4* (2), 1–10. https://doi.org/10.1126/sciadv.aao6724.

(255) Liu, P.; Xie, G.; Li, P.; Zhang, Z.; Yang, L.; Zhao, Y.; Zhu, C.; Kong, X. Y.; Jiang, L.; Wen, L. A Universal Tunable Nanofluidic Diode *via* Photoresponsive Host–Guest Interactions. *NPG Asia Mater.* **2018**, *10* (8), 849–857. https://doi.org/10.1038/s41427-018-0079-5.

(256) Smirnov, S. N.; Vlassiouk, I. V.; Lavrik, N. V. Voltage-Gated Hydrophobic Nanopores. *ACS Nano* **2011**, *5* (9), 7453–7461. https://doi.org/10.1021/nn202392d.

(257) Hou, X.; Hu, Y.; Grinthal, A.; Khan, M.; Aizenberg, J. Liquid-Based Gating Mechanism with

Tunable Multiphase Selectivity and Antifouling Behaviour. *Nature* **2015**, *519* (7541), 70–73. https://doi.org/10.1038/nature14253.

(258) Xu, Y.; Shinomiya, M.; Harada, A. Soft Matter-Regulated Active Nanovalves Locally Self-Assembled in Femtoliter Nanofluidic Channels. *Adv. Mater.* **2016**, *28* (11), 2209–2216. https://doi.org/10.1002/adma.201505132.

(259) Xie, G.; Li, P.; Zhao, Z.; Zhu, Z.; Kong, X. Y.; Zhang, Z.; Xiao, K.; Wen, L.; Jiang, L. Light- and Electric-Field-Controlled Wetting Behavior in Nanochannels for Regulating Nanoconfined Mass Transport. *J. Am. Chem. Soc.* **2018**, *140* (13), 4552–4559. https://doi.org/10.1021/jacs.7b13136.

(260) Xiao, K.; Zhou, Y.; Kong, X.-Y.; Xie, G.; Li, P.; Zhang, Z.; Wen, L.; Jiang, L. Electrostatic-Charge- and Electric-Field-Induced Smart Gating for Water Transportation. *ACS Nano* **2016**, *10* (10), 9703–9709. https://doi.org/10.1021/acsnano.6b05682.

(261) Wen, L.; Hou, X.; Tian, Y.; Zhai, J.; Jiang, L. Bio-Inspired Photoelectric Conversion Based on Smart-Gating Nanochannels. *Adv. Funct. Mater.* **2010**, *20* (16), 2636–2642. https://doi.org/10.1002/adfm.201000239.

(262) Guo, W.; Cao, L.; Xia, J.; Nie, F. Q.; Wen, M.; Xue, J.; Song, Y.; Zhu, D.; Wang, Y.; Jiang, L. Energy Harvesting with Single-Ion-Selective Nanopores: A Concentration-Gradient-Driven Nanofluidic Power Source. *Adv. Funct. Mater.* **2010**, *20* (8), 1339–1344. https://doi.org/10.1002/adfm.200902312.

(263) Cao, L.; Guo, W.; Ma, W.; Wang, L.; Xia, F.; Wang, S.; Wang, Y.; Jiang, L.; Zhu, D. Towards Understanding the Nanofluidic Reverse Electrodialysis System: Well Matched Charge Selectivity and Ionic Composition. *Energy Environ. Sci.* **2011**, *4* (6), 2259–2266. https://doi.org/10.1039/c1ee01088c.

(264) Gao, J.; Guo, W.; Feng, D.; Wang, H.; Zhao, D.; Jiang, L. High-Performance Ionic Diode Membrane for Salinity Gradient Power Generation. *J. Am. Chem. Soc.* **2014**, *136* (35), 12265–12272. https://doi.org/10.1021/ja503692z.

(265) Vlassiouk, I.; Kozel, T. R.; Siwy, Z. S. Biosensing with Nanofluidic Diodes. *J. Am. Chem. Soc.* **2009**, *131* (23), 8211–8220. https://doi.org/10.1021/ja901120f.

(266) Han, C.; Hou, X.; Zhang, H.; Guo, W.; Li, H.; Jiang, L. Enantioselective Recognition in Biomimetic Single Artificial Nanochannels. *J. Am. Chem. Soc.* **2011**, *133* (20), 7644–7647. https://doi.org/10.1021/ja2004939.

(267) Daiguji, H. Ion Transport in Nanofluidic Channels. *Chem. Soc. Rev.* **2010**, *39* (3), 901–911. https://doi.org/10.1039/b820556f.

(268) Cheng, L. J.; Guo, L. J. Nanofluidic Diodes. *Chem. Soc. Rev.* **2010**, *39* (3), 923–938. https://doi.org/10.1039/b822554k.

(269) Chen, Q.; Meng, L.; Li, Q.; Wang, D.; Guo, W.; Shuai, Z.; Jiang, L. Water Transport and Purification in Nanochannels Controlled by Asymmetric Wettability. *Small* **2011**, *7* (15), 2225–2231. https://doi.org/10.1002/smll.201100287.

(270) Doyle, D. A.; Cabral, J. M.; Pfuetzner, R. A.; Kuo, A.; Gulbis, J. M.; Cohen, S. L.; Chait, B. T.; MacKinnon, R. The Structure of the Potassium Channel: Molecular Basis of K+ Conduction and Selectivity. *Science (80-. ).* **1998**, *280* (5360), 69–77. https://doi.org/10.1126/science.280.5360.69.

(271) Nishizawa, M.; Menon, V. P.; Martin, C. R. Metal Nanotubule Membranes with Electrochemically Switchable Ion-Transport Selectivity. *Science (80-. ).* **1995**, *268* (5211), 700–702. https://doi.org/10.1126/science.268.5211.700.

(272) Guo, W.; Xia, H.; Xia, F.; Hou, X.; Cao, L.; Wang, L.; Xue, J.; Zhang, G.; Song, Y.; Zhu, D.;

Wang, Y.; Jiang, L. Current Rectification in Temperature-Responsive Single Nanopores. *ChemPhysChem* **2010**, *11* (4), 859–864. https://doi.org/10.1002/cphc.200900989.

(273) Hou, X.; Dong, H.; Zhu, D.; Jiang, L. Fabrication of Stable Single Nanochannels with Controllable Ionic Rectification. *Small* **2010**, *6* (3), 361–365. https://doi.org/10.1002/smll.200901701.

(274) Yameen, B.; Ali, M.; Neumann, R.; Ensinger, W.; Knoll, W.; Azzaroni, O. Single Conical Nanopores Displaying PH-Tunable Rectifying Characteristics. Manipulating Ionic Transport with Zwitterionic Polymer Brushes. *J. Am. Chem. Soc.* **2009**, *131* (6), 2070–2071. https://doi.org/10.1021/ja8086104.

(275) Zhou, Y.; Guo, W.; Cheng, J.; Liu, Y.; Li, J.; Jiang, L. High-Temperature Gating of Solid-State Nanopores with Thermo-Responsive Macromolecular Nanoactuators in Ionic Liquids. *Adv. Mater.* **2012**, *24* (7), 962–967. https://doi.org/10.1002/adma.201104814.

(276) Wang, L.; Guo, W.; Xie, Y. B.; Wang, X. W.; Xue, J. M.; Wang, Y. G. Nanofluidic Diode Generated by PH Gradient inside Track-Etched Conical Nanopore. *Radiat. Meas.* **2009**, *44* (9–10), 1119–1122. https://doi.org/10.1016/j.radmeas.2009.10.042.

(277) Apel, P. Y.; Korchev, Y. E.; Siwy, Z.; Spohr, R.; Yoshida, M. Diode-like Single-Ion Track Membrane Prepared by Electro-Stopping. *Nucl. Instruments Methods Phys. Res. Sect. B Beam Interact. with Mater. Atoms* **2001**, *184* (3), 337–346. https://doi.org/10.1016/S0168-583X(01)00722-4.

(278) Siwy, Z. S. Ion-Current Rectification in Nanopores and Nanotubes with Broken Symmetry. *Adv. Funct. Mater.* **2006**, *16* (6), 735–746. https://doi.org/10.1002/adfm.200500471.

(279) Siwy, Z.; Apel, P.; Baur, D.; Dobrev, D. D.; Korchev, Y. E.; Neumann, R.; Spohr, R.; Trautmann, C.; Voss, K. O. Preparation of Synthetic Nanopores with Transport Properties Analogous to Biological Channels. *Surf. Sci.* **2003**, *532–535*, 1061–1066. https://doi.org/10.1016/S0039-6028(03)00448-5.

(280) Siwy, Z.; Heins, E.; Harrell, C. C.; Kohli, P.; Martin, C. R. Conical-Nanotube Ion-Current Rectifiers: The Role of Surface Charge. *J. Am. Chem. Soc.* **2004**, *126* (35), 10850–10851. https://doi.org/10.1021/ja047675c.

(281) Siwy, Z.; Apel, P.; Dobrev, D.; Neumann, R.; Spohr, R.; Trautmann, C.; Voss, K. Ion Transport through Asymmetric Nanopores Prepared by Ion Track Etching. *Nucl. Instruments Methods Phys. Res. Sect. B Beam Interact. with Mater. Atoms* **2003**, *208* (1–4), 143–148. https://doi.org/10.1016/S0168-583X(03)00884-X.

(282) Siwy, Z.; Gu, Y.; Spohr, H. A.; Baur, D.; Wolf-Reber, A.; Spohr, R.; Apel, P.; Korchev, Y. E. Rectification and Voltage Gating of Ion Currents in a Nanofabricated Pore. *EPL (Europhysics Lett.* **2002**, *60* (3), 349. https://doi.org/10.1209/EPL/I2002-00271-3.

(283) Cheng, L. J.; Guo, L. J. Rectified Ion Transport through Concentration Gradient in Homogeneous Silica Nanochannels. *Nano Lett.* **2007**, *7* (10), 3165–3171. https://doi.org/10.1021/nl071770c.

(284) Daiguji, H.; Oka, Y.; Shirono, K. Nanofluidic Diode and Bipolar Transistor. *Nano Lett.* **2005**, *5* (11), 2274–2280. https://doi.org/10.1021/nl051646y.

(285) Karnik, R.; Castelino, K.; Duan, C.; Majumdar, A. Diffusion-Limited Patterning of Molecules in Nanofluidic Channels. *Nano Lett.* **2006**, *6* (8), 1735–1740. https://doi.org/10.1021/nl061159y.

(286) Vlassiouk, I.; Siwy, Z. S. Nanofluidic Diode. *Nano Lett.* **2007**, *7* (3), 552–556. https://doi.org/10.1021/nl062924b.

(287) Cheng, L. J.; Guo, L. J. Ionic Current Rectification, Breakdown, and Switching in Heterogeneous

Oxide Nanofluidic Devices. *ACS Nano* **2009**, *3* (3), 575–584. https://doi.org/10.1021/nn8007542.

(288) Alcaraz, A.; Ramírez, P.; García-Giménez, E.; López, M. L.; Andrio, A.; Aguilella, V. M. A PH-Tunable Nanofluidic Diode: Electrochemical Rectification in a Reconstituted Single Ion Channel. *J. Phys. Chem. B* **2006**, *110* (42), 21205–21209. https://doi.org/10.1021/jp063204w.

(289) Miedema, H.; Vrouenraets, M.; Wierenga, J.; Meijberg, W.; Robillard, G.; Eisenberg, B. A Biological Porin Engineered into a Molecular, Nanofluidic Diode. *Nano Lett.* **2007**, *7* (9), 2886–2891. https://doi.org/10.1021/nl0716808.

(290) Ali, M.; Ramirez, P.; Mafé, S.; Neumann, R.; Ensinger, W. A PH-Tunable Nanofluidic Diode with a Broad Range of Rectifying Properties. *ACS Nano* **2009**, *3* (3), 603–608. https://doi.org/10.1021/nn900039f.

(291) Yameen, B.; Ali, M.; Neumann, R.; Ensinger, W.; Knoll, W.; Azzaroni, O. Proton-Regulated Rectified Ionic Transport through Solid-State Conical Nanopores Modified with Phosphate-Bearing Polymer Brushes. *Chem. Commun.* **2010**, *46* (11), 1908–1910. https://doi.org/10.1039/b920870d.

(292) Macrae, M. X.; Blake, S.; Mayer, M.; Yang, J. Nanoscale Ionic Diodes with Tunable and Switchable Rectifying Behavior. *J. Am. Chem. Soc.* **2010**, *132* (6), 1766–1767. https://doi.org/10.1021/ja909876h.

(293) He, Y.; Gillespie, D.; Boda, D.; Vlassiouk, I.; Eisenberg, R. S.; Siwy, Z. S. Tuning Transport Properties of Nanofluidic Devices with Local Charge Inversion. *J. Am. Chem. Soc.* **2009**, *131* (14), 5194–5202. https://doi.org/10.1021/ja808717u.

(294) Guan, W.; Fan, R.; Reed, M. A. Field-Effect Reconfigurable Nanofluidic Ionic Diodes. *Nat. Commun.* **2011**, *2* (1), 1–8. https://doi.org/10.1038/ncomms1514.

(295) Picallo, C. B.; Gravelle, S.; Joly, L.; Charlaix, E.; Bocquet, L. Nanofluidic Osmotic Diodes: Theory and Molecular Dynamics Simulations. *Phys. Rev. Lett.* **2013**, *111* (24), 244501. https://doi.org/10.1103/PhysRevLett.111.244501.

(296) Laohakunakorn, N.; Gollnick, B.; Moreno-Herrero, F.; Aarts, D. G. A. L.; Dullens, R. P. A.; Ghosal, S.; Keyser, U. F. A Landau-Squire Nanojet. *Nano Lett.* **2013**, *13* (11), 5141–5146. https://doi.org/10.1021/nl402350a.

(297) Guo, W.; Tian, Y.; Jiang, L. Asymmetric Ion Transport through Ion-Channel-Mimetic Solid-State Nanopores. *Acc. Chem. Res.* **2013**, *46* (12), 2834–2846. https://doi.org/10.1021/ar400024p.

(298) Mao, P.; Han, J. Fabrication and Characterization of 20 Nm Planar Nanofluidic Channels by Glass-Glass and Glass-Silicon Bonding. *Lab Chip* **2005**, *5* (8), 837–844. https://doi.org/10.1039/b502809d.

(299) Maleki, T.; Mohammadi, S.; Ziaie, B. A Nanofluidic Channel with Embedded Transverse Nanoelectrodes. *Nanotechnology* **2009**, *20* (10). https://doi.org/10.1088/0957-4484/20/10/105302.

(300) Li, H. W.; Kang, D. J.; Blamire, M. G.; Huck, W. T. S. Focused Ion Beam Fabrication of Silicon Print Masters. *Nanotechnology* **2003**, *14* (2), 220–223. https://doi.org/10.1088/0957-4484/14/2/323.

(301) Xu, Y.; Wang, C.; Dong, Y.; Li, L.; Jang, K.; Mawatari, K.; Suga, T.; Kitamori, T. Low-Temperature Direct Bonding of Glass Nanofluidic Chips Using a Two-Step Plasma Surface Activation Process. *Anal. Bioanal. Chem.* **2012**, *402* (3), 1011–1018. https://doi.org/10.1007/s00216-011-5574-2.

(302) Xu, Z.; Wen, J. K.; Liu, C.; Liu, J. S.; Du, L. Q.; Wang, L. D. Research on Forming and Application of U-Form Glass Micro-Nanofluidic Chip with Long Nanochannels. *Microfluid.*

*Nanofluidics* **2009**, *7* (3), 423–429. https://doi.org/10.1007/s10404-009-0407-8.

(303) Mao, P.; Han, J. Massively-Parallel Ultra-High-Aspect-Ratio Nanochannels as Mesoporous Membranes. *Lab Chip* **2009**, *9* (4), 586–591. https://doi.org/10.1039/b809370a.

(304) Nam, K. H.; Suh, Y. D.; Yeo, J.; Woo, D. Manual, *in Situ*, Real-Time Nanofabrication Using Cracking through Indentation. *Sci. Rep.* **2016**, *6*, 2–9. https://doi.org/10.1038/srep18892.

(305) Wong, C. C.; Agarwal, A.; Balasubramanian, N.; Kwong, D. L. Fabrication of Self-Sealed Circular Nano/Microfluidic Channels in Glass Substrates. *Nanotechnology* **2007**, *18* (13). https://doi.org/10.1088/0957-4484/18/13/135304.

(306) Xu, Y.; Matsumoto, N. Flexible and *in Situ* Fabrication of Nanochannels with High Aspect Ratios and Nanopillar Arrays in Fused Silica Substrates Utilizing Focused Ion Beam. *RSC Adv.* **2015**, *5* (62), 50638–50643. https://doi.org/10.1039/c5ra06306j.

(307) Kim, S. J.; Song, Y. A.; Han, J. Nanofluidic Concentration Devices for Biomolecules Utilizing Ion Concentration Polarization: Theory, Fabrication, and Applications. *Chem. Soc. Rev.* **2010**, *39* (3), 912–922. https://doi.org/10.1039/b822556g.

(308) Fanzio, P.; Mussi, V.; Manneschi, C.; Angeli, E.; Firpo, G.; Repetto, L.; Valbusa, U. DNA Detection with a Polymeric Nanochannel Device. *Lab Chip* **2011**, *11* (17), 2961–2966. https://doi.org/10.1039/c1lc20243j.

(309) Cheng, E.; Zou, H.; Yin, Z.; Jurčíček, P.; Zhang, X. Fabrication of 2D Polymer Nanochannels by Sidewall Lithography and Hot Embossing. *J. Micromechanics Microengineering* **2013**, *23* (7). https://doi.org/10.1088/0960-1317/23/7/075022.

(310) Pezzuoli, D.; Angeli, E.; Repetto, D.; Guida, P.; Firpo, G.; Repetto, L. Increased Flexibility in Lab-on-Chip Design with a Polymer Patchwork Approach. *Nanomaterials* **2019**, *9* (12). https://doi.org/10.3390/nano9121678.

(311) Huh, D.; Mills, K. L.; Zhu, X.; Burns, M. A.; Thouless, M. D.; Takayama, S. Tuneable Elastomeric Nanochannels for Nanofluidic Manipulation. *Nat. Mater.* **2007**, *6* (6), 424–428. https://doi.org/10.1038/nmat1907.

(312) Bowden, N.; Huck, W. T. S.; Paul, K. E.; Whitesides, G. M. The Controlled Formation of Ordered, Sinusoidal Structures by Plasma Oxidation of an Elastomeric Polymer. *Appl. Phys. Lett.* **1999**, *75* (17), 2557–2559. https://doi.org/10.1063/1.125076.

(313) Zhu, X.; Mills, K. L.; Peters, P. R.; Bahng, J. H.; Liu, E. H.; Shim, J.; Naruse, K.; Csete, M. E.; Thouless, M. D.; Takayama, S. Fabrication of Reconfigurable Protein Matrices by Cracking. *Nat. Mater.* **2005**, *4* (5), 403–406. https://doi.org/10.1038/nmat1365.

(314) Peng, R.; Li, D. Fabrication of Polydimethylsiloxane (PDMS) Nanofluidic Chips with Controllable Channel Size and Spacing. *Lab Chip* **2016**, *16* (19), 3767–3776. https://doi.org/10.1039/c6lc00867d.

(315) Kim, M.; Ha, D.; Kim, T. Cracking-Assisted Photolithography for Mixed-Scale Patterning and Nanofluidic Applications. *Nat. Commun.* **2015**, *6*, 1–8. https://doi.org/10.1038/ncomms7247.

(316) Park, S. M.; Huh, Y. S.; Craighead, H. G.; Erickson, D. A Method for Nanofluidic Device Prototyping Using Elastomeric Collapse. *Proc. Natl. Acad. Sci. U. S. A.* **2009**, *106* (37), 15549–15554. https://doi.org/10.1073/pnas.0904004106.

(317) Park, Y. S.; Oh, J. M.; Cho, Y. K. Non-Lithographic Nanofluidic Channels with Precisely Controlled Circular Cross Sections. *RSC Adv.* **2018**, *8* (35), 19651–19658. https://doi.org/10.1039/c8ra03496f.

(318) van Kan, J. A.; Zhang, C.; Perumal Malar, P.; van der Maarel, J. R. C. High Throughput Fabrication of Disposable Nanofluidic Lab-on-Chip Devices for Single Molecule Studies. *Biomicrofluidics* **2012**, *6* (3). https://doi.org/10.1063/1.4740231.

(319) Wu, J.; Chantiwas, R.; Amirsadeghi, A.; Soper, S. A.; Park, S. Complete Plastic Nanofluidic Devices for DNA Analysis *via* Direct Imprinting with Polymer Stamps. *Lab Chip* **2011**, *11* (17), 2984–2989. https://doi.org/10.1039/c1lc20294d.

(320) Chantiwas, R.; Hupert, M. L.; Pullagurla, S. R.; Balamurugan, S.; Tamarit-López, J.; Park, S.; Datta, P.; Goettert, J.; Cho, Y. K.; Soper, S. A. Simple Replication Methods for Producing Nanoslits in Thermoplastics and the Transport Dynamics of Double-Stranded DNA through These Slits. *Lab Chip* **2010**, *10* (23), 3255–3264. https://doi.org/10.1039/c0lc00096e.

(321) Thangawng, A. L.; Swartz, M. A.; Glucksberg, M. R.; Ruoff, R. S. Bond-Detach Lithography: A Method for Micro/Nanolithography by Precision PDMS Patterning. *Small* **2007**, *3* (1), 132–138. https://doi.org/10.1002/smll.200500418.

(322) Li, X.; Wang, X.; Jin, J.; Tang, Q.; Tian, Y.; Fu, S.; Cui, Z. Fabrication of Micro/Nano Fluidic System Combining Hybrid Mask-Mould Lithography with Thermal Bonding. *Microelectron. Eng.* **2010**, *87* (5–8), 722–725. https://doi.org/10.1016/j.mee.2009.12.024.

(323) Wu, C.; Lin, T. G.; Zhan, Z.; Li, Y.; Tung, S. C. H.; Tang, W. C.; Li, W. J. Fabrication of All-Transparent Polymer-Based and Encapsulated Nanofluidic Devices Using Nano-Indentation Lithography. *Microsystems Nanoeng.* **2017**, *3* (October 2016). https://doi.org/10.1038/micronano.2016.84.

(324) Takei, S. Ultraviolet Nano Imprint Lithography Using Fluorinated Silicon-Based Resist Materials. *Appl. Phys. Express* **2010**, *3* (2). https://doi.org/10.1143/APEX.3.025203.

(325) Yang, H. Y.; Han, Z. J.; Yu, S. F.; Pey, K. L.; Ostrikov, K.; Karnik, R. Carbon Nanotube Membranes with Ultrahigh Specific Adsorption Capacity for Water Desalination and Purification. *Nat. Commun.* **2013**, *4*. https://doi.org/10.1038/ncomms3220.

(326) Liu, L.; Yang, C.; Zhao, K.; Li, J.; Wu, H. C. Ultrashort Single-Walled Carbon Nanotubes in a Lipid Bilayer as a New Nanopore Sensor. *Nat. Commun.* **2013**, *4*, 1–8. https://doi.org/10.1038/ncomms3989.

(327) Geng, J.; Kim, K.; Zhang, J.; Escalada, A.; Tunuguntla, R.; Comolli, L. R.; Allen, F. I.; Shnyrova, A. V.; Cho, K. R.; Munoz, D.; Wang, Y. M.; Grigoropoulos, C. P.; Ajo-Franklin, C. M.; Frolov, V. A.; Noy, A. Stochastic Transport through Carbon Nanotubes in Lipid Bilayers and Live Cell Membranes. *Nature* **2014**, *514* (7524), 612–615. https://doi.org/10.1038/nature13817.

(328) Niguès, A.; Siria, A.; Vincent, P.; Poncharal, P.; Bocquet, L. Ultrahigh Interlayer Friction in Multiwalled Boron Nitride Nanotubes. *Nat. Mater.* **2014**, *13* (7), 688–693. https://doi.org/10.1038/nmat3985.

(329) Cong, H.; Xu, X.; Yu, B.; Yang, Z.; Zhang, X. A Smart Temperature and Magnetic-Responsive Gating Carbon Nanotube Membrane for Ion and Protein Transportation. *Sci. Rep.* **2016**, *6* (May), 1–10. https://doi.org/10.1038/srep32130.

(330) Tunuguntla, R. H.; Escalada, A.; A Frolov, V.; Noy, A. Synthesis, Lipid Membrane Incorporation, and Ion Permeability Testing of Carbon Nanotube Porins. *Nat. Protoc.* **2016**, *11* (10), 2029–2047. https://doi.org/10.1038/nprot.2016.119.

(331) Sun, X.; Zaric, S.; Daranciang, D.; Welsher, K.; Lu, Y.; Li, X.; Dai, H. Optical Properties of Ultrashort Semiconducting Single-Walled Carbon Nanotube Capsules down to Sub-10 Nm. *J. Am. Chem. Soc.* **2008**, *130* (20), 6551–6555. https://doi.org/10.1021/ja8006929.

(332) Pang, P.; He, J.; Park, J. H.; Krstić, P. S.; Lindsay, S. Origin of Giant Ionic Currents in Carbon Nanotube Channels. *ACS Nano* **2011**, *5* (9), 7277–7283. https://doi.org/10.1021/nn202115s.

(333) Choi, W.; Ulissi, Z. W.; Shimizu, S. F. E.; Bellisario, D. O.; Ellison, M. D.; Strano, M. S. Diameter-Dependent Ion Transport through the Interior of Isolated Single-Walled Carbon Nanotubes. *Nat. Commun.* **2013**, *4*, 1–8. https://doi.org/10.1038/ncomms3397.

(334) Ponomarenko, L. A.; Geim, A. K.; Zhukov, A. A.; Jalil, R.; Morozov, S. V.; Novoselov, K. S.; Grigorieva, I. V.; Hill, E. H.; Cheianov, V. V.; Fal'Ko, V. I.; Watanabe, K.; Taniguchi, T.; Gorbachev, R. V. Tunable Metalinsulator Transition in Double-Layer Graphene Heterostructures. *Nat. Phys.* **2011**, *7* (12), 958–961. https://doi.org/10.1038/NPHYS2114.

(335) Britnell, L.; Gorbachev, R. V.; Jalil, R.; Belle, B. D.; Schedin, F.; Mishchenko, A.; Georgiou, T.; Katsnelson, M. I.; Eaves, L.; Morozov, S. V.; Peres, N. M. R.; Leist, J.; Geim, A. K.; Novoselov, K. S.; Ponomarenko, L. A. Field-Effect Tunneling Transistor Based on Vertical Graphene Heterostructures. *Science (80-. ).* **2012**, *335* (6071), 947–950. https://doi.org/10.1126/science.1218461.

(336) Haigh, S. J.; Gholinia, A.; Jalil, R.; Romani, S.; Britnell, L.; Elias, D. C.; Novoselov, K. S.; Ponomarenko, L. A.; Geim, A. K.; Gorbachev, R. Cross-Sectional Imaging of Individual Layers and Buried Interfaces of Graphene-Based Heterostructures and Superlattices. *Nat. Mater.* **2012**, *11* (9), 764–767. https://doi.org/10.1038/nmat3386.

(337) Georgiou, T.; Jalil, R.; Belle, B. D.; Britnell, L.; Gorbachev, R. V.; Morozov, S. V.; Kim, Y. J.; Gholinia, A.; Haigh, S. J.; Makarovsky, O.; Eaves, L.; Ponomarenko, L. A.; Geim, A. K.; Novoselov, K. S.; Mishchenko, A. Vertical Field-Effect Transistor Based on Graphene-WS 2 Heterostructures for Flexible and Transparent Electronics. *Nat. Nanotechnol.* **2013**, *8* (2), 100–103. https://doi.org/10.1038/nnano.2012.224.

(338) Gorbachev, R. V.; Geim, A. K.; Katsnelson, M. I.; Novoselov, K. S.; Tudorovskiy, T.; Grigorieva, I. V.; MacDonald, A. H.; Morozov, S. V.; Watanabe, K.; Taniguchi, T.; Ponomarenko, L. A. Strong Coulomb Drag and Broken Symmetry in Double-Layer Graphene. *Nat. Phys.* **2012**, *8* (12), 896–901. https://doi.org/10.1038/nphys2441.

(339) Dean, C.; Young, A. F.; Wang, L.; Meric, I.; Lee, G. H.; Watanabe, K.; Taniguchi, T.; Shepard, K.; Kim, P.; Hone, J. Graphene Based Heterostructures. *Solid State Commun.* **2012**, *152* (15), 1275–1282. https://doi.org/10.1016/j.ssc.2012.04.021.